Primordial gravitational waves from triaxially anisotropic pre-inflation

Yu Furuya

A dissertation submitted to Hirosaki University
for the degree of Doctor of Philosophy

January 2020

Abstract

One of the paradigms in modern cosmology is an early accelerated expansion of the universe, called "cosmic inflation", before the big bang. In the era of gravitational astronomy after the discovery of GW150914, there is a growing hope that a detection of primordial gravitational waves (PGWs), emerging from the quantum nature of spacetime during the early accelerated expansion, will be carried out before long by future-planned laser-interferometer experiments in space such as LISA, DECIGO/B-DECIGO and Big Bang Observer, and it will serve as a direct evidence of the occurrence of inflation. If there was a stage preceding inflation, it is well anticipated that the spacetime then was fairly anisotropic and/or inhomogeneous with a magnitude of the order of the energy scale of unified theories, and the dynamics of cosmic inflation lead to homogeneous, isotropic expansion as partly proved by Wald's cosmic no-hair theorem. The aim of my study is to argue that one could read the pre-inflationary initial anisotropy off from directional variations of PGWs. In this thesis, we attempt to perform theoretical/numerical calculations of PGWs in triaxially anisotropic Kasner–de Sitter spacetimes, which represents a homogeneous but anisotropic universe of Bianchi type-I, isotropized by a positive cosmological constant Λ. Quantization in such an anisotropic background has been argued to be problematic due to the presence of an initial singularity where the anisotropy diverges. We circumvent this difficulty by introducing "the time for quantization" after the singularity where certain adiabatic conditions for the fields are met, so that the standard procedure of second quantization can be carried out. We demonstrate that our prescription for determining the quantum energy spectrum is useful in making physically meaningful predictions for the primordial gravitational waves in triaxially anisotropic Kasner–de Sitter backgrounds. As a *sanity check*,

it is confirmed that, with a moderate assumption on the choice of the quantum state, the power spectrum and distribution of PGWs on sufficiently short wave-length scales recover the one for de Sitter inflation, namely, scale invariant and isotropic. Moreover, we perform a detailed analysis of the directional dependence of the time evolution of PGWs. As a result, it is found that the predicted angular distribution map of the growth factor of PGWs on large scales exhibits topologically distinctive patterns according to the degree of the pre-inflationary anisotropy. Such a qualitative topological nature of the sky-map of the growth factor should have impacts on the final intensity of PGWs. Particularly, the regions where our quantization prescription is ineffective could correspond to greater growths, which might serve as a potential probe for the pre-inflationary initial anisotropy with future all-sky observations of gravitational waves. The success of observation of such topological nature would be not only useful for searching the initial anisotropy but also be a proof of the presence of a "pre-inflation" stage of the universe.

Acknowledgements

I most gratefully acknowledge the valuable guidance of Dr. Yuuiti Sendouda in all situations of this study. Without his attentive guidance, I could not complete this thesis. I thank incisive comments by Yuki Niiyama based on his deep knowledge of the theory of gravity. I was helped by his knowledge on theoretical calculations of PGWs. I would like to show my appreciation for Dr. Hideki Asada for valuable indications in various situations. It was beneficial to me to learn from studies in Asada Lab. related to gravitational waves originating from celestial objects. I would like to offer my special thanks to Dr. Kei Yamada. I was able to have meaningful discussions in a workshop where he invited me, and discussions with Dr. Masato Minamitsuji were particularly useful. As a matter of course, I acknowledge other past and present members of our laboratory. They gave interesting information in various fields to me.

Preface

Organization of this thesis: Chapter 1 reviews some of the modern paradigms in the research fields of cosmology and astrophysics and introduces the whole purpose of the studies presented in this thesis. In particular, the theoretical and observational motivations for studying the state of the extremely early universe preceding cosmic inflation, pre-inflationary state, are presented. In Chapter 2, we show derivation of gravitational wave equations in the Kasner–de Sitter cosmological model, a (pre-)inflation model with a primordial anisotropy, where this part is mostly based on Reference [PPU07]. In Chapter 3, we consider quantization of primordial gravitational waves, suggesting a prescription for circumventing the initial Kasner singularity. In Chapter 4, we perform detailed analyses of directional dependence of the time evolution of tensor fluctuations in general directions. In Chapter 5, we conclude this thesis.

Notations: Throughout the thesis, we use the natural units with $c = \hbar = k_{\mathrm{B}} = 8\pi G = 1$. In general, Greek indices $\mu, \nu, \cdots$ of vectors and tensors run through $0, 1, 2, 3$, while Latin indices $i, j, \cdots$ through $1, 2, 3$. Note, however, that, in Chapters 2–4, λ and λ' are used to represent tensor polarizations and a and b for vector polarizations. We employ the Einstein summation convention, such as

$$\begin{aligned} a^{\mu}\, b_{\mu} &\equiv \sum_{\mu=0}^{3} a^{\mu}\, b_{\mu} = a^{0}\, b_{0} + a^{1}\, b_{1} + a^{2}\, b_{2} + a^{3}\, b_{3}\,, \\ A^{i}\, B_{i} &\equiv \sum_{i=1}^{3} A^{i}\, B_{i} = A^{1}\, B_{1} + A^{2}\, B_{2} + A^{3}\, B_{3}\,. \end{aligned} \tag{1}$$

Brackets are used to denote symmetrization and anti-symmetrization of tensor indices as

$$T_{(ij)} \equiv \frac{1}{2}\left(T_{ij} + T_{ji}\right), \quad T_{[ij]} \equiv \frac{1}{2}\left(T_{ij} - T_{ji}\right). \tag{2}$$

We will use the arrow notation to denote spatial contravariant vectors such as $\vec{V} \equiv (V^1, V^2, V^3)$. The Minkowski spacetime metric is $\eta_{\mu\nu} \equiv \mathrm{diag}(-1,\, 1,\, 1,\, 1)$. The sign convention for the Riemann tensor of a metric $g_{\mu\nu}$ is $R_{\mu\nu\rho\sigma} = \frac{1}{2}\,\partial_\nu\partial_\rho g_{\mu\sigma} + \dots$.

Declaration: This thesis includes materials presented in the following two papers co-authored by myself and my colleagues:

Yu Furuya, Yuki Niiyama and Yuuiti Sendouda, "Probing pre-inflationary anisotropy with directional variations in the gravitational wave background", Journal of Cosmology and Astroparticle Physics **1701**, 009 (2017)

and

Yu Furuya, Yuki Niiyama and Yuuiti Sendouda, "A quantisation procedure in the presence of an initial Kasner singularity: primordial gravitational waves from triaxially anisotropic pre-inflation", Classical and Quantum Gravity **36**, 085007 (2019).

Contents

List of figures

Chapter 1

Introduction

1.1 Standard cosmology, big bang and its problems

The idea of the big-band theory [Gam46] is that the universe expanded from a very high-density and high-temperature state, which is based on General Relativity and the cosmological principle, i.e., an assumption that the universe is isotropic and homogeneous on large scales. In this theory, the geometry of the universe is described by the Friedmann–Lemaître–Robertson–Walker (FLRW) metric [Fri22; Lem27; Rob35; Rob36a; Rob36b; Wal37] given by

$$\mathrm{d}s^2 = -\mathrm{d}t^2 + a(t)^2\,\gamma_{ij}\,\mathrm{d}x^i\,\mathrm{d}x^j\,, \tag{1.1}$$

where a is the scale factor and γ_{ij} is the 3-metric for a homogeneous and isotropic space.

The big-bang theory enjoyed great success in explaining important observational facts, the Hubble–Lemaître law [Lem27; Hub29], big-bang nucleosynthesis (BBN), i.e., the light-element abundances at present [Pit+18], and the isotropic cosmic microwave background (CMB) [PW65; Fix+96].

However, at the same time, the big-bang theory was suffering from a few serious problems as briefly explained below.

The horizon problem: From the CMB observations [PW65; Fix+96], the observable universe is almost isotropic and homogeneous in the sky to a precision of $\mathcal{O}(10^{-5})$. On the other hand, the whole sky as seen by us is much larger than the section of the particle horizon at the epoch of last scattering of CMB photons, and any two points separated by a Hubble distance at a certain time could not have had causal relationship in the

past. This would mean that all the patches of the universe should have the same initial condition to a precision of $\mathcal{O}(10^{-5})$, which sounds unnatural.

The flatness problem: The observable universe is almost flat, $|\Omega_{\rm K0}| \lesssim 0.01$ [Ala+17; Agh+18], where $\Omega_{\rm K0}$ is the curvature parameter at the present time. Since $\Omega_{\rm K0} \propto 1/(a\,H)^2$, where $H \equiv \dot{a}/a$ and the dot denotes derivative with respect to t, it can be found that the the curvature parameter at the epoch of BBN, $\Omega_{\rm K}(t_{\rm BBN})$, was less than 10^{-16}, which is unnaturally small.

The magnetic-monopole problem: According to the predictions of certain grand unification theories (GUTs) of particle physics, magnetic monopoles should be produced efficiently at phase transitions in the hot early universe. However, they have not been found experimentally to date.

These problems are unavoidable within the standard big-bang theory, where it is assumed that the universe was dominated by radiation or matter components at all times up to now, so the universe always underwent decelerated expansion.

1.2 Cosmic inflation

The basic concept of cosmic inflation [Gut81; Sat81] was originally proposed as a possible solution to the horizon, flatness and magnetic-monopole problems in the big-bang theory described in the previous section. Inflation is generically characterized as being a period of accelerated expansion preceding the hot big bang. The minimal mathematical requirement for the occurrence of inflation is $\ddot{a} > 0$, where the dot denotes derivative with respect to t. The most generic class of inflation is of the power-law type, whose scale-factor grows in time as $a \propto t^{\beta}$ with $\beta > 1$, which can be supported by a slow-rolling scalar field. Another special but typical class is the de Sitter solution [de 17; de 18] with $a \propto {\rm e}^{\sqrt{\Lambda/3}\,t}$ realized in the presence of a positive cosmological constant Λ.

If inflation occurred, it could stretch the particle horizon at that moment beyond our event horizon at the present time. Also, the accelerated expansion can suppress the curvature parameter. Moreover, the number density of the magnetic-monopole at the present time can become negligibly small. If the energy-scale of inflation is $\sim 10^{15}\,{\rm GeV}$, then the required e-fold is $N \gtrsim 60$ for the consistency with the observations.

Just after, it was realized that the quantum nature of inflation could even work as the seed of the structures present in the late-time universe [Haw82; Sta82; GP82;

BST83]. Indeed, inflation has been evidenced by the observations of the various structures in the universe made in the past decades including the nearly scale-invariant power spectrum of the matter power spectrum spanning the scales from CMB to galaxy scales [Ade+16b; Ala+17; Agh+18] and the anisotropy of the CMB [Smo+92; Ben+13; Ade+16b; Agh+18].

The inflationary theory has established its status as a paradigm of modern cosmology.

1.3 Primordial gravitational waves from inflation

A subject currently attracting a particular attention in this field is the search for the primordial gravitational waves (PGWs) emerging from the quantum nature of spacetime during inflation [MC81], which is thought to be a *direct* evidence of the occurrence of inflation. Detection of PGWs, indirect or direct, is considered to be a decisive evidence of the occurrence of primordial inflation.

Indirect search for PGWs is indeed one of the purposes of measuring the B-mode polarizations in the CMB [SZ97; KKS97a; KKS97b], but its detection has not yet been accomplished. Past and ongoing projects for CMB B-mode polarization measurement at low multipoles include POLARBEAR [Ade+14a], ACTpol [Nae+14], BICEP2/Keck array and Planck [Ade+15] (see also [Ade+14b]), and SPTpol [Kei+15]. Many future experiments are also planned, such as POLARBEAR-2 and Simons Array [Suz+16], and LiteBIRD [Mat+14]. Several constraints on tensor perturbations from the current bound on the CMB B-mode have been obtained in [Ade+15; Ade+16a; Agh+18].

Meanwhile, there has been a growing hope for directly detecting the PGWs since the great success of observing gravitational waves from binary celestial bodies by the LIGO and Virgo collaborations [Abb+16b; Abb+16a; Abb+17a; Abb+17b; Abb+17c; Abb+17d]. Actually, direct detection of such PGWs in the low-frequency bands is one of the ultimate goals of future-planned laser-interferometer experiments in space such as LISA [AS+12], DECIGO/B-DECIGO [SKN01; Nak+16] and Big Bang Observer [CC05].

1.4 Anisotropic pre-inflation: beyond the inflation paradigm

Despite the bunch of observational successes, the origin of inflation has been left as a deep mystery. The well-established standard model (SM) of particle physics is considered not to answer this question. Rather, there are hopes that, at such high-energy regimes relevant to inflation, some elementary particle theory beyond SM, such as grand unification theories (GUTs) or superstrings, can come into play and be responsible for the mechanism of inflation.

At the same time, one of the next goals beyond confirming the occurrence of inflation should be determination of its initial state. Since inflation is not a truly eternal phenomenon, there must be some moment at which it set in. This is not necessarily the "beginning of the universe" and it is even anticipated that there were preceding *pre-inflationary* stages.

There is a general expectation that there were anisotropies and/or inhomogeneities of order the energy scale of unified theories like GUTs or superstrings. Investigations of early anisotropies may bring us useful information to construct the theory of elementary particles beyond SM and even quantum gravity. Then, what is to be understood is how the universe has evolved into the currently observed homogeneous and isotropic state.

A general expectation is that the current geometry of the universe, well approximated by the the FLRW metric (1.1) over a Hubble patch, was realized by inflation. Apart from homogeneity, Wald's cosmic no-hair theorem [Wal83] states that a homogeneous but anisotropic universe inevitably evolve towards isotropic de Sitter space in the presence of a (large enough) positive cosmological constant Λ. The cosmological models with an anisotropic space are classified into the so-called Bianchi types [EM69].

Although the primordial anisotropies are not supposed to persist after inflation, it is generically expected that they would have impacts on the evolution of cosmological perturbations. Indeed, several observational signatures of an anisotropic pre-inflation were discussed in [GCP07; GKP08; PPU08]. Among others, a remarkable finding is that amplification of gravitational waves occurs during the pre-inflationary Kasner regime [GKP08; KUP11], whose efficiency varies with the direction in the sky. In particular, in [GKP08], Gümrükçüoğlu *et al.* investigated such gravitational waves from an inflationary background driven by a scalar field. However, Gümrükçüoğlu *et al.*'s analysis in

[GKP08] was restricted to a particular background with axisymmetry. In fact, there is an initial singularity in the presence of general, "triaxial" anisotropy, where Weyl tensor squared diverges. The presence of singularity lies as a major obstacle when attempting to obtain reliable predictions from any calculations because identification of the unique quantum vacuum state is rendered difficult as discussed in [GCP07; PPU08]. In this sense, understanding of the quantum nature of anisotropic universe should be considered still at an immature stage.

1.5 Purpose of the thesis

The purpose of the thesis is to give further insights into the connection between direction-dependent gravitational waves and primordial pre-inflationary anisotropies. In order to accomplish this, we take the Kasner–de Sitter metric as a simpler background in which initially anisotropic expansion of space is isotropized due to a cosmological constant Λ rather than a scalar field. As analyzed in [GKP08; KUP11], the amplification of gravitational waves originates from an instability in the tensor sector and we expect even our simple model captures its essential features. This simple model also allows us to generate the all-sky map of gravitational-wave intensity from which we could decode the degree of the primordial anisotropy. Moreover, we discuss foundations of quantizing fields in the presence of a general triaxial anisotropy in order to derive reliable predictions.

Chapter 2

Gravitational waves equations in anisotropic universe

In this chapter, we review the formalism for the study of PGWs originating from anisotropic early universe and give its specific form in the case of the Kasner–de Sitter (KdS) background. In Section 2.1, we describe the background cosmological setup modeled by the KdS solution. In Section 2.2, we review the basic equations for cosmological perturbations in general Bianchi type-I spacetime formulated in [PPU07]. In Section 2.3, we give the specific form of the PGWs equations in KdS.

2.1 Kasner–de Sitter pre-inflation model

2.1.1 Bianchi type-I metric

In cosmic time, the general Bianchi type-I metric in comoving coordinates is given by

$$\mathrm{d}s^2 = -\mathrm{d}t^2 + \sum_{i=1}^{3} X_i^2(t)\,(\mathrm{d}x^i)^2\,. \tag{2.1}$$

The x^i-axes will be referred to as *principal axes* of anisotropic expansion. The metric (2.1) includes the Friedmann–Lemaître universe as a subcase when $X_1 = X_2 = X_3$. We define the average scale factor as

$$a(t) = [X_1(t)\,X_2(t)\,X_3(t)]^{1/3}\,, \tag{2.2}$$

and it characterizes the volume expansion. From this definition, it follows that we can recast the metric (2.1) by $X_i \to a\,\mathrm{e}^{\beta_i}$ as

$$\mathrm{d}s^2 = -\mathrm{d}t^2 + a^2(t)\,\gamma_{ij}\,\mathrm{d}x^i\,\mathrm{d}x^j\,, \tag{2.3}$$

where γ_{ij} is the *induced metric* defined by

$$\gamma_{ij} = \exp\left(2\beta_i(t)\right)\,\delta_{ij}\,, \tag{2.4}$$

with the constraint

$$\sum_{i=1}^{3}\beta_i = 0\,. \tag{2.5}$$

Note that, here and hereafter, the subscript of β_i is merely a label, not tensor index of a vector, which is not subject to the Einstein summation rule. The inverse of the induced metric is defined by

$$\gamma^{ij} = \exp\left(-2\beta_i(t)\right)\,\delta^{ij}\,, \tag{2.6}$$

where clearly $\gamma^{ik}\,\gamma_{kj} = \delta^i{}_j$. The indices of spatial tensors will be raised and lowered by γ^{ij} and γ_{ij}. The isotropic expansion of the space is characterized by the Hubble parameter defined as

$$H \equiv \frac{\dot{a}}{a}\,, \tag{2.7}$$

where a dot denotes differentiation with respect to t, and the anisotropy of the expansion is characterized by the shear tensor defined as

$$\hat{\sigma}_{ij} \equiv \frac{1}{2}\,\dot{\gamma}_{ij}\,. \tag{2.8}$$

Introducing the conformal time as $\mathrm{d}t = a\,\mathrm{d}\eta$, we can recast the metric (2.3) as

$$\mathrm{d}s^2 = a^2\left[-\mathrm{d}\eta^2 + \gamma_{ij}\,\mathrm{d}x^i\,\mathrm{d}x^j\right]. \tag{2.9}$$

In a similar way to that in cosmic time, the comoving Hubble parameter $\mathcal{H}$ is defined by

$$\mathcal{H} \equiv \frac{a'}{a}\,, \tag{2.10}$$

where a prime denotes differentiation with respect to η, and the conformal shear tensor σ_{ij} is defined by

$$\sigma_{ij} \equiv \frac{1}{2}\,\gamma'_{ij}\,. \tag{2.11}$$

Hereafter we shall refer to $\mathcal{H}$ as Hubble and σ_{ij} as shear. As is clear from the definition, the shear tensor is traceless, $\sigma^i{}_i = 0$, and we define the scalar shear as

$$\sigma^2 \equiv \sigma_{ij}\,\sigma^{ij} = \sum_{i=1}^{3} (\beta_i')^2\,. \tag{2.12}$$

2.1.2 Geometric quantities and background Einstein equation

The geometric quantities in a Bianchi type-I spacetime are as follows. The non-vanishing components of the Christoffel symbols are given by

$$\Gamma^0{}_{00} = \mathcal{H}\,, \quad \Gamma^0{}_{ij} = \mathcal{H}\,\gamma_{ij} + \sigma_{ij}\,, \quad \Gamma^i{}_{0j} = \mathcal{H}\,\delta^i{}_j + \sigma^i{}_j\,. \tag{2.13}$$

The non-vanishing components of the Riemann tensor are given by

$$\begin{aligned} R_{0i0j} &= -a^2\,\left(\mathcal{H}'\,\gamma_{ij} + \mathcal{H}\,\sigma_{ij} + (\sigma_{ij})' - \sigma_{jk}\,\sigma^k{}_i\right)\,, \\ R_{ijkl} &= 2a^2\,\left(\mathcal{H}^2\,\gamma_{i[k}\,\gamma_{l]j} + \mathcal{H}\,\gamma_{i[k}\,\sigma_{l]j} + \mathcal{H}\,\sigma_{i[k}\,\gamma_{l]j} + \sigma_{i[k}\,\sigma_{l]j}\right)\,. \end{aligned} \tag{2.14}$$

The non-vanishing components of the Ricci tensor are given by

$$\begin{aligned} R_{00} &= -3\mathcal{H}' - \sigma^2\,, \\ R_{ij} &= \left(\mathcal{H}' + 2\mathcal{H}^2\right)\,\gamma_{ij} + 2\mathcal{H}\,\sigma_{ij} + (\sigma_{ij})' - 2\sigma_{ik}\,\sigma^k{}_j\,. \end{aligned} \tag{2.15}$$

The Ricci scalar is given by

$$R = a^{-2}\,\left(6\mathcal{H}' + 6\mathcal{H}^2 + \sigma^2\right)\,. \tag{2.16}$$

The non-vanishing components of the Einstein tensor are given by

$$\begin{aligned} G_{00} &= 3\mathcal{H}^2 - \frac{1}{2}\,\sigma^2\,, \\ G_{ij} &= -2\mathcal{H}'\,\gamma_{ij} - \mathcal{H}^2\,\gamma_{ij} + 2\mathcal{H}\,\sigma_{ij} + (\sigma_{ij})' - \frac{1}{2}\,\sigma^2\,\gamma_{ij} - 2\sigma_{ik}\,\sigma^k{}_j\,. \end{aligned} \tag{2.17}$$

In anisotropic spacetimes, the Weyl tensor no longer vanishes. The non-vanishing components of the Weyl tensor are given by

$$\begin{aligned} C_{0i0j} &= a^2\,\left[-\frac{1}{2}\,(\sigma_{ij})' + \frac{1}{3}\,\sigma^2\,\gamma_{ij}\right]\,, \\ C_{ijkl} &= a^2\,\Bigg[2\sigma_{i[k}\,\sigma_{l]j} - \gamma_{i[k}\,(\sigma_{l]j})' + \gamma_{j[k}\,(\sigma_{l]i})' + 2\gamma_{i[k}\,\sigma_{l]m}\,\sigma^m{}_j - 2\gamma_{j[k}\,\sigma_{l]m}\,\sigma^m{}_i \\ &\quad - \frac{1}{3}\,\gamma_{i[k}\,\gamma_{l]j}\,\sigma^2\Bigg]\,, \end{aligned} \tag{2.18}$$

and we define a Weyl-curvature invariant as

$$\begin{aligned} C^2 &\equiv C_{\mu\nu\rho\sigma}\,C^{\mu\nu\rho\sigma} \\ &= a^{-4}\,\left[2\sigma^{i\prime}{}_j\,\sigma^{j\prime}{}_i + 8\sigma^{i\prime}{}_j\,(\sigma^2)^j{}_i + 2(\sigma^2)^i{}_j\,(\sigma^2)^j{}_i + \frac{1}{3}\,(\sigma^2)^2\right]\,. \end{aligned} \tag{2.19}$$

If a cosmological constant Λ is the only source for the cosmological dynamics, the Einstein equation is

$$G^\mu{}_\nu = -\Lambda\,\delta^\mu{}_\nu\,. \tag{2.20}$$

The independent equations are then given by

$$\mathcal{H}^2 = \frac{a^2\,\Lambda}{3} + \frac{1}{6}\,\sigma^2\,, \quad \mathcal{H}' = \frac{a^2\,\Lambda}{3} - \frac{1}{3}\,\sigma^2\,, \quad (\sigma^i{}_j)' = -2\mathcal{H}\,\sigma^i{}_j\,, \tag{2.21}$$

and we obtain a relation

$$\mathcal{H}' = \mathcal{H}^2 - \frac{1}{2}\,\sigma^2\,. \tag{2.22}$$

2.1.3 Kasner–de Sitter solution

Hereafter we consider the so-called Kasner–de Sitter (KdS) metric as a simple model for an inflationary universe with an initial anisotropy. It is an exact solution to the

cosmological equations (2.21), whose line element is given by

$$\mathrm{d}s^2 = -\mathrm{d}t^2 + a_{\mathrm{iso}}^2 \, \sinh^{2/3}(3H_\Lambda t) \sum_{i=1}^{3} \tanh^{2q_i}\left(\frac{3H_\Lambda t}{2}\right) (\mathrm{d}x^i)^2 \,, \tag{2.23}$$

where a_{iso} is an arbitrary positive constant, $H_\Lambda \equiv \sqrt{\Lambda/3}$, and the three exponents q_i $(i = 1, 2, 3)$ satisfy the constraints

$$\sum_{i=1}^{3} q_i = 0 \,, \quad \sum_{i=1}^{3} q_i^2 = \frac{2}{3} \,. \tag{2.24}$$

We define the average scale factor $a(t)$ and the spatial metric $\gamma_{ij}(t)$ by

$$a(t) \equiv a_{\mathrm{iso}} \, \sinh^{1/3}(3H_\Lambda t) \,, \quad \gamma_{ij}(t) \equiv \tanh^{2q_i}\left(\frac{3H_\Lambda t}{2}\right) \delta_{ij} \,. \tag{2.25}$$

Recall that the conformal time η is defined by $\mathrm{d}\eta = \mathrm{d}t/a(t)$ and a prime denotes differentiation with respect to η. Then, the average Hubble parameter $\mathcal{H}$ and the shear tensor σ_{ij} are respectively given as

$$\begin{aligned} \mathcal{H} &\equiv \frac{a'}{a} = a_{\mathrm{iso}} \, H_\Lambda \, \frac{\cosh(3H_\Lambda t)}{\sinh^{2/3}(3H_\Lambda t)} \,, \\ \sigma_{ij} &\equiv \frac{1}{2} \, \gamma'_{ij} = 3q_i \, a_{\mathrm{iso}} \, H_\Lambda \, \frac{\tanh^{2q_i}\left(\frac{3H_\Lambda t}{2}\right)}{\sinh^{2/3}(3H_\Lambda t)} \, \delta_{ij} \,. \end{aligned} \tag{2.26}$$

Clearly, this metric belongs to the class of Bianchi type-I cosmological model [EM69].

At earlier times with $t \ll H_\Lambda^{-1}$, the metric behaves like a vacuum Kasner solution [Kas21]

$$a(t) \simeq a_{\mathrm{iso}} \, (3H_\Lambda t)^{1/3} \,, \quad \gamma_{ij}(t) \simeq \left(\frac{3H_\Lambda t}{2}\right)^{2q_i} \delta_{ij} \,, \tag{2.27}$$

while at later times with $t \gg H_\Lambda^{-1}$, the metric asymptotes to a de Sitter solution [de 17; de 18],

$$a(t) \simeq 2^{-1/3} \, a_{\mathrm{iso}} \, \mathrm{e}^{H_\Lambda t} \,, \quad \gamma_{ij}(t) \simeq \delta_{ij} \,. \tag{2.28}$$

Hence the KdS metric describes a universe evolving from an anisotropic initial phase to an isotropic inflation driven by Λ. The isotropization is achieved around the time

$t_{\rm iso} \equiv H_\Lambda^{-1}$ and the constant $a_{\rm iso}$ serves as the normalization of the scale factor at the beginning of the isotropic de Sitter inflation.

This simple (pre-)inflationary model has some flaws as a realistic setup for the early universe such as lacking of mechanisms to realize a decline of the expansion rate and to exit from the inflationary phase, i.e., reheating. In what follows, we assume some appropriate mechanism, not described here, to work in ending inflation at later stage, while the metric at earlier stages is approximated by (2.23). More precisely, what we assume on observational grounds is that the superhorizon fluctuations re-entering the cosmological horizon at late times after reheating have exited the horizon at the early era when the metric is well approximated by (2.23). Since the presence of global anisotropies on cosmological scales is observationally not favored, we should require $a_{\rm iso}\, H_\Lambda \lesssim a(t_0)\, H_0$, where $t_0 \approx 13.8\,{\rm Gyr}$ is the present age of the universe and $H_0 = H(t_0) \approx 67.4\,{\rm km\,s^{-1}\,Mpc^{-1}}$ [Agh+18] is the Hubble constant. Note that this condition is equivalent to the one for evading the horizon and flatness problems.

It is useful to introduce an angular parameter Θ to express the exponents q_i as

$$q_1 = \frac{2}{3}\sin\left(\Theta - \frac{2\pi}{3}\right), \quad q_2 = \frac{2}{3}\sin\left(\Theta - \frac{4\pi}{3}\right), \quad q_3 = \frac{2}{3}\sin\Theta\,. \tag{2.29}$$

The parameter Θ quantifies the degree of anisotropy of pre-inflationary cosmological expansion. With no loss of generality, we can restrict our attention to a range $\frac{7\pi}{6} \le \Theta \le \frac{9\pi}{6}$, within which the order of the exponents is $q_1 \ge q_2 \ge q_3$, see Figure 2.1. Any KdS metric is equivalent, up to relabeling the axes and/or reversing their orientations, to one with the value of Θ lying in the above range. The expansion of the universe is axisymmetric for $\Theta = \frac{7\pi}{6}$ ($(q_1, q_2, q_3) = (\frac{2}{3}, -\frac{1}{3}, -\frac{1}{3})$) ("oblate") and for $\Theta = \frac{9\pi}{6}$ ($(q_1, q_2, q_3) = (\frac{1}{3}, \frac{1}{3}, -\frac{2}{3})$) ("prolate"). In the following analysis we shall often take $\Theta = \frac{8\pi}{6}$ as a fiducial value, for which the anisotropy exponents are $(q_1, q_2, q_3) = (\frac{1}{\sqrt{3}}, 0, -\frac{1}{\sqrt{3}})$.

An important property of the KdS metric is that it has an initial singularity at $t = 0$, where the Weyl-curvature invariant $C_{\mu\nu\rho\sigma}\, C^{\mu\nu\rho\sigma}$ diverges, unless $\Theta = \frac{7\pi}{6}$; Indeed, it is represented in terms of Θ as

$$C^2 = C^{\mu\nu}{}_{\rho\sigma}\, C^{\rho\sigma}{}_{\mu\nu} = 48 H_\Lambda^4\, \frac{1 + \cosh^2(3H_\Lambda\, t) + 2\sin 3\Theta\, \cosh(3H_\Lambda\, t)}{\sinh^4(3H_\Lambda\, t)}\,. \tag{2.30}$$

To avoid this *Kasner singularity*, we have to introduce an initial time $t_{\rm ini} > 0$. Moreover, as we shall see, its existence will play an essential role in making the ordinary prescription

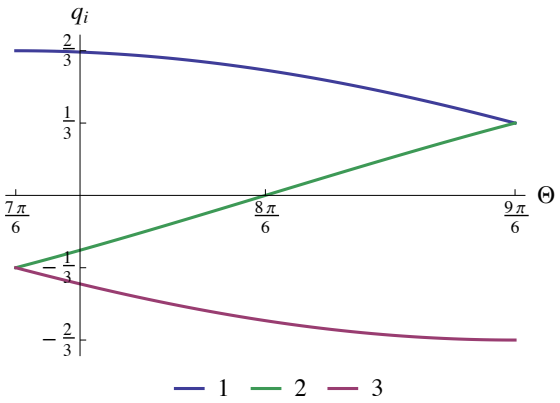

Figure 2.1: Values of q_i for $\frac{7\pi}{6} \leq \Theta \leq \frac{9\pi}{6}$.

for quantization of fields impracticable. How to circumvent this difficulty will be the main subject of Chapter 3.

2.2 Gauge-invariant formalism for cosmological perturbations in general Bianchi type-I spacetime

In this section, before focusing on the specific inflation model, we will show basic PGWs equations in general Bianchi type-I spacetime [EM69]. Our calculations rely on the gauge-invariant formulation of perturbations in Bianchi type-I cosmology developed by Pereira *et al.* [PPU07]. Qualitative differences of calculations from that in the isotropic case are as follows: (a) The norm and direction of wavevectors are time-dependent, and (b) the gauge invariant variables are no longer composed independently of scalar, vector and tensor components of perturbed variables due to the presence of shear in background. At the end of this section, we show polarization decomposition of components of the first-order Einstein tensor.

2.2.1 Gauge invariant variables and first-order Einstein tensor

We apply the gauge-invariant formulation of cosmological perturbations in Bianchi type-I models developed by Pereira *et al.* [PPU07]. In this formalism, the general perturbed metric $g_{\mu\nu}$, decomposed into the background and the perturbations as $g_{\mu\nu} = \bar{g}_{\mu\nu} + \delta g_{\mu\nu}$,

is given by

$$(\bar{g}_{\mu\nu} + \delta g_{\mu\nu})\,\mathrm{d}x^\mu\,\mathrm{d}x^\nu = a(\eta)^2\,\left[-(1+2A)\,\mathrm{d}\eta^2 + 2B_i\,\mathrm{d}x^i\,\mathrm{d}\eta + (\gamma_{ij} + h_{ij})\,\mathrm{d}x^i\,\mathrm{d}x^j\right]\,, \tag{2.31}$$

where the $(0i)$ and (ij) components are respectively decomposed into the scalar, vector, and tensor variables as

$$B_i = \partial_i B + \bar{B}_i\,, \quad h_{ij} = 2\,(\gamma_{ij} + \mathcal{H}^{-1}\,\sigma_{ij})\,C + 2\partial_{ij}E + 2\partial_{(i}E_{j)} + 2E_{ij}\,, \tag{2.32}$$

where the vector and tensor variables satisfy $\partial_i \bar{B}^i = \partial_i E^i = \partial_i E^i{}_j = E^i{}_i = 0$. Recall that the induced metric γ_{ij} and its inverse γ^{ij} are used to raise and lower the indices of the spatial vectors and tensors.

In order to construct gauge-invariant variables, let us consider an active transformation of the coordinate system. The coordinates of any point change according to

$$x^\mu \to \tilde{x}^\mu = x^\mu - \xi^\mu(x^\nu)\,, \tag{2.33}$$

where ξ is a vector field as small as the perturbations and the right-arrow means the active transformation of the coordinate system. Accordingly, the spacetime metric transforms as

$$g_{\mu\nu} \to \tilde{g}_{\mu\nu} = g_{\mu\nu} + \mathcal{L}_\xi g_{\mu\nu}\,, \tag{2.34}$$

where $\mathcal{L}_\xi g_{\mu\nu}$ is the Lie derivative of $g_{\mu\nu}$ along ξ. It follows that

$$\delta g_{\mu\nu} \to \delta g_{\mu\nu} + \mathcal{L}_\xi \bar{g}_{\mu\nu} \tag{2.35}$$

at first order in the perturbations. The vector field ξ can be decomposed into a scalar and vector part as

$$\xi^0 = T(x^i, \eta)\,, \quad \xi^i = \partial^i L(x^i, \eta) + L^i(x^j, \eta)\,, \tag{2.36}$$

with $\partial_i L^i(x^i,\eta)=0$, where $\partial^i \equiv \gamma^{ij}\,\partial_j$. The transformations of the metric perturbations are given as

$$\begin{aligned} A &\to A + T' + \mathcal{H}\,T\,,\\ B &\to B - T + L'\,,\\ C &\to C + \mathcal{H}\,T\,,\\ E &\to E + L\,, \end{aligned} \tag{2.37}$$

for the scalar variables, and as

$$\begin{aligned} \bar{B}_i &\to \bar{B}_i + \gamma_{ij}\,(L^j)' - 2\sigma_{ij}\,\partial^j L\,,\\ E_i &\to E_i + L_i\,, \end{aligned} \tag{2.38}$$

for the vector variables. The tensor variable is gauge-invariant,

$$E_{ij} \to E_{ij}\,. \tag{2.39}$$

From the gauge transformations (2.37), we can construct a set of gauge-invariant variables for the scalar sector defined by

$$\Phi \equiv A + \frac{1}{a}\left[a\,\left(B - E'\right)\right]'\,, \tag{2.40}$$

$$\Psi \equiv -C - \mathcal{H}\,\left(B - E'\right)\,. \tag{2.41}$$

As is clear from above, only two degrees of freedom remain, while the other two are absorbed. On the other hand, from the gauge transformations (2.38), a gauge invariant vector perturbation is found as

$$\Phi_i \equiv \bar{B}_i - \gamma_{ij}\,(E^j)' + 2\sigma_{ij}\,\partial^j E\,. \tag{2.42}$$

When the induced metric γ is time independent and hence $\sigma_{ij}=0$, it is obvious that these variables reduce to the standard Bardeen variables defined in the Friedmann–Lemaître case [Bar80].

We will work in the conformal Newtonian gauge defined by the conditions

$$B = E = E_i = 0\,. \tag{2.43}$$

Then the gauge-invariant variables are reduced as

$$\Phi = A\,, \quad \Psi = -C\,, \quad \Phi_i = B_i\,. \tag{2.44}$$

After some calculations, the components of the first-order Einstein tensor in terms of the gauge-invariant variables are eventually given as

$$\begin{aligned}
a^2\,\delta G^0{}_0 &= \sigma^j{}_i\,E^{i\prime}{}_j + 6\mathcal{H}\,\Psi' - 2\triangle\Psi + \frac{\sigma^i{}_j}{\mathcal{H}}\,\partial^j{}_i\Psi - \sigma^j{}_i\,\left(\frac{\sigma^i{}_j}{\mathcal{H}}\,\Psi\right)' \\
&\quad + 6\mathcal{H}^2\,\Phi - \sigma^2\,\Phi - \sigma^i{}_j\,\partial_i\Phi^j\,, \qquad (2.45) \\
a^2\,\delta G^0{}_i &= \sigma^k{}_j\,\partial_i E^j{}_k - 2\sigma^k{}_j\,\partial_k E^j{}_i - 2\partial_i\Psi' + 3\sigma^j{}_i\,\partial_j\Psi + \partial_j\left(\frac{\sigma^j{}_i}{\mathcal{H}}\,\Psi\right)' - \frac{\sigma^2}{\mathcal{H}}\,\partial_i\Psi \\
&\quad - 2\mathcal{H}\,\partial_i\Phi + \sigma^j{}_i\,\partial_j\Phi + \frac{1}{2}\,\triangle\Phi_i\,, \qquad (2.46) \\
a^2\,\delta G^i{}_j &= E^{i\prime\prime}{}_j + 2\mathcal{H}\,E^{i\prime}{}_j - \triangle E^i{}_j + 2\sigma^i{}_k\,E^{k\prime}{}_j - 2\sigma^k{}_j\,E^{i\prime}{}_k \\
&\quad + 2\left(\sigma^{i\prime}{}_k + 2\mathcal{H}\,\sigma^i{}_k\right)\,E^k{}_j - 2\left(\sigma^{k\prime}{}_j + 2\mathcal{H}\,\sigma^k{}_j\right)\,E^i{}_k - \sigma^n{}_m\,E^{m\prime}{}_n\,\delta^i{}_j \\
&\quad + 2\delta^i{}_j\,\Psi'' + 4\mathcal{H}\,\delta^i{}_j\,\Psi' - 3\sigma^i{}_j\,\Psi' \\
&\quad - \left(\frac{\sigma^j{}_i}{\mathcal{H}}\,\Psi\right)'' - 2\mathcal{H}\,\left(\frac{\sigma^j{}_i}{\mathcal{H}}\,\Psi\right)' + \sigma^n{}_m\,\left(\frac{\sigma^m{}_n}{\mathcal{H}}\,\Psi\right)'\,\delta^i{}_j \\
&\quad - \delta^i{}_j\,\triangle\Psi + \partial^i{}_j\Psi + \frac{\sigma^j{}_i}{\mathcal{H}}\,\triangle\Psi - \frac{\sigma^k{}_j}{\mathcal{H}}\,\partial^i{}_k\Psi - \frac{\sigma^i{}_k}{\mathcal{H}}\,\partial^k{}_j\Psi + \delta^i{}_j\,\frac{\sigma^m{}_n}{\mathcal{H}}\,\partial^n{}_m\Psi \\
&\quad + 2\mathcal{H}\,\delta^i{}_j\,\Phi' - \partial^i{}_j\Phi + \delta^i{}_j\,\triangle\Phi + 2\left(2\mathcal{H}' + \mathcal{H}^2\right)\delta^i{}_j\,\Phi \\
&\quad - \sigma^i{}_j\,\Phi' - 2\left(\sigma^{i\prime}{}_j + 2\mathcal{H}\,\sigma^i{}_j\right)\Phi + \sigma^2\,\delta^i{}_j\,\Phi \\
&\quad - \frac{1}{2}\,\partial^i\Phi'_j - \frac{1}{2}\,\gamma^{ik}\,\partial_j\Phi'_k + \sigma^i{}_k\,\partial^k\Phi_j + \sigma^k{}_j\,\partial_k\Phi^i + \sigma^n{}_m\,\partial_n\Phi^m\,\delta^i{}_j \\
&\quad - \mathcal{H}\,\partial^i\Phi_j - \mathcal{H}\,\partial_j\Phi^i\,, \qquad (2.47)
\end{aligned}$$

where we defined $\partial^i{}_j \equiv \gamma^{ik}\,\partial_k\partial_j$ and $\triangle \equiv \gamma^{ij}\,\partial_i\partial_j$.

2.2.2 Time-dependent orthogonal basis

As usual, we will parameterize the harmonic modes of waves by a set of constants (k_1, k_2, k_3), which are regarded as the covariant components of a wavevector in the (x^1, x^2, x^3) comoving coordinate frame. Then, any function of spacetime can be de-

composed by a Fourier transformation as

$$f(x^j,\eta)=\int\frac{\mathrm{d}^3k_i}{(2\pi)^{3/2}}\,\hat{f}(k_i,\eta)\,\mathrm{e}^{\mathrm{i}k_ix^i}\,, \tag{2.48}$$

with

$$\hat{f}(k_j,\eta)=\int\frac{\mathrm{d}^3x^i}{(2\pi)^{3/2}}\,f(x^i,\eta)\,\mathrm{e}^{-\mathrm{i}k_ix^i}\,. \tag{2.49}$$

What is unusual is that, on an anisotropic spacetime, the contravariant components $k^i\equiv k_j\,\gamma^{ij}$ are no longer constant. Hereafter, we assume that the early anisotropic expansion of the universe is isotropized through inflation. Then the contravariant wavevector $\vec{k}\equiv(k^1,k^2,k^3)$ changes its direction and norm,

$$\sqrt{k_i\,k^i}=\sqrt{\mathrm{e}^{-2\beta_1}\,k_1^2+\mathrm{e}^{-2\beta_2}\,k_2^2+\mathrm{e}^{-2\beta_3}\,k_3^2}\,, \tag{2.50}$$

during the anisotropic regime, and after the universe is isotropized, it comes to coincide with its covariant dual as $\lim_{t\to\infty}\vec{k}=(k_1,k_2,k_3)$.

It is useful to introduce time-dependent polar angles (β,γ) to parameterize the normalized wavevector as [PPU08]

$$\hat{\vec{k}}\equiv\frac{\vec{k}}{\sqrt{k_i\,k^i}}=\begin{pmatrix}\mathrm{e}^{-\beta_1}\,\sin\beta\,\cos\gamma\\ \mathrm{e}^{-\beta_2}\,\sin\beta\,\sin\gamma\\ \mathrm{e}^{-\beta_3}\,\cos\beta\end{pmatrix}\,. \tag{2.51}$$

The orthonormal polarization vector basis perpendicular to $\hat{\vec{k}}$ is introduced as

$$\begin{aligned}\vec{e}_{(1)}&\equiv\begin{pmatrix}\mathrm{e}^{-\beta_1}\,(\cos\beta\,\cos\gamma\,\cos\alpha-\sin\gamma\,\sin\alpha)\\ \mathrm{e}^{-\beta_2}\,(\cos\beta\,\sin\gamma\,\cos\alpha+\cos\gamma\,\sin\alpha)\\ -\mathrm{e}^{-\beta_3}\,\sin\beta\,\cos\alpha\end{pmatrix}\,,\\ \vec{e}_{(2)}&\equiv\begin{pmatrix}-\mathrm{e}^{-\beta_1}\,(\cos\beta\,\cos\gamma\,\sin\alpha+\sin\gamma\,\cos\alpha)\\ -\mathrm{e}^{-\beta_2}\,(\cos\beta\,\sin\gamma\,\sin\alpha-\cos\gamma\,\cos\alpha)\\ \mathrm{e}^{-\beta_3}\,\sin\beta\,\sin\alpha\end{pmatrix}\,,\end{aligned} \tag{2.52}$$

where the arbitrary angle α represents the rotation degree of freedom of $(\vec{e}_{(1)}, \vec{e}_{(2)})$ around $\vec{\hat{k}}$. As in [PPU08], we determine α by imposing a condition

$$\alpha' = -\gamma' \cos\beta \,. \tag{2.53}$$

Accordingly, the orthonormal tensor basis is defined in terms of the vector basis as

$$\epsilon^{+}_{ij} \equiv \frac{e^{(1)}_i \, e^{(1)}_j - e^{(2)}_i \, e^{(2)}_j}{\sqrt{2}} \,, \quad \epsilon^{\times}_{ij} \equiv \frac{e^{(1)}_i \, e^{(2)}_j + e^{(2)}_i \, e^{(1)}_j}{\sqrt{2}} \,, \tag{2.54}$$

where we will refer to them as the "+" and "×" modes, respectively.

2.2.3 Mode decomposition

We define a projection operator onto the subspace perpendicular to k^i as

$$P_{ij} \equiv \gamma_{ij} - \hat{k}_i \, \hat{k}_j = e^{(1)}_i \, e^{(1)}_j + e^{(2)}_i \, e^{(2)}_j \tag{2.55}$$

satisfying

$$P^i{}_j \, P^j{}_k = P^i{}_k \,, \quad P^i{}_j \, k^j = 0 \,, \quad P^{ij} \, \gamma_{ij} = 2 \,. \tag{2.56}$$

Using this operator, any three-dimensional vector V_i and any three-dimensional symmetric tensor field T_{ij} are decomposed as

$$V_i = (\hat{k}^j \, \hat{k}_i + P^j{}_i) \, V_j \equiv \hat{k}_i \, V_{\parallel} + {}_{\perp}V_i \,, \tag{2.57}$$

and

$$\begin{aligned} T_{ij} &= (\hat{k}^k \, \hat{k}_i \, \hat{k}^l \, \hat{k}_j + \hat{k}^k \, \hat{k}_i \, P^l{}_j + P^k{}_i \, \hat{k}^l \, \hat{k}_j + P^k{}_i \, P^l{}_j) \, T_{kl} \\ &\equiv \hat{k}_i \, \hat{k}_j \, T_{\parallel\parallel} + \hat{k}_i \, {}_{\perp}T_{\parallel j} + \hat{k}_j \, {}_{\perp}T_{i\parallel} + {}_{\perp}T_{ij} \,, \end{aligned} \tag{2.58}$$

respectively, where we introduced abbreviated notations such that the subscript $\parallel$ represents contraction with $\hat{k}^i$ and the subscript $\perp$ represents projection onto the two-dimensional surface by $P^i{}_j$. If $\parallel$ and $\perp$ exist together in an expression of a tensor, the contraction should be done before the projection.

Projected two-dimensional vectors and symmetric tensors can be decomposed into their scalar, vector and tensor modes. A vector satisfying $k^i \, V_i = 0$ can be expanded by

the vector basis e^i_a as

$$V^i = \sum_{a=(1),(2)} V_a \, e^i_a \,, \quad V_a \equiv V_i \, e^i_a \,. \tag{2.59}$$

The number of independent components of a symmetric tensor T_{ij} satisfying $k^i \, T_{ij} = T_i{}^i = 0$ is two, and therefore T_{ij} can be decomposed by the tensor basis ϵ^λ_{ij} as

$$T_{ij} = \sum_{\lambda=+,\times} T_\lambda \, \epsilon^\lambda_{ij} \,, \quad T_\lambda \equiv T_{ij} \, \epsilon^{ij}_\lambda \,. \tag{2.60}$$

2.2.4 Decomposition of the shear tensor

Let us decompose the shear tensor σ_{ij} . At the beginning, we make (2+1) decomposition,

$$\sigma_{ij} = \hat{k}_i \, \hat{k}_j \, \sigma_{\parallel\parallel} + 2\hat{k}_{(i} {}_\perp\sigma_{j)\parallel} + {}_\perp\sigma_{ij} \,. \tag{2.61}$$

Since σ_{ij} is traceless, $\sigma_i{}^i = \sigma_{\parallel\parallel} + P^{ij} \, {}_\perp\sigma_{ij} = 0$, it is useful to rearrange the expression as a sum of manifestly traceless terms as

$$\sigma_{ij} = \left(\hat{k}_i \, \hat{k}_j - \frac{1}{2} \, P_{ij} \right) \, \sigma_{\parallel\parallel} + 2\hat{k}_{(i} {}_\perp\sigma_{j)\parallel} + \left({}_\perp\sigma_{ij} - \frac{1}{2} \, P_{ij} \, P^{kl} \, {}_\perp\sigma_{kl} \right) \,. \tag{2.62}$$

Thus, by defining the scalar, vector, and tensor components as

$$\begin{aligned} \sigma^{(\mathrm{S})} &\equiv \sigma_{ij} \, \hat{k}^i \, \hat{k}^j = \sigma_{\parallel\parallel} \,, \\ \sigma^{(\mathrm{V})}_a &\equiv \sigma_{ij} \, \hat{k}^{(i} \, e^{j)}_a = {}_\perp\sigma_{i\parallel} \, e^i_a \,, \\ \sigma^{(\mathrm{T})}_\lambda &\equiv \sigma_{ij} \, \epsilon^{ij}_\lambda = {}_\perp\sigma_{ij} \, \epsilon^{ij}_\lambda \,, \end{aligned} \tag{2.63}$$

we can decompose the shear tensor σ_{ij} as

$$\sigma_{ij} = \frac{3}{2} \, \left(\hat{k}_i \, \hat{k}_j - \frac{1}{3} \, \gamma_{ij} \right) \, \sigma^{(\mathrm{S})} + 2\hat{k}_{(i} \, \sum_a e^a_{j)} \, \sigma^{(\mathrm{V})}_a + \sum_\lambda \sigma^{(\mathrm{T})}_\lambda \, \epsilon^\lambda_{ij} \tag{2.64}$$

and σ^2 as

$$\sigma^2 = \frac{3}{2} \, \left(\sigma^{(\mathrm{S})} \right)^2 + 2 \sum_a \left(\sigma^{(\mathrm{V})}_a \right)^2 + \sum_\lambda \left(\sigma^{(\mathrm{T})}_\lambda \right)^2 \,. \tag{2.65}$$

For the time derivatives, we will use similar notations

$$\begin{aligned}
(\sigma')^{(\mathrm{S})} &\equiv (\sigma^i{}_j)' \, \hat{k}_i \, \hat{k}^j \,, \quad (\sigma')^{(\mathrm{V})}_a \equiv (\sigma^i{}_j)' \, \hat{k}_i \, e^j_a \,, \quad (\sigma')^{(\mathrm{T})}_\lambda \equiv (\sigma^i{}_j)' \, \epsilon_\lambda{}^j{}_i \,, \\
(\sigma'')^{(\mathrm{S})} &\equiv (\sigma^i{}_j)'' \, \hat{k}_i \, \hat{k}^j \,, \quad (\sigma'')^{(\mathrm{V})}_a \equiv (\sigma^i{}_j)'' \, \hat{k}_i \, e^j_a \,, \quad (\sigma'')^{(\mathrm{T})}_\lambda \equiv (\sigma^i{}_j)'' \, \epsilon_\lambda{}^j{}_i \,.
\end{aligned} \tag{2.66}$$

From Equation (2.21), we obtain the time derivatives of the shear components as

$$\begin{aligned}
(\sigma^{(\mathrm{S})})' &= -2\mathcal{H} \, \sigma^{(\mathrm{S})} - 2 \sum_a \left(\sigma^{(\mathrm{V})}_a\right)^2 \,, \\
(\sigma^{(\mathrm{V})}_a)' &= -2\mathcal{H} \, \sigma^{(\mathrm{V})}_a + \frac{3}{2} \, \sigma^{(\mathrm{S})} \, \sigma^{(\mathrm{V})}_a - \sum_{\lambda,b} \mathcal{M}^\lambda_{ab} \, \sigma^{(\mathrm{V})}_b \, \sigma^{(\mathrm{T})}_\lambda \,, \\
(\sigma^{(\mathrm{T})}_\lambda)' &= -2\mathcal{H} \, \sigma^{(\mathrm{T})}_\lambda + 2 \sum_{a,b} \mathcal{M}^\lambda_{ab} \, \sigma^{(\mathrm{V})}_a \, \sigma^{(\mathrm{V})}_b
\end{aligned} \tag{2.67}$$

and as

$$\begin{aligned}
(\sigma')^{(\mathrm{S})} &= -2\mathcal{H} \, \sigma^{(\mathrm{S})} \,, \\
(\sigma')^{(\mathrm{V})}_a &= -2\mathcal{H} \, \sigma^{(\mathrm{V})}_a \,, \\
(\sigma')^{(\mathrm{T})}_\lambda &= -2\mathcal{H} \, \sigma^{(\mathrm{T})}_\lambda \,, \\
(\sigma^2)' &= -4\mathcal{H} \, \sigma^2 \,, \\
(\sigma^i{}_j)'' &= (4\mathcal{H}^2 - 2\mathcal{H}') \, \sigma^i{}_j \,, \\
(\sigma'')^{(\mathrm{S})} &= (4\mathcal{H}^2 - 2\mathcal{H}') \, \sigma^{(\mathrm{S})} = (2\mathcal{H}^2 + \sigma^2) \, \sigma^{(\mathrm{S})} \,, \\
(\sigma'')^{(\mathrm{V})}_a &= (4\mathcal{H}^2 - 2\mathcal{H}') \, \sigma^{(\mathrm{V})}_a = (2\mathcal{H}^2 + \sigma^2) \, \sigma^{(\mathrm{V})}_a \,, \\
(\sigma'')^{(\mathrm{T})}_\lambda &= (4\mathcal{H}^2 - 2\mathcal{H}') \, \sigma^{(\mathrm{T})}_\lambda = (2\mathcal{H}^2 + \sigma^2) \, \sigma^{(\mathrm{T})}_\lambda \,.
\end{aligned} \tag{2.68}$$

2.2.5 Decomposition of the first-order Einstein tensor

In this subsection, we show polarization decomposition of the components of the first-order Einstein tensor. First, we define the vector and tensor gauge-invariant variables as

$$\begin{aligned}
\Phi_a &\equiv e^i_a \, \Phi_i \,, \quad \Phi_i = \sum_a e^a_i \, \Phi_a \,, \\
E_\lambda &\equiv \epsilon^{ij}_\lambda \, E_{ij} \,, \quad E_{ij} = \sum_\lambda \epsilon^\lambda_{ij} \, E_\lambda \,,
\end{aligned} \tag{2.69}$$

and we introduce useful notations

$$\begin{aligned} \epsilon^{\lambda}_{ij} &\equiv \sum_{a,b} \mathcal{M}^{\lambda}_{ab}\, e^{a}_{i}\, e^{b}_{j}\,, \quad Q_{i}{}^{j} \equiv e^{(1)}_{i}\, e^{j}_{(2)} - e^{(2)}_{i}\, e^{j}_{(1)}\,, \\ \zeta^{\lambda}{}_{\lambda'} &\equiv \delta^{\lambda}_{+}\, \delta^{\times}_{\lambda'} - \delta^{\lambda}_{\times}\, \delta^{+}_{\lambda'}\,, \quad \mathcal{N}_{ab} \equiv Q_{ij}\, e^{i}_{a}\, e^{j}_{b}\,, \end{aligned} \tag{2.70}$$

with

$$\mathcal{M}^{+}_{ab} = \frac{1}{\sqrt{2}} \begin{pmatrix} 1 & 0 \\ 0 & -1 \end{pmatrix}\,, \quad \mathcal{M}^{\times}_{ab} = \frac{1}{\sqrt{2}} \begin{pmatrix} 0 & 1 \\ 1 & 0 \end{pmatrix}\,. \tag{2.71}$$

By using these notations, time derivatives of the gauge-invariant variables are given as

$$\Phi'_{i} = \sum_{a} \left[\Phi'_{a}\, e^{a}_{i} - \frac{1}{2}\, \sigma^{(\mathrm{S})}\, \Phi_{a}\, e^{a}_{i} + 2\sigma^{(\mathrm{V})}_{a}\, \Phi_{a}\, \hat{k}_{i} + \sum_{\lambda,b} \sigma^{(\mathrm{T})}_{\lambda}\, \Phi_{a}\, \mathcal{M}^{\lambda}_{ab}\, e^{b}_{i} \right]\,, \tag{2.72}$$

$$E^{i'}_{\ j} = \sum_{\lambda} \left[E'_{\lambda}\, \epsilon^{\lambda i}{}_{j} + E_{\lambda}\, Q^{i}{}_{j}\, \zeta_{\lambda(1-\lambda)}\, \sigma^{(\mathrm{T})}_{(1-\lambda)} + 2E_{\lambda} \sum_{a,b} \sigma^{(\mathrm{V})}_{b}\, \mathcal{M}^{\lambda}_{ab}\, e^{i}_{a}\, \hat{k}_{j} \right]\,, \tag{2.73}$$

where

$$(1-\lambda) \equiv \begin{cases} \times\ (\lambda = +) \\ +\ (\lambda = \times) \end{cases}\,. \tag{2.74}$$

Moreover, their polarization components are given as

$$\begin{aligned} \hat{k}^{i}\, \Phi'_{i} &= 2 \sum_{a} \sigma^{(\mathrm{V})}_{a}\, \Phi_{a}\,, \\ e^{i}_{a}\, \Phi'_{i} &= \Phi'_{a} - \frac{1}{2}\, \sigma^{(\mathrm{S})}\, \Phi_{a} + \sum_{\lambda,b} \sigma^{(\mathrm{T})}_{\lambda}\, \mathcal{M}^{\lambda}_{ba}\, \Phi_{b}\,, \end{aligned} \tag{2.75}$$

and as

$$\begin{aligned}
\hat{k}_i \, E^{i\prime}{}_j &= 0 \,, \\
\hat{k}_i \, \hat{k}^j \, E^{i\prime}{}_j &= \hat{k}_i \, e^j_a \, E^{i\prime}{}_j = 0 \,, \\
e^a_i \, \hat{k}^j \, E^{i\prime}{}_j &= 2 \sum_{\lambda,b} \sigma^{(\mathrm{V})}_b \, \mathcal{M}^\lambda_{ab} \, E_\lambda \,, \\
e^a_i \, e^j_b \, E^{i\prime}{}_j &= \sum_\lambda \left[\mathcal{M}^\lambda_{ab} \, E'_\lambda + \sigma^{(\mathrm{T})}_{1-\lambda} \, \mathcal{N}_{ab} \, \zeta_{\lambda(1-\lambda)} \, E_\lambda \right] \,, \\
\epsilon_\lambda{}^j{}_i \, E^{i\prime}{}_j &= E'_\lambda \,, \\
\epsilon_\lambda{}^j{}_i \, E^{i\prime\prime}{}_j &= E''_\lambda + 2\zeta_{\lambda(1-\lambda)} \, \sigma^{(\mathrm{T})}_{(1-\lambda)} \sum_{\lambda'} \zeta_{\lambda'(1-\lambda')} \, \sigma^{(\mathrm{T})}_{(1-\lambda')} \, E_{\lambda'} \,.
\end{aligned} \tag{2.76}$$

So far, preparation for the decomposition of the Einstein tensor has completed and we now show its concrete form.

Decomposition of $\delta G^0{}_0$ In Fourier space, Equation (2.45) is expressed as

$$\begin{aligned}
a^2 \, \delta G^0{}_0 = {} & \sigma^j{}_i \, E^{i\prime}{}_j - \mathrm{i} \, \sigma^i{}_j \, k_i \, \Phi^j + 6\mathcal{H} \, \Psi' + 2k^2 \, \Psi - \frac{\sigma^i{}_j}{\mathcal{H}} \, k^j \, k_i \, \Psi - \sigma^j{}_i \left(\frac{\sigma^i{}_j}{\mathcal{H}} \Psi \right)' \\
& + 6\mathcal{H}^2 \, \Phi - \sigma^2 \, \Phi \,.
\end{aligned} \tag{2.77}$$

By substituting the prepared equations into above, $\delta G^0{}_0$ is expressed as

$$\begin{aligned}
a^2 \, \delta G^0{}_0 = {} & \sum_\lambda \left[E'_\lambda \, \sigma^{(\mathrm{T})}_\lambda - 2E_\lambda \sum_{a,b} \sigma^{(\mathrm{V})}_a \, \sigma^{(\mathrm{V})}_b \, \mathcal{M}^\lambda_{ab} \right] - \mathrm{i} \, k \sum_a \sigma^{(\mathrm{V})}_a \, \Phi_a \\
& + 6\mathcal{H} \, \Psi' - \sigma^2 \left(\frac{\Psi}{\mathcal{H}} \right)' + k^2 \left(2 - \frac{\sigma^{(\mathrm{S})}}{\mathcal{H}} \right) \Psi - \frac{1}{2} \frac{(\sigma^2)'}{\mathcal{H}} \Psi \\
& + 6\mathcal{H}^2 \, \Phi - \sigma^2 \, \Phi \,.
\end{aligned} \tag{2.78}$$

It is coordinate-transformation-invariant in three-dimensional space and already scalar-like in terms of rotations of the polarization basis around $\vec{k}$ in the two-dimensional plane.

Decomposition of $\delta G^0{}_i$ We can decompose $\delta G^0{}_i$ (2.46) as

$$\delta G^0{}_i = \hat{k}_i \, \delta G^0{}_\parallel + {}_\perp \delta G^0{}_i \,, \tag{2.79}$$

where the $\hat{k}$-direction component

$$a^2\,\delta G^0{}_{\parallel} = \mathrm{i}\,k\Bigg[\sum_\lambda \sigma^{(\mathrm{T})}_\lambda\,E_\lambda - 2\Psi' + \left(\frac{\Psi}{\mathcal{H}}\right)'\sigma^{(\mathrm{S})} + \frac{(\sigma^{(\mathrm{S})})'}{\mathcal{H}}\,\Psi - \frac{\sigma^2}{\mathcal{H}}\,\Psi + 3\sigma^{(\mathrm{S})}\,\Psi \\ - 2\mathcal{H}\,\Phi + \sigma^{(\mathrm{S})}\,\Phi\Bigg] \tag{2.80}$$

is scalar-like, and the projected components

$$a^2\,{}_\perp\delta G^0{}_i = -2\mathrm{i}\,k\,{}_\perp\sigma^\parallel{}_j\,E^j{}_i - \frac{1}{2}\,k^2\,\Phi_i \\ + \mathrm{i}\,k\,{}_\perp\sigma^\parallel{}_i\left(\frac{\Psi}{\mathcal{H}}\right)' + \mathrm{i}\,P^k{}_i\,k_j\,(\sigma^j{}_k)'\,\frac{\Psi}{\mathcal{H}} + 3\mathrm{i}\,k\,{}_\perp\sigma^\parallel{}_i\,\Psi + \mathrm{i}\,k\,{}_\perp\sigma^\parallel{}_i\,\Phi \tag{2.81}$$

are vector-like in the two-dimensional plane. Moreover, the projected components can be decomposed into polarization components as

$$a^2\,e^i_a\,{}_\perp\delta G^0{}_i = -2\mathrm{i}\,k\sum_{b,\lambda}\mathcal{M}_{ab}\,\sigma^{(\mathrm{V})}_b\,E_\lambda - \frac{1}{2}\,k^2\,\Phi_a \\ + \mathrm{i}\,k\,\sigma^{(\mathrm{V})}_a\left(\frac{\Psi}{\mathcal{H}}\right)' + \mathrm{i}\,k\,(\sigma')^{(\mathrm{V})}_a\,\frac{\Psi}{\mathcal{H}} + 3\mathrm{i}\,k\,\sigma^{(\mathrm{V})}_a\,\Psi + \mathrm{i}\,k\,\sigma^{(\mathrm{V})}_a\,\Phi\,. \tag{2.82}$$

Decomposition of $\boldsymbol{\delta G^i{}_j}$ We decompose $\delta G^i{}_j$ (2.47) into the trace part and the traceless part as

$$\delta G^i{}_j = \frac{1}{3}\,\delta G^k_k\,\delta^i{}_j + \delta\mathbb{G}^i{}_j\,, \quad \delta\mathbb{G}^k{}_k = 0\,. \tag{2.83}$$

The trace part is given as

$$a^2\,\delta G^k{}_k = E^{k\prime\prime}{}_k + 2\mathcal{H}\,E^{k\prime}{}_k - 3\sigma^n{}_m\,E^{m\prime}{}_n - \mathrm{i}\,k^k\,\Phi'_k + 5\mathrm{i}\,\sigma^n{}_m\,k_n\,\Phi^m \\ + 6\Psi'' + 12\mathcal{H}\,\Psi' + 3\sigma^n{}_m\left(\frac{\sigma^m{}_n}{\mathcal{H}}\,\Psi\right)' + 2k^2\,\Psi - \frac{\sigma^m{}_n}{\mathcal{H}}\,k^n\,k_m\,\Psi \\ + 6\mathcal{H}\,\Phi' - 2k^2\,\Phi + 6\,(2\mathcal{H}' + \mathcal{H}^2)\,\Phi + 3\sigma^2\,\Phi\,, \tag{2.84}$$

and is represented with the polarization components as

$$\begin{aligned}\frac{1}{3}\,a^2\,\delta G^k{}_k = &-\sum_\lambda\left[\left(\sigma^{(\mathrm{T})}_\lambda\,E_\lambda\right)' - (\sigma')^{(\mathrm{T})}_\lambda\,E_\lambda\right] + \mathrm{i}\,k\,\sum_a \sigma^{(\mathrm{V})}_a\,\Phi_a \\ &+ 2\Psi'' + 4\mathcal{H}\,\Psi' + \frac{1}{2}\,(\sigma^2)'\,\frac{\Psi}{\mathcal{H}} + \sigma^2\,\left(\frac{\Psi}{\mathcal{H}}\right)' + \frac{2}{3}\,k^2\,\Psi - \frac{1}{3}\,\frac{\sigma^{(\mathrm{S})}}{\mathcal{H}}\,k^2\,\Psi \\ &+ 2\mathcal{H}\,\Phi' - \frac{2}{3}\,k^2\,\Phi + 2\left(2\mathcal{H}' + \mathcal{H}^2\right)\,\Phi + \sigma^2\,\Phi\,.\end{aligned} \tag{2.85}$$

The traceless part is given as

$$\begin{aligned}a^2\,\delta\mathbb{G}^i{}_j = &\,E^{i\prime\prime}{}_j + 2\mathcal{H}\,E^{i\prime}{}_j + k^2\,E^i{}_j + 2\sigma^i{}_k\,E^{k\prime}{}_j - 2\sigma^k{}_j\,E^{i\prime}{}_k \\ &+ 2\left(\sigma^{i\prime}{}_k + 2\mathcal{H}\,\sigma^i{}_k\right)\,E^k{}_j - 2\left(\sigma^{k\prime}{}_j + 2\mathcal{H}\,\sigma^k{}_j\right)\,E^i{}_k \\ &- \frac{1}{2}\,\mathrm{i}\,k^i\,\Phi'_j - \frac{1}{2}\,\mathrm{i}\,\gamma^{ik}\,k_j\,\Phi'_k + \mathrm{i}\,\sigma^i{}_k\,k^k\,\Phi_j + \mathrm{i}\,\sigma^k{}_j\,k_k\,\Phi^i - \mathrm{i}\,\mathcal{H}\,k^i\,\Phi_j - \mathrm{i}\,\mathcal{H}\,k_j\,\Phi^i \\ &- 3\sigma^i{}_j\,\Psi' - \sigma^{i\prime\prime}{}_j\,\frac{\Psi}{\mathcal{H}} - 2\sigma^{i\prime}{}_j\,\left(\frac{\Psi}{\mathcal{H}}\right)' - \sigma^i{}_j\,\left(\frac{\Psi}{\mathcal{H}}\right)'' - 2\sigma^{i\prime}{}_j\,\Psi - 2\mathcal{H}\,\sigma^i{}_j\,\left(\frac{\Psi}{\mathcal{H}}\right)' \\ &- \left(k^i\,k_j - \frac{1}{3}\,\delta^i{}_j\,k^2\right)\,\Psi - \frac{\sigma^i{}_j}{\mathcal{H}}\,k^2\,\Psi + \frac{\sigma^k{}_j}{\mathcal{H}}\,k^i\,k_k\,\Psi + \frac{\sigma^i{}_k}{\mathcal{H}}\,k^k\,k_j\,\Psi \\ &- \frac{2}{3}\,\delta^i{}_j\,\frac{\sigma^{(\mathrm{S})}}{\mathcal{H}}\,k^2\,\Psi + \left(k^i\,k_j - \frac{1}{3}\,\delta^i{}_j\,k^2\right)\,\Phi - \sigma^i{}_j\,\Phi' - 2\left(\sigma^{i\prime}{}_j + 2\mathcal{H}\,\sigma^i{}_j\right)\,\Phi\end{aligned} \tag{2.86}$$

Moreover, the traceless part $\delta\mathbb{G}^i{}_j$ is decomposed as

$$\delta\mathbb{G}^i{}_j = \hat{k}^i\,\hat{k}_j\,\mathbb{G}^{\parallel}{}_{\parallel} + \hat{k}^i\,\delta\mathbb{G}^{\parallel}{}_j + \hat{k}_j\,\delta\mathbb{G}^i{}_{\parallel} + {}_{\perp}\delta\mathbb{G}^i{}_j\,, \tag{2.87}$$

where the independent components are

$$
\begin{aligned}
a^2\,\delta\mathbb{G}^{\parallel}{}_{\parallel} &= 4\sum_{\lambda,a,b}\sigma_a^{(\mathrm{V})}\,\sigma_b^{(\mathrm{V})}\,\mathcal{M}^{\lambda}_{ab}\,E_\lambda - 2\mathrm{i}\,k\sum_a \sigma_a^{(\mathrm{V})}\,\Phi_a \\
&\quad - 3\sigma^{(\mathrm{S})}\,\Psi' - (\sigma'')^{(\mathrm{S})}\,\frac{\Psi}{\mathcal{H}} - 2(\sigma')^{(\mathrm{S})}\,\left(\frac{\Psi}{\mathcal{H}}\right)' - \sigma^{(\mathrm{S})}\,\left(\frac{\Psi}{\mathcal{H}}\right)'' \\
&\quad - 2(\sigma')^{(\mathrm{S})}\,\Psi - 2\mathcal{H}\,\sigma^{(\mathrm{S})}\,\left(\frac{\Psi}{\mathcal{H}}\right)' - \frac{2}{3}\,k^2\,\Psi + \frac{1}{3}\,\frac{\sigma^{(\mathrm{S})}}{\mathcal{H}}\,k^2\,\Psi \\
&\quad + \frac{2}{3}\,k^2\,\Phi - \sigma^{(\mathrm{S})}\,\Phi' - 2a^2\,\mathbb{G}^{\parallel}{}_{\parallel}\,\Phi\,, \qquad (2.88)\\
a^2\,{}_{\perp}\delta\mathbb{G}^{\parallel}{}_i &= 2\,{}_{\perp}\sigma^{\parallel}{}_j\,{}_{\perp}(E^{j\prime}{}_i) + 2a^2\,{}_{\perp}\mathbb{G}^{\parallel}{}_j\,E^j{}_i - \frac{1}{2}\,\mathrm{i}\,k\,{}_{\perp}\Phi'_i - \mathrm{i}\,k\,\mathcal{H}\,\Phi_i + \mathrm{i}\,k\,\sigma^{(\mathrm{S})}\,\Phi_i \\
&\quad - 3\,{}_{\perp}\sigma^{\parallel}{}_i\,\Psi' - {}_{\perp}(\hat{k}_j\,\sigma^{j\prime\prime}{}_i)\,\frac{\Psi}{\mathcal{H}} - 2\,{}_{\perp}(\hat{k}_j\,\sigma^{j\prime}{}_i)\,\left(\frac{\Psi}{\mathcal{H}}\right)' - {}_{\perp}\sigma^{\parallel}{}_i\,\left(\frac{\Psi}{\mathcal{H}}\right)'' \\
&\quad - 2{}_{\perp}(\hat{k}_j\,\sigma^{j\prime}{}_i)\,\Psi - 2\mathcal{H}\,{}_{\perp}\sigma^{\parallel}{}_i\,\left(\frac{\Psi}{\mathcal{H}}\right)' - {}_{\perp}\sigma^{\parallel}{}_i\,\Phi' - 2a^2\,{}_{\perp}\mathbb{G}^{\parallel}{}_i\,\Phi \qquad (2.89)
\end{aligned}
$$

and

$$
\begin{aligned}
a^2\,{}_{\perp}\delta\mathbb{G}^{i}{}_j &= {}_{\perp}(E^{i\prime\prime}{}_j) + 2\mathcal{H}\,{}_{\perp}(E^{i\prime}{}_j) + k^2\,E^i{}_j + 2\,{}_{\perp}\left(\sigma^i{}_k\,E^{k\prime}{}_j\right) - 2\,{}_{\perp}\left(\sigma^k{}_j\,E^{i\prime}{}_k\right) \\
&\quad + 2a^2\,{}_{\perp}\mathbb{G}^i{}_k\,{}_{\perp}E^k{}_j - 2a^2\,{}_{\perp}\left(\mathbb{G}^k{}_j\,E^i{}_k\right) \\
&\quad + \mathrm{i}\,{}_{\perp}\sigma^i{}_{\parallel}\,k\,\Phi_j + \mathrm{i}\,{}_{\perp}\sigma^{\parallel}{}_j\,k\,\Phi^i \\
&\quad - 3\,{}_{\perp}\sigma^i{}_j\,\Psi' - {}_{\perp}\left(\frac{\sigma^i{}_j}{\mathcal{H}}\,\Psi\right)' - 2\mathcal{H}\,{}_{\perp}\left(\frac{\sigma^i{}_j}{\mathcal{H}}\,\Psi\right)' \\
&\quad + \frac{1}{3}\,P^i{}_j\,k^2\,\Psi - \frac{{}_{\perp}\sigma^i{}_j}{\mathcal{H}}\,k^2\,\Psi - \frac{2}{3}\,P^i{}_j\,\sigma^{(\mathrm{S})}\,k^2\,\frac{\Psi}{\mathcal{H}} \\
&\quad - \frac{1}{3}\,P^i{}_j\,k^2\,\Phi - {}_{\perp}\sigma^i{}_j\,\Phi' - 2a^2\,{}_{\perp}\mathbb{G}^i{}_j\,\Phi\,. \qquad (2.90)
\end{aligned}
$$

The polarization-projected components of ${}_{\perp}\delta\mathbb{G}^{\parallel}{}_i$ and ${}_{\perp}\delta\mathbb{G}^{i}{}_j$ are given as

$$
\begin{aligned}
a^2\,e^i_a\,{}_{\perp}\delta\mathbb{G}^{\parallel}{}_i &= 2\sum_{\lambda,b}\sigma_b^{(\mathrm{V})}\,\mathcal{M}^{\lambda}_{ab}\,E'_\lambda - 2\sum_{\lambda,b}\sigma_b^{(\mathrm{V})}\,\mathcal{N}_{ab}\,\zeta_{\lambda(1-\lambda)}\,\sigma^{(\mathrm{T})}_{(1-\lambda)}\,E_\lambda + 2a^2\,{}_{\perp}\mathbb{G}^{\parallel}{}_j\,E^j{}_i\,e^i_a \\
&\quad - \frac{1}{2}\,\mathrm{i}\,k\,\Phi'_a - \frac{1}{2}\,\mathrm{i}\,k\sum_{\lambda,b}\sigma_\lambda^{(\mathrm{T})}\,\mathcal{M}^{\lambda}_{ab}\,\Phi_b + \frac{5}{4}\,\mathrm{i}\,k\,\sigma^{(\mathrm{S})}\,\Phi_a - \mathrm{i}\,k\,\mathcal{H}\,\Phi_a \\
&\quad - 3\sigma_a^{(\mathrm{V})}\,\Psi' - (\sigma'')^{(\mathrm{V})}_a\,\frac{\Psi}{\mathcal{H}} - 2(\sigma')^{(\mathrm{V})}_a\,\left(\frac{\Psi}{\mathcal{H}}\right)' - \sigma_a^{(\mathrm{V})}\,\left(\frac{\Psi}{\mathcal{H}}\right)'' \\
&\quad - 2(\sigma')^{(\mathrm{V})}_a\,\Psi - 2\mathcal{H}\,\sigma_a^{(\mathrm{V})}\,\left(\frac{\Psi}{\mathcal{H}}\right)' - \sigma_a^{(\mathrm{V})}\,\Phi' - 2a^2\,{}_{\perp}\mathbb{G}^{\parallel}{}_i\,e^i_a\,\Phi \qquad (2.91)
\end{aligned}
$$

and

$$
\begin{aligned}
a^2\,\epsilon_\lambda{}^j{}_i\,\delta\mathbb{G}^i{}_j = {} & E_\lambda'' + 2\mathcal{H}\,E_\lambda' + k^2\,E_\lambda - 2\zeta_{\lambda(1-\lambda)}\,\sigma^{(\mathrm{T})}_{(1-\lambda)}\sum_{\lambda'}\zeta_{\lambda'(1-\lambda')}\,\sigma^{(\mathrm{T})}_{(1-\lambda')}\,E_{\lambda'} \\
& - 2\sum_a\left(\sigma^{(\mathrm{V})}_a\right)^2\,E_\lambda + 2\mathrm{i}\,k\sum_{a,b}\mathcal{M}^\lambda_{ab}\,\sigma^{(\mathrm{V})}_a\,\Phi_b \\
& - 3\sigma^{(\mathrm{T})}_\lambda\,\Psi' - (\sigma'')^{(\mathrm{T})}_\lambda\,\frac{\Psi}{\mathcal{H}} - 2(\sigma')^{(\mathrm{T})}_\lambda\left(\frac{\Psi}{\mathcal{H}}\right)' - \sigma^{(\mathrm{T})}_\lambda\left(\frac{\Psi}{\mathcal{H}}\right)'' \\
& - 2(\sigma')^{(\mathrm{T})}_\lambda\,\Psi - 2\mathcal{H}\,\sigma^{(\mathrm{T})}_\lambda\left(\frac{\Psi}{\mathcal{H}}\right)' - \frac{\sigma^{(\mathrm{T})}_\lambda}{\mathcal{H}}\,k^2\,\Psi \\
& - \sigma^{(\mathrm{T})}_\lambda\,\Phi' - 2a^2\,{}_\perp\mathbb{G}^i{}_j\,\epsilon_\lambda{}^j{}_i\,\Phi\,,
\end{aligned}
\tag{2.92}
$$

respectively.

So far, we have completed rewriting each component of the perturbed Einstein tensor by using the gauge-invariant variables and their polarization components.

2.3 PGWs equations in KdS

Now let us focus on the case of Kasner–de Sitter background. Since there is no matter source, the first-order Einstein equation is

$$
\delta G^\mu{}_\nu = 0\,. \tag{2.93}
$$

As we will confirm, the number of dynamical degrees freedom in this case is two.

Now, we perform simplification of the Einstein tensor. The gauge-invariant variables $\Phi\,,\Psi\,,\Phi_a$ can be all represented by E_λ. To do so, we start to define a useful scalar variable X as

$$
X \equiv \Phi + \Psi + \left(\frac{\Psi}{\mathcal{H}}\right)'\,. \tag{2.94}
$$

From this definition and Equation (2.22), we obtain the following expressions

$$\begin{aligned}\Psi' &= \mathcal{H}(X-\Phi) - \frac{\sigma^2}{2\mathcal{H}}\Psi\,,\\ \Psi'' &= \mathcal{H}\left(X'-\Phi'\right) + \left(\mathcal{H}^2-\sigma^2\right)(X-\Phi) + \frac{5\sigma^2}{2}\,\Psi\,.\end{aligned} \tag{2.95}$$

By using these expressions, we can remove Φ from each component of the linear Einstein equation $\delta G^{\mu}{}_{\nu} = 0$ as follows. In the scalar parts, from Equations (2.78), (2.80), (2.85) and (2.88),

$$\begin{aligned}0 &= \sum_{\lambda}\left[\left(\sigma^{(\mathrm{T})}_{\lambda}\,E_{\lambda}\right)' + 2\mathcal{H}\,\sigma^{(\mathrm{T})}_{\lambda}\,E_{\lambda}\right] - \mathrm{i}\,k\sum_{a}\sigma^{(\mathrm{V})}_{a}\,\Phi_a\\ &\quad + \left(6\mathcal{H}^2-\sigma^2\right)\,X + \frac{2\mathcal{H}-\sigma^{(\mathrm{S})}}{\mathcal{H}}\,k^2\,\Psi\,, \qquad (2.96)\\ 0 &= \sum_{\lambda}\sigma^{(\mathrm{T})}_{\lambda}\,E_{\lambda} - 2\mathcal{H}\,X + \sigma^{(\mathrm{S})}\,X\,, \qquad (2.97)\\ 0 &= -\sum_{\lambda}\left[\left(\sigma^{(\mathrm{T})}_{\lambda}\,E_{\lambda}\right)' + 2\mathcal{H}\,\sigma^{(\mathrm{T})}_{\lambda}\,E_{\lambda}\right] + \mathrm{i}\,k\sum_{a}\sigma^{(\mathrm{V})}_{a}\,\Phi_a\\ &\quad + 2\mathcal{H}\,X' + \left(6\mathcal{H}^2-\sigma^2\right)\,X + \frac{1}{3}\,\frac{2\mathcal{H}-\sigma^{(\mathrm{S})}}{\mathcal{H}}\,k^2\,\Psi - \frac{2}{3}\,k^2\,\Phi\,, \qquad (2.98)\\ 0 &= 4\sum_{\lambda,a,b}\sigma^{(\mathrm{V})}_{a}\,\sigma^{(\mathrm{V})}_{b}\,\mathcal{M}^{\lambda}_{ab}\,E_{\lambda} - 2\mathrm{i}\,k\sum_{a}\sigma^{(\mathrm{V})}_{a}\,\Phi_a\\ &\quad - \sigma^{(\mathrm{S})}\,X' - \frac{1}{3}\,\frac{2\mathcal{H}-\sigma^{(\mathrm{S})}}{\mathcal{H}}\,k^2\,\Psi + \frac{2}{3}\,k^2\,\Phi\,. \qquad (2.99)\end{aligned}$$

In the vector parts, from (2.82) and (2.91),

$$0 = -2\sum_{\lambda,b}\sigma^{(\mathrm{V})}_{b}\mathcal{M}^{\lambda}_{ab}\,E_{\lambda} + \frac{\mathrm{i}}{2}\,k\,\Phi_a + \sigma^{(\mathrm{V})}_{a}\,X\,, \tag{2.100}$$

$$\begin{aligned}0 &= 2\sum_{\lambda,b}\sigma^{(\mathrm{V})}_{b}\,\mathcal{M}^{\lambda}_{ab}\,E'_{\lambda} - 2\sum_{\lambda,b}\sigma^{(\mathrm{V})}_{b}\,\mathcal{N}_{ab}\,\zeta_{\lambda(1-\lambda)}\,\sigma^{(\mathrm{T})}_{(1-\lambda)}\,E_{\lambda} - \frac{1}{2}\,\mathrm{i}\,k\,\Phi'_a\\ &\quad - \frac{1}{2}\,\mathrm{i}\,k\sum_{\lambda,b}\sigma^{(\mathrm{T})}_{\lambda}\,\mathcal{M}^{\lambda}_{ab}\,\Phi_b - \mathrm{i}\,k\,\mathcal{H}\,\Phi_a + \frac{5}{4}\,\mathrm{i}\,k\,\sigma^{(\mathrm{S})}\,\Phi_a - \sigma^{(\mathrm{V})}_{a}\,X'\,. \qquad (2.101)\end{aligned}$$

In the tensor part, from (2.92),

$$0 = E_\lambda'' + 2\mathcal{H}\,E_\lambda' + k^2\,E_\lambda - 2\,\zeta_{\lambda(1-\lambda)}\,\sigma^{(\mathrm{T})}_{(1-\lambda)}\sum_{\lambda'}\zeta_{\lambda'(1-\lambda')}\,\sigma^{(\mathrm{T})}_{(1-\lambda')}\,E_{\lambda'} - 2\sum_a\left(\sigma^{(\mathrm{V})}_a\right)^2 E_\lambda$$
$$+ 2\mathrm{i}\,k\sum_{a,b}\mathcal{M}^\lambda_{ab}\,\sigma^{(\mathrm{V})}_a\,\Phi_b - \sigma^{(\mathrm{T})}_\lambda\,X' - \frac{\sigma^{(\mathrm{T})}_\lambda}{\mathcal{H}}\,k^2\,\Psi\,. \tag{2.102}$$

Here, we rewrite Equation (2.97) as

$$X = \frac{1}{2\mathcal{H} - \sigma^{(\mathrm{S})}}\sum_\lambda \sigma^{(\mathrm{T})}_\lambda E_\lambda\,. \tag{2.103}$$

Then we can replace X with E_λ. Moreover, with Equation (2.100), we can represent Φ_a in terms of E_λ as

$$\mathrm{i}\,k\,\Phi_a = 4\sum_{\lambda,b}\mathcal{M}^\lambda_{ab}\,\sigma^{(\mathrm{V})}_b\,E_\lambda - \frac{2\sigma^{(\mathrm{V})}_a}{2\mathcal{H} - \sigma^{(\mathrm{S})}}\sum_\lambda \sigma^{(\mathrm{T})}_\lambda\,E_\lambda\,, \tag{2.104}$$

and we can remove X and Φ_a from Equation (2.96) as

$$k^2\,\Psi = -\frac{\mathcal{H}}{2\mathcal{H} - \sigma^{(\mathrm{S})}}\sum_\lambda\left[\sigma^{(\mathrm{T})}_\lambda\,E_\lambda' + \frac{6\mathcal{H}^2 - \sigma^2 - a^{-2}\left(a^2\,\sigma^{(\mathrm{S})}\right)'}{2\mathcal{H} - \sigma^{(\mathrm{S})}}\,\sigma^{(\mathrm{T})}_\lambda\,E_\lambda - a^{-2}\left(a^2\,\sigma^{(\mathrm{T})}_\lambda\right)'E_\lambda\right]. \tag{2.105}$$

Also, we can represent Φ in terms of E_λ using Equation (2.99). As the last step, by summing up Equations (2.98) and (2.99), we obtain the following relation

$$0 = \left(2\mathcal{H} - \sigma^{(\mathrm{S})}\right)X' + \left(6\mathcal{H}^2 - \sigma^2\right)X + \sum_\lambda\left[-a^{-2}\left(a^2\,\sigma^{(\mathrm{T})}_\lambda\right)'E_\lambda - \sigma^{(\mathrm{T})}_\lambda\,E_\lambda'\right]$$
$$- \frac{a^{-2}\left(a^2\,\sigma^{(\mathrm{S})}\right)'}{2\mathcal{H} - \sigma^{(\mathrm{S})}}\sum_\lambda\sigma^{(\mathrm{T})}_\lambda\,E_\lambda\,. \tag{2.106}$$

Then, we obtain an expression for the time derivative of X as

$$X' = \sum_\lambda\frac{\sigma^{(\mathrm{T})}_\lambda}{2\mathcal{H} - \sigma^{(\mathrm{S})}}\,E_\lambda' + \sum_\lambda\left(\frac{\sigma^{(\mathrm{T})}_\lambda}{2\mathcal{H} - \sigma^{(\mathrm{S})}}\right)'E_\lambda$$
$$= \frac{1}{2\mathcal{H} - \sigma^{(\mathrm{S})}}\sum_\lambda\left(\sigma^{(\mathrm{T})}_\lambda\,E_\lambda\right)' - \frac{2\mathcal{H}^2 - \sigma^2 - \sigma^{(\mathrm{S})\prime}}{\left(2\mathcal{H} - \sigma^{(\mathrm{S})}\right)^2}\sum_\lambda\sigma^{(\mathrm{T})}_\lambda\,E_\lambda\,. \tag{2.107}$$

Finally, substituting all the relations obtained so far into Equation (2.102), we obtain the gravitational-wave equations as

$$\begin{aligned} 0 = {} & E_\lambda'' + 2\mathcal{H}\, E_\lambda' + k^2\, E_\lambda - 2\zeta_{\lambda(1-\lambda)}\, \sigma^{(\mathrm{T})}_{(1-\lambda)} \sum_{\lambda'} \zeta_{\lambda'(1-\lambda')}\, \sigma^{(\mathrm{T})}_{(1-\lambda')}\, E_{\lambda'} \\ & + \sigma^{(\mathrm{T})}_\lambda\, \frac{12\mathcal{H}^2 - 2\sigma^2 - 2a^{-2}\, \left(a^2\, \sigma^{(\mathrm{S})}\right)'}{\left(2\mathcal{H} - \sigma^{(\mathrm{S})}\right)^2} \sum_{\lambda'} \sigma^{(\mathrm{T})}_{\lambda'}\, E_{\lambda'} \\ & - \frac{2a^{-2}}{2\mathcal{H} - \sigma^{(\mathrm{S})}} \sum_{\lambda'} \left[\left(a^2\, \sigma^{(\mathrm{T})}_\lambda\right)'\, \sigma^{(\mathrm{T})}_{\lambda'} + \left(a^2\, \sigma^{(\mathrm{T})}_{\lambda'}\right)'\, \sigma^{(\mathrm{T})}_\lambda \right] E_{\lambda'} \\ & - a^{-2}\, \left(a^2\, \sigma^{(\mathrm{S})}\right)'\, E_\lambda\,. \end{aligned} \tag{2.108}$$

Here, as announced, the gravitational-wave equations are described in terms of E_λ only.

Introducing $\mu_\lambda \equiv a\, E_\lambda$, the equations of motion for gravitational waves (2.108) are rewritten as (see also [PPU07])

$$\mu_+'' + \omega_+^2\, \mu_+ + \xi\, \mu_\times = 0\,, \quad \mu_\times'' + \omega_\times^2\, \mu_\times + \xi\, \mu_+ = 0\,, \tag{2.109}$$

where

$$\begin{aligned} \omega_+^2 &\equiv \gamma^{ij}\, k_i\, k_j - \frac{a''}{a} - \frac{\left(a^2\, \sigma^{(\mathrm{S})}\right)'}{a^2} - 2\, \left(\sigma^{(\mathrm{T})}_\times\right)^2 - \frac{2}{a^2} \left(\frac{a^2\, \left(\sigma^{(\mathrm{T})}_+\right)^2}{2\mathcal{H} - \sigma^{(\mathrm{S})}} \right)'\,, \\ \omega_\times^2 &\equiv \gamma^{ij}\, k_i\, k_j - \frac{a''}{a} - \frac{\left(a^2\, \sigma^{(\mathrm{S})}\right)'}{a^2} - 2\, \left(\sigma^{(\mathrm{T})}_+\right)^2 - \frac{2}{a^2} \left(\frac{a^2\, \left(\sigma^{(\mathrm{T})}_\times\right)^2}{2\mathcal{H} - \sigma^{(\mathrm{S})}} \right)' \end{aligned} \tag{2.110}$$

and

$$\xi \equiv 2\sigma^{(\mathrm{T})}_+\, \sigma^{(\mathrm{T})}_\times - \frac{2}{a^2} \left(\frac{a^2\, \sigma^{(\mathrm{T})}_+\, \sigma^{(\mathrm{T})}_\times}{2\mathcal{H} - \sigma^{(\mathrm{S})}} \right)'\,. \tag{2.111}$$

Correspondingly, the second-order action for μ_λ was also obtained by Pereira *et al.* [PPU07]. Discarding scalar fields in Equation (5.20) in [PPU07], one obtains the action integral for tensor perturbations

$$S_2 = \sum_{\lambda=+,\times} \frac{1}{2} \int \mathrm{d}^3 k_i\, \mathrm{d}\eta\, \left[\mu_\lambda'\, \mu_\lambda'^{\,*} - \omega_\lambda^2\, \mu_\lambda\, \mu_\lambda^{\,*} - \xi\, \mu_\lambda^*\, \mu_{1-\lambda} \right]\,, \tag{2.112}$$

where the index "$1-\lambda$" is $\times$ for $\lambda = +$ and $+$ for $\lambda = \times$.

Chapter 3

Quantization of PGWs in anisotropic pre-inflation

In order to make a quantitative prediction for PGWs from anisotropic pre-inflation, we discuss their initial conditions. The most standard way to determine the initial values of PGWs in ordinary scenarios like de Sitter inflation is to perform canonical quantization of tensor perturbations on an isotropic cosmological background. In the anisotropic setup, one might think that a standard procedure of quantization could still work since the action for the tensor perturbations (2.112) has an analogous shape to (coupled) double scalar fields. This is not the case, though, for ω_λ^2 given by (2.110) generically blows up as approaching to the initial singularity due to the growing background anisotropy. In this chapter, we begin with clarifying the problems in quantization in anisotropic pre-inflation and discuss a prescription which may enable us to evade the problem [FNS19].

3.1 Problems in quantization

To see the diverging behavior of ω_λ^2 , it is instructive to consider how the contravariant wavevector $\vec{k}$ rotates under the influence of anisotropic expansion based on (2.51). As going back in time towards the initial singularity at $t = 0$, any wavevector $\vec{k}$ with non-vanishing k^1 component tends to be aligned to the k^1-axis, as one can see the limits of

the Euler angles defined in (2.51) :

$$\begin{aligned}\lim_{t\to 0}\beta &= \lim_{t\to 0}\cos^{-1}\left(\frac{k_3\,\mathrm{e}^{-\beta_3}}{\sqrt{\sum_{i=1}^{3}k_i^2\,\mathrm{e}^{-2\beta_i}}}\right)=\frac{\pi}{2}\,,\\ \lim_{t\to 0}\gamma &= \lim_{t\to 0}\tan^{-1}\left(\frac{k_2\,\mathrm{e}^{-\beta_2}}{k_1\,\mathrm{e}^{-\beta_1}}\right)=0\,.\end{aligned} \tag{3.1}$$

In such an asymptotic regime, the frequency squared ω_λ^2 can be estimated approximating $k^2/k^1 \sim k^3/k^1 \sim 0$ as

$$\omega_\lambda^2 \sim k_1^2\left(\frac{3H_\Lambda t}{2}\right)^{-2q_1} + a_{\mathrm{iso}}^2\,H_\Lambda^2\,\frac{1-9\,\delta_\lambda^{\times}\,(q_2-q_3)^2}{(3H_\Lambda t)^{4/3}}\,. \tag{3.2}$$

This expression illuminates the generic divergent behavior of ω_λ^2 as $t\to 0$.

The usual procedure of second quantization in cosmological background relies upon the existence of suitable modes which oscillate harmonically in the asymptotic past region. In an anisotropic setup, the above observation implies that the variable μ_λ is not the best quantity to quantize, but we should seek for a more suitable variable which can behave like a simple harmonic oscillator.

Now, let us rewrite the equations of motion for μ_λ (2.109) in terms of the new variable and time coordinate [PPU08]

$$\chi_\lambda = f(\eta)\,\mu_\lambda\,,\quad \mathrm{d}\tau = f(\eta)^2\,\mathrm{d}\eta\,. \tag{3.3}$$

Defining

$$\Omega_\lambda^2 \equiv \frac{\omega_\lambda^2}{f^4}+\frac{(f^{-1})''}{f^3}\,,\quad \Xi\equiv\frac{\xi}{f^4}\,, \tag{3.4}$$

the equations of motion for χ_λ read

$$\begin{aligned}\ddot{\chi}_+ + \Omega_+^2\,\chi_+ + \Xi\,\chi_\times &= 0\,,\\ \ddot{\chi}_\times + \Omega_\times^2\,\chi_\times + \Xi\,\chi_+ &= 0\,,\end{aligned} \tag{3.5}$$

where the dots denote derivatives with respect to τ . Here, apart from the subtlety of the interaction term, there arises a possibility of making Ω_λ^2 constant by choosing some function f so that χ_λ behaves as a harmonic oscillator.

Let us consider a generic power-law function $f(\eta) = (a_{\rm iso} H_\Lambda \eta)^p$ as in [PPU08]. Then the new frequency squared Ω_λ^2 is evaluated near the singularity, unless $k_1 = 0$, as

$$\Omega_\lambda^2 \sim \frac{k_1^2}{2^{q_1}\,(a_{\rm iso} H_\Lambda \eta)^{4p+3q_1}} + a_{\rm iso}^2\, H_\Lambda^2\, \frac{(2p+1)^2 - 9\,\delta_\lambda^\times\,(q_2-q_3)^2}{4\,(a_{\rm iso} H_\Lambda \eta)^{4p+2}}\,. \tag{3.6}$$

The oblate axisymmetric KdS, $(q_1, q_2, q_3) = (2/3, -1/3, -1/3)$, is the exceptional case where the powers of the terms in Ω_λ^2 becomes identical. Moreover, by choosing $p = -1/2$, it becomes *positive* constant $\Omega_\lambda^2 \sim k_1^2$ unless $k_1 = 0$. Namely, in this case, quantization can be carried out except for the "planar modes" with $k_1 = 0$. For this reason, several authors have studied primordial perturbations of quantum origin in this particular symmetric background [GCP07; KM10; DP12; DKP12; DKP14; BPM15].

In any other cases of background, all the indices q_i $(i = 1, 2, 3)$ are smaller than $2/3$, so the second term in (3.6) always dominates. Then, setting $p = -1/2$ eliminates the time dependence in the leading term, but this leads to a *negative* frequency squared for the cross mode $(\lambda = \times)$

$$\Omega_\times^2 \sim -\frac{9\,(q_2-q_3)^2}{4}\,(a_{\rm iso}\,H_\Lambda)^2\,, \tag{3.7}$$

which forbids the usual quantization procedure.[1]

Now, one realizes that the problem just arises from the ordinary prescription of quantization that is founded on asymptotic behaviors of the mode functions, which is ill-behaved in the current setup due to the existence of the initial singularity. However, the initial singularity is often a source of difficulties and its existence is disfavored on the physical background. It is rather natural to suppose that the history of the universe began with some finite curvature at some moment $t = t_{\rm ini} > 0$, and quantization of the field contents are done at or after $t_{\rm ini}$.

If we introduce a finite initial time $t_{\rm ini}$, then there arises a chance that the wave-number terms dominate in ω_λ^2 at or after $t_{\rm ini}$, and the frequency squared after transformation may be evaluated as

$$\Omega_\lambda^2 \sim \sum_{i=1}^{3} \frac{k_i^2}{2^{q_i}\,(a_{\rm iso} H_\Lambda \eta)^{4p+3q_i}}\,. \tag{3.8}$$

[1] This analysis supplements the considerations in [PPU08], in which they focused upon adiabaticity conditions.

Once the dominant term among the three components above, to be indicated by the index $i_{\max}$, is identified, setting $p = -3\,q_{i_{\max}}/4$ results in a positive, constant frequency squared $\Omega_\lambda^2 \sim k_{i_{\max}}^2$. Note that this is analogous to the case of "oblate" axisymmetric backgrounds, where quantization can be carried out except for the "planar" modes [GCP07; KM10; DP12; DKP12; DKP14; BPM15].

In what follows, we proceed this idea and give a viable prescription of quantization in triaxially anisotropic universe.

3.2 Behaviors of transformed variables

For the sake of brevity, we collectively call the following three functions of time (and not of wavenumber) as ${}^{(i)}f$ $(i = 1, 2, 3)$:

$$\begin{aligned} {}^{(1)}f &= \left(\gamma^{11}\right)^{1/4} = \tanh^{-q_1/2}\left(\frac{3H_\Lambda t}{2}\right), \\ {}^{(2)}f &= \left(\gamma^{22}\right)^{1/4} = \tanh^{-q_2/2}\left(\frac{3H_\Lambda t}{2}\right), \\ {}^{(3)}f &= \left(\gamma^{33}\right)^{1/4} = \tanh^{-q_3/2}\left(\frac{3H_\Lambda t}{2}\right). \end{aligned} \tag{3.9}$$

With them, the wave-number terms in ω_λ^2 can be written as

$$\gamma^{ij}\,k_i\,k_j = {}^{(1)}f^4\,k_1^2 + {}^{(2)}f^4\,k_2^2 + {}^{(3)}f^4\,k_3^2\,. \tag{3.10}$$

Since the factors ${}^{(i)}f^4$ depend on time to the distinctive powers in a triaxially anisotropic background ($q_1 > q_2 > q_3$), only one of the above three terms should dominate at any moment. Keeping this in mind, let us consider a transformation using ${}^{(i)}f$ as the transformation function f:

$${}^{(i)}\chi_\lambda = {}^{(i)}f\,\mu_\lambda\,, \quad \mathrm{d}{}^{(i)}\tau = {}^{(i)}f^2\,\mathrm{d}\eta\,. \tag{3.11}$$

Then the frequency squared for the new variable ${}^{(i)}\chi_\lambda$ is written as

$$\begin{aligned} {}^{(i)}\Omega_\lambda^2 &= \frac{\omega_\lambda^2}{{}^{(i)}f^4} + \frac{\left({}^{(i)}f^{-1}\right)''}{{}^{(i)}f^3} \\ &= k_i^2 + \sum_{j\neq i} k_j^2\,\tanh^{-2(q_j-q_i)}\left(\frac{3H_\Lambda t}{2}\right) + \cdots, \end{aligned} \tag{3.12}$$

where only the terms relevant to the norm of wavevector were shown in the second line. Now we introduce the time for quantization $t = t_*$, which is not necessarily $t_{\rm ini}$ but can be any moment after it. Then, once a wavevector (k_1, k_2, k_3) is given, one can decide whether each of the functions $\{{}^{(1)}f, {}^{(2)}f, {}^{(3)}f\}$ can satisfy the condition

$$k_i^2 \gtrsim \sum_{j\neq i} k_j^2 \, \tanh^{-2(q_j - q_i)} \left(\frac{3H_\Lambda t_*}{2} \right) , \tag{3.13}$$

and it is under this condition that a variable ${}^{(i)}\chi_\lambda$ has an approximately constant frequency squared ${}^{(i)}\Omega_\lambda^2 \sim k_i^2$. We regard such a variable as "suitable for quantization".

Figure 3.1 shows the time evolution of the squared frequencies ${}^{(i)}\Omega_\lambda^2$ for the transformed variables ${}^{(i)}\chi_\lambda = {}^{(i)}f\,\mu_\lambda$ $(i = 1, 2, 3)$ with a wavenumber $k_1 = k_2 = k_3 = (10/\sqrt{3})\, a_{\rm iso}\, H_\Lambda$. The background is triaxially anisotropic, with the exponents $(q_1, q_2, q_3) = (1/\sqrt{3}, 0, -1/\sqrt{3})$ $(\Theta = 8\pi/6)$. In this case, ${}^{(1)}\Omega_\lambda^2$ stays constant in a wide range of time (top-left), whereas ${}^{(2)}\Omega_\lambda^2$ and ${}^{(3)}\Omega_\lambda^2$ are not (top-right and bottom). This tendency is a consequence of the fact that the wavenumber term in ω_λ^2 can be approximated as

$$\gamma^{ij}\, k_i\, k_j \simeq {}^{(1)}f^4\, k_1^2 \quad (t \ll t_{\rm iso}\,, q_1 > q_2 > q_3) \tag{3.14}$$

thanks to the hierarchy ${}^{(1)}f \gg {}^{(2)}f \gg {}^{(3)}f$. This applies to a wide range of the choice of wavevector (k_1, k_2, k_3) .

The figures illuminate that the advantage of taking ${}^{(1)}\chi_\lambda$ as a quantity to quantize, since it would oscillates harmonically for the longest period. However, as seen in the figure, ${}^{(1)}\Omega_\lambda^2$ ceases to stay constant for smaller t , where the terms other than the wavenumber become dominant. As discussed in the previous section, this is inevitable if a mode really approaches to the initial singularity at $t = 0$. Quantitatively, in this particular but typical example, we may conclude that ${}^{(1)}\chi_\lambda$ should be the most sensible choice of a variable for quantization as long as we quantize at some moment between $t = 10^{-6}\, H_\Lambda^{-1}$ and $10^{-2}\, H_\Lambda^{-1}$.

Likewise, once the time of quantization is given, we examine whether or not each variable ${}^{(i)}\chi_\lambda$ $(i = 1, 2, 3)$ is suitable for quantization. We suggest the following working criterion for the usefulness of a variable ${}^{(i)}\chi_\lambda$ in quantization: If

$${}^{(i)}\Omega_\lambda^2 > 0 \tag{3.15}$$

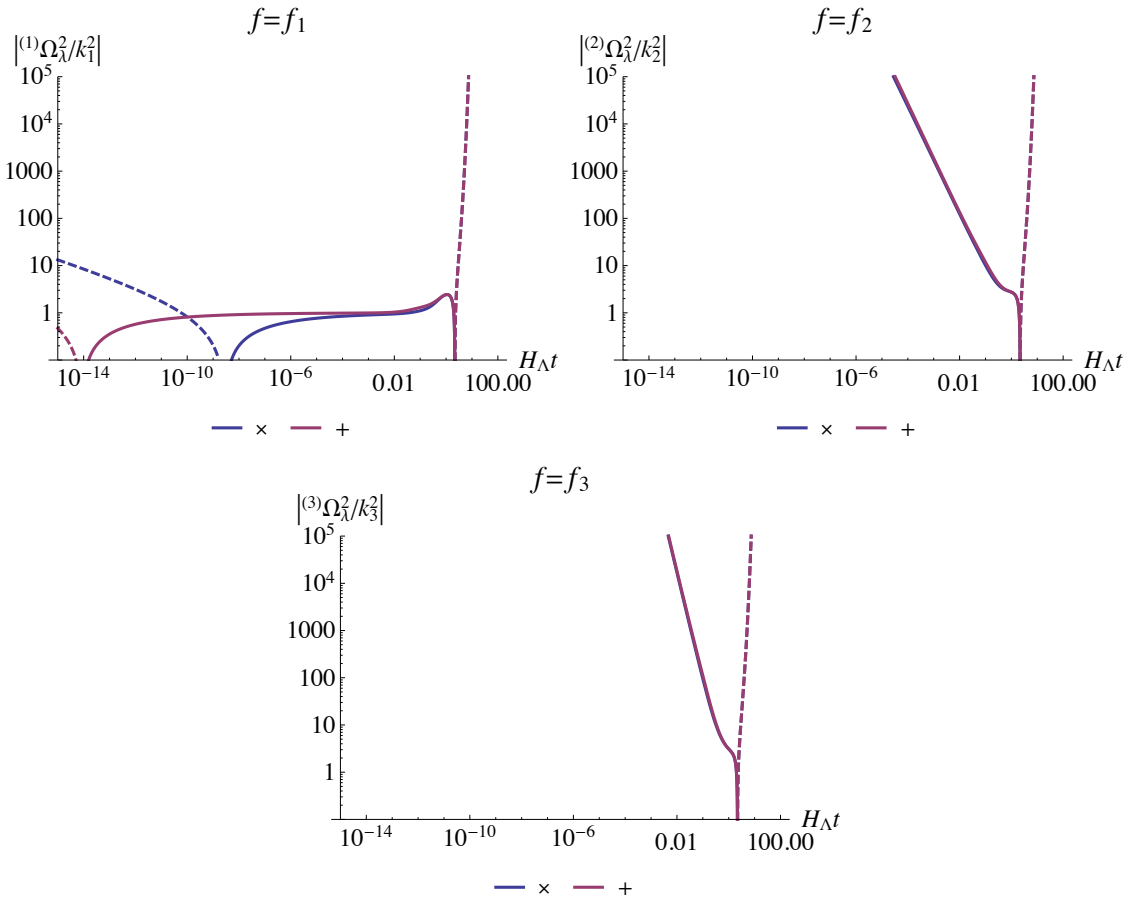

Figure 3.1: Time evolution of the frequencies squared for ${}^{(i)}f$-transformed variables ${}^{(i)}\chi_\lambda$: ${}^{(1)}\Omega^2_\lambda$ (top-left), ${}^{(2)}\Omega^2_\lambda$ (top-right) and ${}^{(3)}\Omega^2_\lambda$ (bottom). The mode has a wavenumber $k_1 = k_2 = k_3 = (10/\sqrt{3})\, a_{\rm iso}\, H_\Lambda$ and the background is triaxially anisotropic with the exponents $(q_1, q_2, q_3) = (1/\sqrt{3}, 0, -1/\sqrt{3})$ ($\Theta = 8\pi/6$). The lines are dashed where the values are negative.

and

$$ {}^{(i)}R_\lambda \equiv \left| \frac{1}{{}^{(i)}\Omega_\lambda^2} \frac{\mathrm{d}^{(i)}\Omega_\lambda}{\mathrm{d}^{(i)}\tau} \right| \ll 1 \tag{3.16} $$

are satisfied simultaneously, ${}^{(i)}\chi_\lambda$ is a sensible choice of variable for quantization.

Figure 3.2 shows which of $\{{}^{(1)}R_\lambda, {}^{(2)}R_\lambda, {}^{(3)}R_\lambda\}$ is the smallest for each direction of (k_1, k_2, k_3) with several wavenumbers $k \equiv \sqrt{k_1^2 + k_2^2 + k_3^2}$. These figures are the Mercator projection of the "celestial sphere" parameterized by the polar angle θ and azimuth angle ϕ defined as

$$ \begin{aligned} k_1 &= k \, \sin\theta \, \cos\phi \,, \\ k_2 &= k \, \sin\theta \, \sin\phi \,, \\ k_3 &= k \, \cos\theta \,. \end{aligned} \tag{3.17} $$

In the figures, regions labelled with "i" ($i = 1, 2, 3$) correspond to where ${}^{(i)}R_\lambda$ is the smallest of the three. For the cross mode ($\lambda = \times$, right column), there appear regions labelled as "None" (black). For those wavenumbers, none of the three frequencies squared ${}^{(i)}\Omega_\lambda^2$ is positive, which implies none of the variables ${}^{(i)}\chi_\lambda$ is suitable for quantization. This does not necessarily mean quantization is impossible, for it merely alerts the failure of our restricted procedure, but in the current work, we would not proceed to quantize such modes.

We see that the ${}^{(1)}f$-transformed variable ${}^{(1)}\chi_\lambda$ is the most suitable choice for quantization in a vast area on the celestial sphere. This is a direct consequence of the hierarchy ${}^{(1)}f \gg {}^{(2)}f \gg {}^{(3)}f$ for $t \ll H_\Lambda^{-1}$. Other variables could take over only when k_1 is tiny, in the vicinity of the circumferences with $\phi = \pi/2, 3\pi/2$ where $k_1 = 0$. In the almost whole region on those circumferences, ${}^{(2)}\chi_\lambda$ is superior to ${}^{(3)}\chi_\lambda$ because of, again, the above hierarchy.

3.3 Conditions for sensible quantization

To sum up, we expect that quantization in the triaxially anisotropic Kasner–de Sitter universe can be carried out to good approximation if there is some moment t_* around which the following conditions are fulfilled:

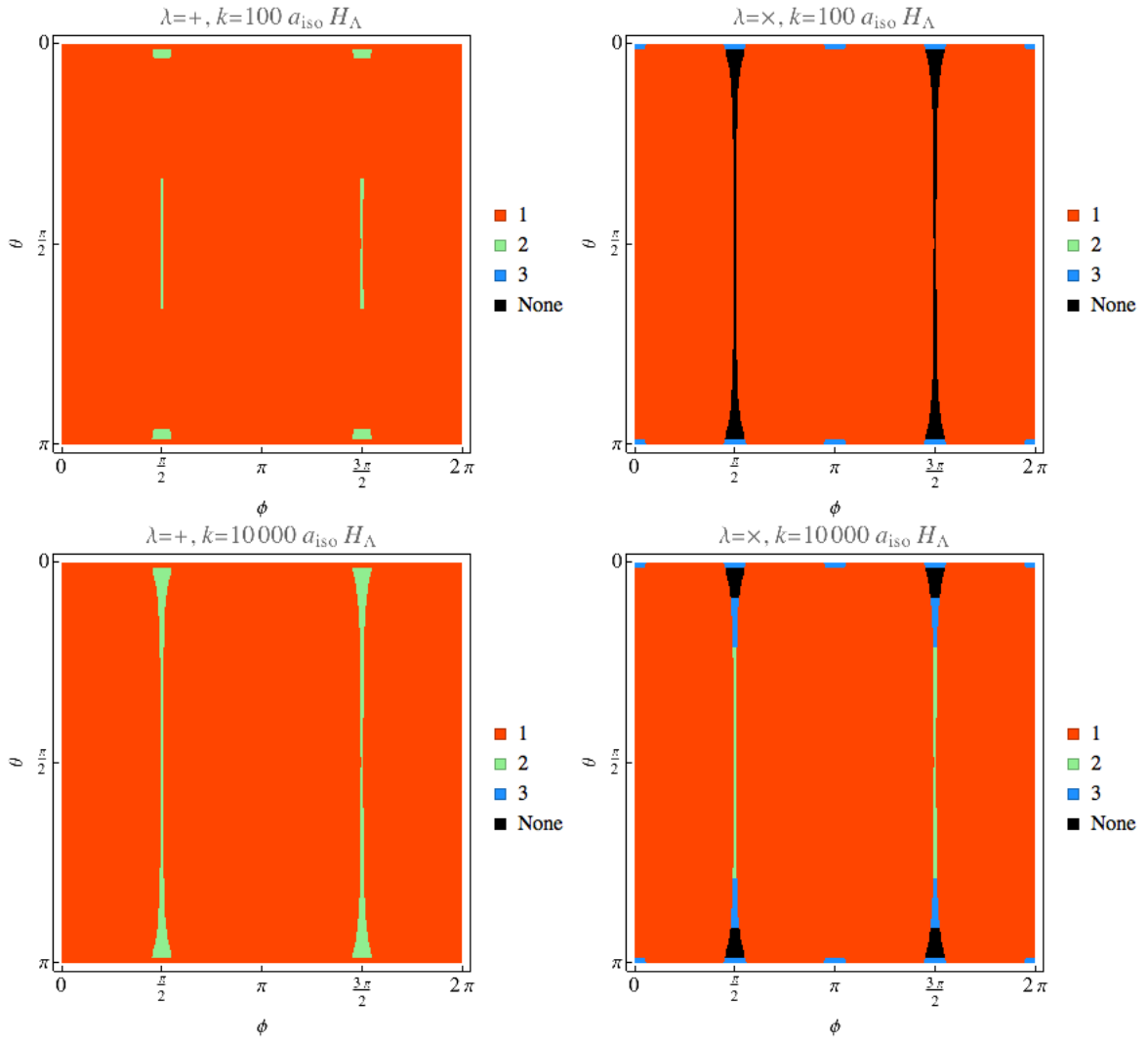

Figure 3.2: Showing of which ${}^{(i)}R_\lambda$ $(i = 1, 2, 3)$ is the smallest for each mode pointing the direction specified by the polar angles (θ, ϕ) in the celestial sphere. Regions labelled by "i" indicates ${}^{(i)}R_\lambda$ is the smallest, whereas in the regions labelled by "None", ${}^{(i)}\Omega^2_\lambda < 0$ for $\forall i$. The background anisotropy is triaxial ($\Theta = 8\pi/6$) and the wavenumber is $k = 10^2\, a_{\rm iso}\, H_\Lambda\,, 10^4\, a_{\rm iso}\, H_\Lambda$ from top to bottom.

- At least one of the transformed variables $\{{}^{(1)}\chi_\lambda\,,{}^{(2)}\chi_\lambda\,,{}^{(3)}\chi_\lambda\}$ has positive, nearly constant frequency squared.
- Interaction between the polarization modes are weak. Decoupling of the modes in the short wave-length regime has been partly confirmed in [PPU07], and we expect that the interaction is weak as long as the WKB approximation is valid.

The role of the above conditions is only to provide us the means to determine the energy spectrum of the fields at $t = t_*$. Here, to choose an adequate quantum state is a completely different problem which we would not answer at this stage. A typical situation is that, although the state with the lowest energy at $t = t_*$ is a tempting choice, it may not remain the ground state throughout the whole anisotropic expansion unlike the Bunch–Davies vacuum in isotropic de Sitter. We can however expect that the knowledge of the energy spectrum should serve as a useful clue to choose the favored state on physical backgrounds.

In the following discussions, we assume that we can decide which of ${}^{(i)}\chi_\lambda$ is the most suitable choice of a variable to quantize for a given wavevector (k_1, k_2, k_3) within a given setup. With this in mind, the index (i) is omitted unless it is necessary.

Once a variable suitable for quantization is given, a standard procedure of second quantization can be carried out. What we need is the normalization condition imposed on each mode.

The second-order action of χ_λ is given by transforming the second-order action for μ_λ (2.112) as

$$S_2 \simeq \sum_{\lambda=+,\times} \frac{1}{2} \int \mathrm{d}^3 k_i \, \mathrm{d}\eta \, \left[\mu'_\lambda \, {\mu'_\lambda}^* - \omega_\lambda^2 \, \mu_\lambda \, {\mu_\lambda}^*\right] \tag{3.18}$$

$$= \sum_{\lambda=+,\times} \frac{1}{2} \int \mathrm{d}^3 k_i \, \mathrm{d}\tau \, \left[\dot{\chi}_\lambda \, \dot{\chi}_\lambda{}^* - \Omega_\lambda^2 \, \chi_\lambda \, \chi_\lambda{}^*\right] \tag{3.19}$$

up to surface term, where we have dropped the interaction term. The operator version of the canonical variable

$$\hat{\chi}_\lambda = \hat{a}^\lambda_{k_i} \, u_\lambda \,, \tag{3.20}$$

where $\hat{a}_\lambda$ ($\hat{a}_{\lambda'}{}^\dagger$) is the annihilation (creation) operator and u_λ the appropriately normalized mode function with positive frequency. The canonical quantization condition to be

satisfied by the operators is

$$\left[\hat{a}^{\lambda}_{k_i}\,,\hat{a}^{\lambda'\dagger}_{k'_i}\right]=\delta_{\lambda\lambda'}\,\delta^3(k_i-k'_i)\,,\quad\text{otherwise}\quad 0\,. \tag{3.21}$$

We decide the normalization constant of the modes u_λ by the Wronskian matrix determinant W as

$$W\left[u_\lambda\,,\frac{\mathrm{d}u_\lambda}{\mathrm{d}\tau}\right]=u_\lambda\,\frac{\mathrm{d}u^*_\lambda}{\mathrm{d}\tau}-u^*_\lambda\,\frac{\mathrm{d}u_\lambda}{\mathrm{d}\tau}=\mathrm{i}\,. \tag{3.22}$$

In order to estimate the expectation value of fluctuation, we define the quantum vacuum by

$$\hat{a}^{\lambda}_{k_i}|0\rangle=0\,, \tag{3.23}$$

and we construct the Fock space in the standard way.

3.4 PGWs from quantum fluctuations in triaxial KdS

In this section, we apply the formulation for quantizing PGWs in triaxial KdS backgrounds. Throughout the numerical calculations, the background anisotropy is fixed and specified by $(q_1,q_2,q_3)=(1/\sqrt{3},0,-1/\sqrt{3})$ ($\Theta=8\pi/6$), and the time of quantization is $t_*=10^{-5}\,H_\Lambda^{-1}$ unless otherwise stated. This value of t_* corresponds to the Planck scale if the energy scale of isotropic inflation is around the GUT scale.

The vacuum expectation value of fluctuation of tensor modes are calculated as

$$\langle 0|\hat{E}_{ij}(x^i,\tau)\,\hat{E}^{ij}(x^i,\tau)|0\rangle=\frac{1}{a^2\,f^2}\sum_{\lambda=+,\times}\int\frac{\mathrm{d}^3k_i}{(2\pi)^3}\,|u_\lambda(k_i,\tau)|^2\,, \tag{3.24}$$

where u_λ is the positive frequency mode appropriately normalized at the time of quantization, $t=t_*$. The final value of the classical expectation value at the end of inflation is calculated by evolving the mode function up to $t\gg t_{\rm iso}$, where the modes *freeze out* after their horizon exit. We shall give analytic and numerical evaluations for the gravitational-wave power spectrum and angular distribution.

3.4.1 Analytic evaluation with WKB approximation

The mode function u_λ can be approximated by the (zeroth-order) WKB solution

$$u_\lambda^{\rm WKB}(k_i,\tau)=\frac{1}{\sqrt{2\,\Omega_\lambda(k_i,\tau)}}{\rm e}^{-{\rm i}\int^\tau {\rm d}\tau'\,\Omega_\lambda(k_i,\tau')}\,, \tag{3.25}$$

as long as the so-called WKB parameter

$$Q_\lambda(k_i,\tau)=-\frac{1}{2\,\Omega_\lambda^2}\left[\frac{1}{\Omega_\lambda}\frac{{\rm d}^2\Omega_\lambda}{{\rm d}\tau^2}-\frac{3}{2}\left(\frac{1}{\Omega_\lambda}\frac{{\rm d}\Omega_\lambda}{{\rm d}\tau}\right)^2\right] \tag{3.26}$$

is tiny.[2] It is now clear from the previous analyses that modes with sufficiently large wavenumber (k_1,k_2,k_3) have approximately constant Ω_λ^2, hence $|Q_\lambda|\ll 1$. The normalization for $u_\lambda^{\rm WKB}$ is given in terms of the Wronskian matrix determinant as

$$W\left[u_\lambda^{\rm WKB},\frac{{\rm d}u_\lambda^{\rm WKB}}{{\rm d}\tau}\right]={\rm i}\,. \tag{3.27}$$

As expected, for a wide range of wavenumber (k_1,k_2,k_3), the ${}^{(1)}f$-transformed variable ${}^{(1)}\chi_\lambda$ behaves much like a harmonic oscillator with ${}^{(1)}\Omega_\lambda^2\simeq k_1^2$ as long as it does not approach too close to the singularity $t=0$ or $t=t_{\rm iso}$. Figure 3.3 shows the evolution of the WKB parameter $|{}^{(1)}Q_\lambda|$ for ${}^{(1)}\chi_\lambda$ and its waveform for $k_1=k_2=k_3=k/\sqrt{3}=(100/\sqrt{3})\,a_{\rm iso}\,H_\Lambda$. The initial condition for the numerical calculation at $t=t_*=10^{-5}\,H_\Lambda^{-1}$ is so taken as to match the analytic WKB mode function.

As t approaches to the time of isotropization $t_{\rm iso}$, the WKB mode function is isotropized as

$$|u_\lambda^{\rm WKB}|^2\sim\frac{1}{2\,\Omega_\lambda}\to\frac{1}{2\,\sqrt{k_1^2+k_2^2+k_3^2}}\,. \tag{3.28}$$

Then, after the transition to ordinary, isotropic de Sitter inflation at $t=t_{\rm iso}$, the tensor perturbations decay as $|E_\lambda|\propto a^{-1}$ until they exit the horizon when $a=k/H_\Lambda$. Therefore

[2] The function $u_\lambda^{\rm WKB}$ satisfies

$$\frac{{\rm d}^2u_\lambda^{\rm WKB}}{{\rm d}\tau^2}+[1-Q_\lambda]\;\Omega_\lambda^2\,u_\lambda^{\rm WKB}=0\,.$$

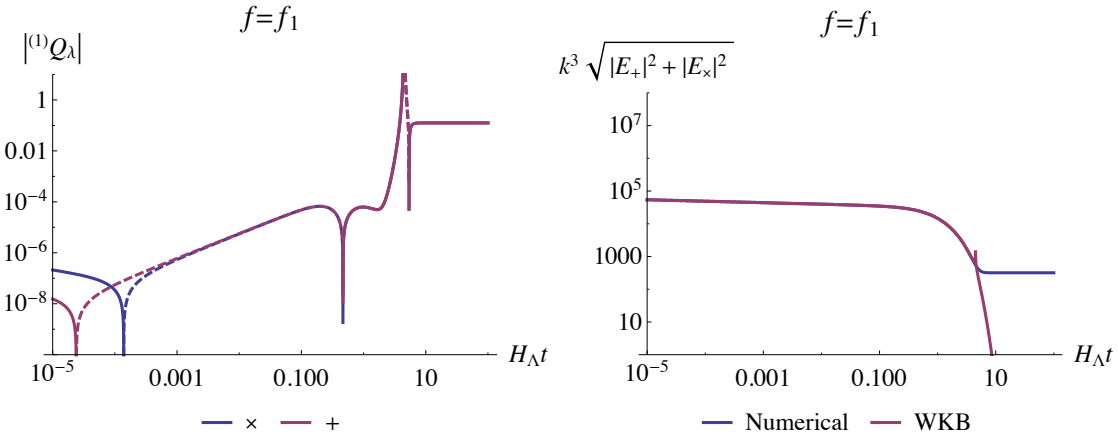

Figure 3.3: Time evolution of the WKB parameter ${}^{(1)}Q_\lambda$ (left) and comparison of the WKB solution with the numerical solution (right) for a mode with $k_1 = k_2 = k_3 = k/\sqrt{3} = (100/\sqrt{3})\, a_{\rm iso}\, H_\Lambda$. The lines for ${}^{(1)}Q_\lambda$ are dashed when the values are negative.

the power spectrum of PGWs after inflation is estimated as

$$\begin{aligned} P_{\rm T} &\equiv \sum_{\lambda=+,\times} 4\,|E_\lambda(a = k/H_\Lambda)|^2 \\ &= 64\pi\, G\, \frac{|u_\lambda|^2}{a^2\, f^2}\bigg|_{a=k/H_\Lambda} \\ &\approx \frac{8\pi\, G\, H_\Lambda^2}{k^3}\,. \end{aligned} \tag{3.29}$$

This expression depends only on the norm of wavenumber, $k = \sqrt{k_1^2 + k_2^2 + k_3^2}$, and agrees with the one in de Sitter inflation, that is, isotropic and scale-invariant.

In the above simple estimate, we assumed that the WKB approximation is valid all the way after the time of quantization t_* up to the time of isotropization $t_{\rm iso}$. However, if the WKB condition is violated somewhere on the way during the anisotropic regime, then the prediction can differ and some imprints of the initial anisotropy could be left in the sky map of the gravitational-wave background as we studied in [FNS17]. Inspection of such possibilities is beyond the scope of this thesis and left in future studies.

3.4.2 Numerical calculations: all-sky map of primordial gravitational waves originating quantum fluctuations

Finally, we confirm the previous estimate for the gravitational-wave intensity by numerical means.

Shown in Figure 3.4 are the all-sky maps of the intensity of PGWs for wavenumbers $k = 10^2\, a_{\rm iso}\, H_\Lambda$ and $10^4\, a_{\rm iso}\, H_\Lambda$. The values are normalized by that of ordinary de Sitter inflation.

One can see that the prediction in the triaxial KdS coincides with that of isotropic de Sitter inflation for the range of wavelength considered and wide range of direction. There are some features, though: In the polar regions where $|k_3| \gg |k_1|, |k_2|$, there is an apparent enhancement of the PGWs. At this stage, we do not claim this should be a real signature of the initial anisotropy because there vast violations of the WKB approximation occur. The regions without value (in black) correspond to where all of ${}^{(i)}\Omega_\lambda^2$ $(i = 1, 2, 3)$ have negative values. We do not try to compute anything in such regions since our approximation method lacks a power of prediction.

At the end, we show a result for a different background anisotropy. Figure 3.5 shows the sky map for wavenumber $k = 100\, a_{\rm iso}\, H_\Lambda$ for a nearly "prolate" axisymmetric background characterized by the anisotropy parameter $\Theta = 0.99 \times 6\pi/9$.

A conceptually subtle but reasonable difference from the triaxial case presented in the top panels of Figure 3.4 is that, in the triaxial case, the "uncomputable" region (in black) makes a great circle, while in the axisymmetric case it localizes in the vicinity of the axis of symmetry, i.e., k_3-axis. We do not claim it serves as an observational signature to distinguish the primordial anisotropy at this stage, because it is merely a manifestation of the limitation of our approximation method. Still, we could direct our intention to what really happens in those regions. We leave development of approximation method applicable in such regions in future studies.

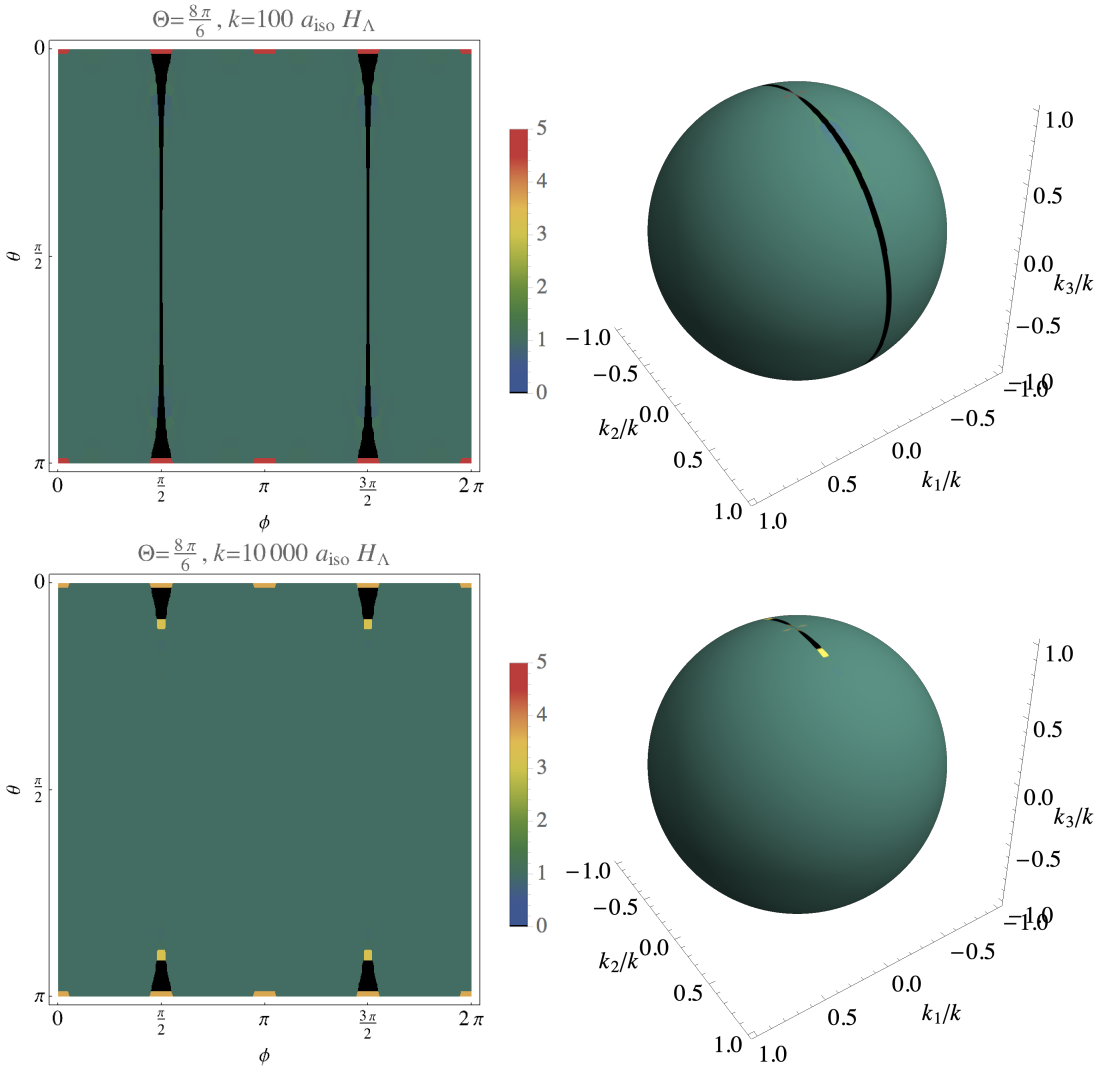

Figure 3.4: All-sky maps of PGW intensity for wavenumbers $k = 10^2\, a_{\rm iso}\, H_\Lambda$ (top) and $10^4\, a_{\rm iso}\, H_\Lambda$ (bottom) in the presence of a background anisotropy characterized by the indices $(q_1, q_2, q_3) = (1/\sqrt{3}, 0, -1/\sqrt{3})$ ($\Theta = 8\pi/6$). The values are normalized by those of de Sitter inflation and they are approximately unity in the vast region. In regions without a value (black), all ${}^{(i)}\Omega_\times^2$ ($i = 1, 2, 3$) are negative and we do not try to compute values.

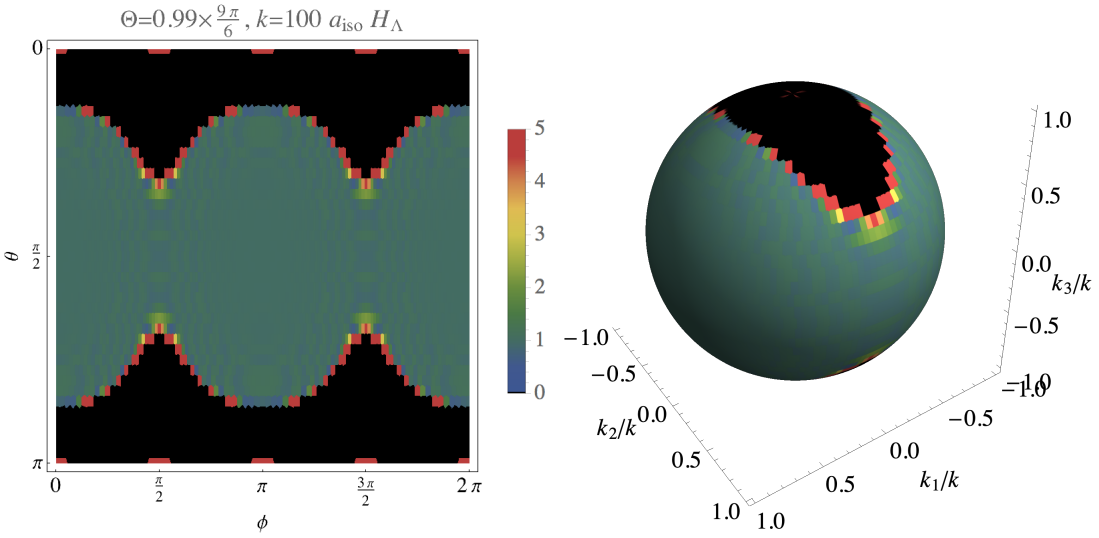

Figure 3.5: All-sky map of the intensity of gravitational waves with wavenumber $k = 10^2\, a_{\rm iso}\, H_\Lambda$ for nearly "prolate" axisymmetric background characterized by the anisotropy parameter $\Theta = 0.99 \times 6\pi/9$. Compared to the top panels in Figure 3.4, the "uncomputable" region localizes near the symmetry k_3-axis.

Chapter 4

Analyses of direction-dependent evolution of PGWs

In the previous chapter, we considered the initial condition of PGWs and power spectra of PGWs in KdS spacetime. Unfortunately, our prescription is not predictive with respect to the "uncomputable" regions. Nevertheless, the "uncomputable" region might include potential information for searching the initial anisotropy by future observations. Therefore, in this chapter, we perform detailed analyses of time evolutions of modes instead of the predictive power spectrum, and we attempt to read off the initial anisotropy from qualitative characteristics of directional dependences of time evolutions of modes.

Since we are interested in gravitational waves currently on large scales and since we require $a_{\rm iso}\, H_\Lambda \lesssim a(t_0)\, H_0$, we only consider modes which had a shorter wavelength than the Hubble radius at the isotropization time $t_{\rm iso} = H_\Lambda^{-1}$. We will take $k = \mathcal{O}(10\text{–}10^3) \times a_{\rm iso}\, H_\Lambda$ as reference values for the wavenumber.

4.1 Rotation of wavevector during anisotropic expansion

In this section we analyze time evolutions of gravitational waves labeling them with the *final* wavevector

$$\lim_{t\to\infty} \vec{k} = (k_1, k_2, k_3)\,. \tag{4.1}$$

The main object of interest in our current study is the distribution of gravitational-wave intensity on a sphere of radius

$$k \equiv \sqrt{{k_1}^2 + {k_2}^2 + {k_3}^2} \tag{4.2}$$

defined in the k-space, which, after being reflected through the origin and mapped to the celestial sphere, will provide an all-sky map of a gravitational wave background which we will be able to observe at a comoving wavenumber k. Note that the norm of a wavevector $\vec{k}$ depends on time and is given by

$$|\vec{k}| = \sqrt{\gamma^{11}\,{k_1}^2 + \gamma^{22}\,{k_2}^2 + \gamma^{33}\,{k_3}^2}\,. \tag{4.3}$$

Since there is a natural correspondence between the k-space and the position space, we sometimes mix up them with each other and even use common terminologies. For instance, a term "principal axes of expansion" may refer to both the x^i-axes in the position space and the k^i-axes in the k-space depending on the context.

Figure 4.1 is a portrait of the time derivatives of $\vec{k}$ drawn on the unit sphere in the k-space (left) and the Mercator projection of a portion of the sphere (right).

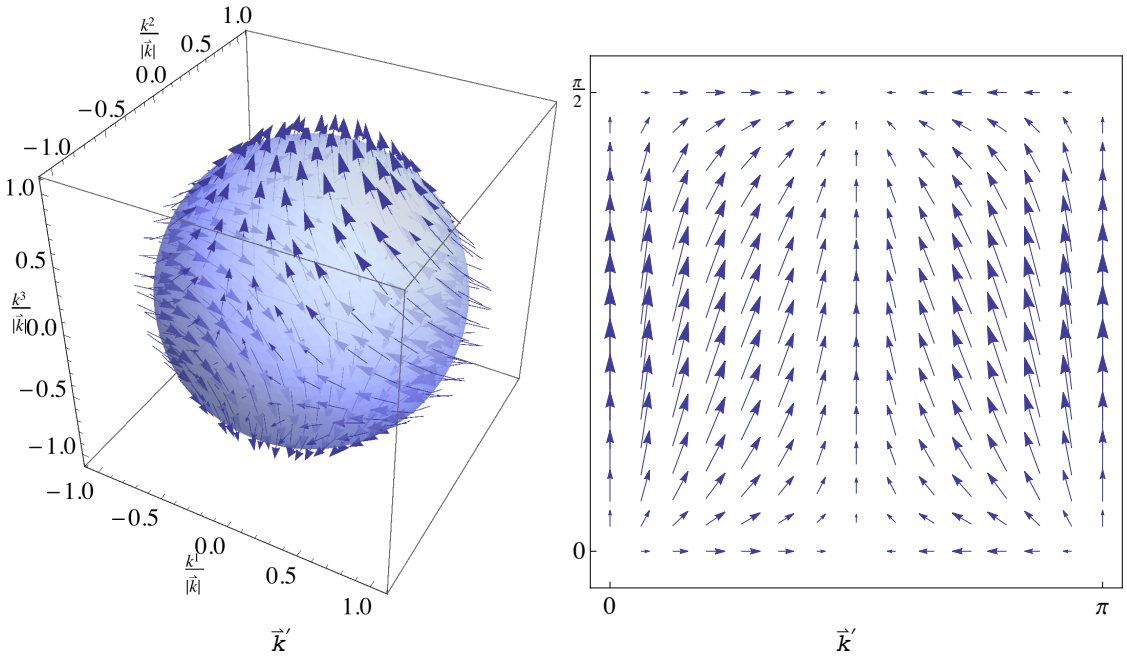

Figure 4.1: Left: A phase portrait of the time derivative $\vec{k}'$ in the k-space. Right: The Mercator projection of the half hemisphere specified by $k^1 \geq 0$ and $k^3 \geq 0$. The background is characterized by the anisotropy parameter $\Theta = \frac{8\pi}{6}$.

The general trend is that a wavevector $\vec{k}$ changes its direction towards the q_3 axis. This is because, as implied by Equation (2.51), $\vec{k}$ tends to rotate towards the principal axis of the slowest expansion of the three, i.e., with the smallest exponent q_i .

In the exceptional cases when $\vec{k}$ is aligned to one of the principal axes, only the norm changes with time but the direction does not, as understood from (2.51). Also, those quarter circumferences of the spheres connecting two principal axes (e.g. equator) are special in that if the endpoint of a wavevector lies on some of them, then it remains to do so, rotating from the direction of the faster axis to the slower. This is understood as follows. In order to parameterize a wavevector pointing somewhere on one of such quarter circumferences, we shall denote quantities associated with the axis of faster expansion by a superscript "(fast)" and those with the slower axis by "(slow)". For example, if one considers a circumference specified by $k_i = 0$, then $k_i^{(\mathrm{fast})}$ and $k_i^{(\mathrm{slow})}$ denote the covariant components of the wavevector along the faster and the slower axes, respectively. Then, we introduce an angle parameter ψ_i and a modulus k as

$$\tan\psi_i \equiv \frac{k_i^{(\mathrm{fast})}}{k_i^{(\mathrm{slow})}}\,, \quad k \equiv \sqrt{\left(k_i^{(\mathrm{slow})}\right)^2 + \left(k_i^{(\mathrm{fast})}\right)^2}\,. \tag{4.4}$$

Hence, the ratio of the contravariant components evolves during the anisotropic phase, $t \ll H_\Lambda^{-1}$, as

$$\begin{aligned} \frac{k^{i(\mathrm{fast})}}{k^{i(\mathrm{slow})}} &= \tan\psi_i \left[\tanh\left(\frac{3H_\Lambda t}{2}\right)\right]^{2(q_i^{(\mathrm{slow})} - q_i^{(\mathrm{fast})})} \\ &\simeq \tan\psi_i \left(\frac{3H_\Lambda t}{2}\right)^{2(q_i^{(\mathrm{slow})} - q_i^{(\mathrm{fast})})}\,. \end{aligned} \tag{4.5}$$

If $k_i^{(\mathrm{fast})} < k_i^{(\mathrm{slow})}$, the wavevector is *finally* aligned closer to the slower axis. From Equation (4.5), the time at which $\vec{k}$ comes to the midpoint of the two axes, i.e., at an angle of $\frac{\pi}{4}$, is estimated as

$$H_\Lambda t_{\mathrm{mid}} \simeq \frac{2}{3}\left(\frac{k_i^{(\mathrm{fast})}}{k_i^{(\mathrm{slow})}}\right)^{1/[2(q_i^{(\mathrm{fast})} - q_i^{(\mathrm{slow})})]}\,. \tag{4.6}$$

On the other hand, if $k_i^{(\mathrm{fast})} > k_i^{(\mathrm{slow})}$, $\vec{k}$ is initially closer to the faster axis and remains so until the end of the anisotropic Kasner regime.

From the above analysis, we can deduce that the direction of a wavevector pointing in general directions can only move within one of the quarter hemispheres bounded by such special quarter circumferences. It follows that, thanks to the symmetry of the background, it is sufficient for our purpose to consider only one of those quarter hemispheres and we shall hereafter restrict on the one specified by $k^i \geq 0$ $(i = 1, 2, 3)$.

In the k-space, a normalized wavevector $\hat{\vec{k}} = (k^1/|\vec{k}|, k^2/|\vec{k}|, k^3/|\vec{k}|)$ with one vanishing component $k^i = 0$ $(i = 1, 2, 3)$ points on one of the quarter circumferences of the unit sphere, which we shall call C_i. See Figure 4.2 for the definitions of the circumferences C_i and angles ψ_i $(i = 1, 2, 3)$.

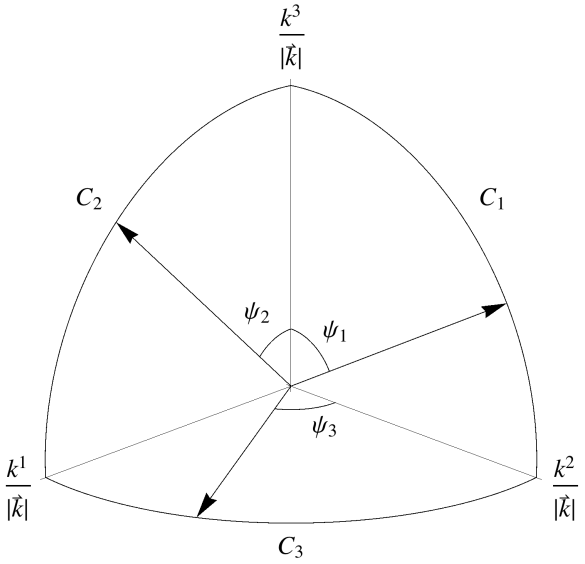

Figure 4.2: Illustration of the angles ψ_i and circumferences C_i on the unit sphere in the k-space. The arrows are examples of normalized final wavevector $\lim_{t\to\infty} \hat{\vec{k}} = (k_1/k, k_2/k, k_3/k)$ lying on each C_i.

4.2 Evolution of modes aligned with the principal axes

We first consider the evolution of modes whose wavevector is aligned to either of the principal axes. Let k_i be the only non-vanishing covariant component. Then the wavevector $\vec{k}$ is kept aligned with the k^i-axis while its squared norm evolves with time as

$$k_i\, k^i = k_i^2\, \tanh^{-2q_i}\left(\frac{3H_\Lambda t}{2}\right) . \tag{4.7}$$

The projected components of the shear tensor are greatly simplified in this case as[1]

$$\sigma^{(\mathrm{S})} = 3q_i \frac{a_{\mathrm{iso}} H_\Lambda}{(a/a_{\mathrm{iso}})^2}\,, \quad \left|\sigma_+^{(\mathrm{T})}\right| = \frac{3\Delta_i}{\sqrt{2}} \frac{a_{\mathrm{iso}} H_\Lambda}{(a/a_{\mathrm{iso}})^2}\,, \quad \sigma_{(1)}^{(\mathrm{V})} = \sigma_{(2)}^{(\mathrm{V})} = \sigma_\times^{(\mathrm{T})} = 0\,, \tag{4.8}$$

where we have introduced $\Delta_i \equiv \max_{j\neq i} q_j - \min_{j\neq i} q_j$, which quantifies the +-component of the shear. See Figure 4.3 for the dependence of Δ_i on Θ for each i . For $\sigma_\times^{(\mathrm{T})} = 0$, the interaction term ξ in the gravitational-wave equations vanishes identically, see (2.111), so the two polarization modes are decoupled.

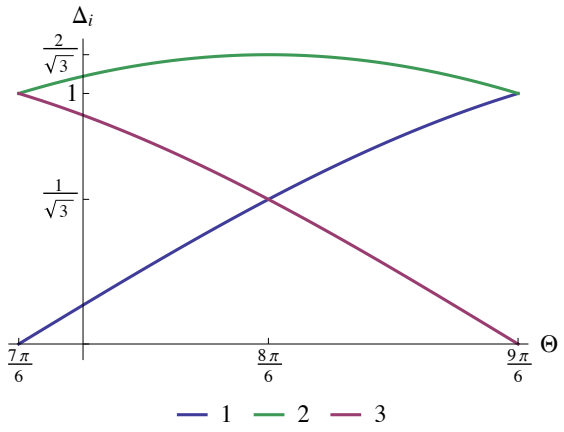

Figure 4.3: Values of $\Delta_i = \max_{j\neq i} q_j - \min_{j\neq i} q_j$.

Substituting Equations (4.7) and (4.8) into (2.110), we obtain the squared frequencies ω_λ^2 as

$$\begin{aligned}
\frac{\omega_\times^2}{a_{\mathrm{iso}}^2 H_\Lambda^2} &= \frac{k_i^2}{a_{\mathrm{iso}}^2 H_\Lambda^2} \tanh^{-2q_i}\left(\frac{3H_\Lambda t}{2}\right) + \frac{2-\cosh(6H_\Lambda t)}{(a/a_{\mathrm{iso}})^4} - \frac{9\Delta_i^2}{(a/a_{\mathrm{iso}})^4}\,, \\
\frac{\omega_+^2}{a_{\mathrm{iso}}^2 H_\Lambda^2} &= \frac{k_i^2}{a_{\mathrm{iso}}^2 H_\Lambda^2} \tanh^{-2q_i}\left(\frac{3H_\Lambda t}{2}\right) + \frac{2-\cosh(6H_\Lambda t)}{(a/a_{\mathrm{iso}})^4} + \frac{6\Delta_i^2\,(a/a_{\mathrm{iso}})^2}{\left[(2/3)\,\cosh(3H_\Lambda t) - q_i\right]^2}\,.
\end{aligned} \tag{4.9}$$

The leading contributions from each term during the early anisotropic regime ($t \ll t_{\mathrm{iso}} = H_\Lambda^{-1}$) are found as

$$\begin{aligned}
\frac{\omega_\times^2}{a_{\mathrm{iso}}^2 H_\Lambda^2} &\supset \frac{k_i^2}{a_{\mathrm{iso}}^2 H_\Lambda^2} \left(\frac{3H_\Lambda t}{2}\right)^{-2q_i} + \frac{1}{(3H_\Lambda t)^{4/3}} - \frac{9\Delta_i^2}{(3H_\Lambda t)^{4/3}}\,, \\
\frac{\omega_+^2}{a_{\mathrm{iso}}^2 H_\Lambda^2} &\supset \frac{k_i^2}{a_{\mathrm{iso}}^2 H_\Lambda^2} \left(\frac{3H_\Lambda t}{2}\right)^{-2q_i} + \frac{1}{(3H_\Lambda t)^{4/3}} + \frac{6\Delta_i^2\,(3H_\Lambda t)^{2/3}}{(2/3-q_i)^2}\,,
\end{aligned} \tag{4.10}$$

[1]The sign of $\sigma_+^{(\mathrm{T})}$ is not needed because only its square will appear.

where we have assumed $q_i < \frac{2}{3}$. The shear tensor gives a negative contribution $\propto -\Delta_i^2/(H_\Lambda t)^{4/3}$ to $\omega_\times^2$, which is missing in ω_+^2 in contrast.

In Figure 4.4, we show typical time evolutions of $\omega_\times^2$ (blue) and ω_+^2 (red) for modes aligned with either of the three principal axes. The three figures correspond to the cases when $\vec{k} \parallel k^1$-axis (top-left), $\vec{k} \parallel k^2$-axis (top-right), and $\vec{k} \parallel k^3$-axis (bottom), where the final wavenumber is $k_i = 100\, a_{\rm iso}\, H_\Lambda$ $(i = 1, 2, 3)$ and the background anisotropy parameter is $\Theta = \frac{8\pi}{6}$, for which $(q_1, q_2, q_3) = (\frac{1}{\sqrt{3}}, 0, -\frac{1}{\sqrt{3}})$ and $(\Delta_1, \Delta_2, \Delta_3) = (\frac{1}{\sqrt{3}}, \frac{2}{\sqrt{3}}, \frac{1}{\sqrt{3}})$. Since $\Delta_i > \frac{1}{3}$ for all i in this case, the squared frequency $\omega_\times^2$ should turn negative once the shear term dominates as implied by (4.10). To illuminate this, the lines for $\omega_\times^2$ are dashed when taking negative values. It is observed that there is a large negative contribution to $\omega_\times^2$ from the shear at the earliest stage of the anisotropic phase ($t \ll t_{\rm iso} = H_\Lambda^{-1}$) except for the k^1-axis-aligned mode (top-left panel), for which $\omega_\times^2$ is dominated by the $k_i\, k^i$ term throughout the time range considered, $10^{-5} < H_\Lambda t \lesssim 1$, although the shear would eventually dominate if one were allowed to go back in time indefinitely.

Shown in Figure 4.5 are the waveforms of the above three axis-aligned modes obtained by numerically integrating (2.109). As expected from the behaviors of $\omega_\times^2$, the $\times$-mode grows substantially while the shear term is giving a dominant contribution.

These waveforms of gravitational waves can be analytically understood as follows. First let us consider the $\times$-mode. The asymptotic form of $\omega_\times^2$ for $H_\Lambda t \ll 1$ is

$$\omega_\times^2 \sim \frac{k_i^2}{\left(2^{1/3} a_{\rm iso} H_\Lambda \eta\right)^{3q_i}} + \frac{1 - 9\Delta_i^2}{4\eta^2}\,, \tag{4.11}$$

where, in converting the time coordinates, we have used a relation

$$H_\Lambda t = \frac{2\sqrt{2}}{3}\, \left(a_{\rm iso} H_\Lambda \eta\right)^{3/2} \left[1 + \frac{\left(a_{\rm iso} H_\Lambda \eta\right)^3}{6} + \mathcal{O}(a_{\rm iso} H_\Lambda \eta)^6\right]. \tag{4.12}$$

Since $q_i < \frac{2}{3}$ for a triaxial KdS metric, $\omega_\times^2$ is dominated by the shear term ($\propto \eta^{-2}$) at earlier times and by the $k_i\, k^i$ term ($\propto \eta^{-3q_i}$) at later times. The growth of $\times$-mode is expected to stall around the transition between these two regimes, whose time is estimated as

$$a_{\rm iso} H_\Lambda \eta_{\rm stall} = \left[\frac{|9\Delta_i^2 - 1|}{2^{2-q_i}} \left(\frac{a_{\rm iso} H_\Lambda}{k_i}\right)^2\right]^{1/(2-3q_i)} \tag{4.13}$$

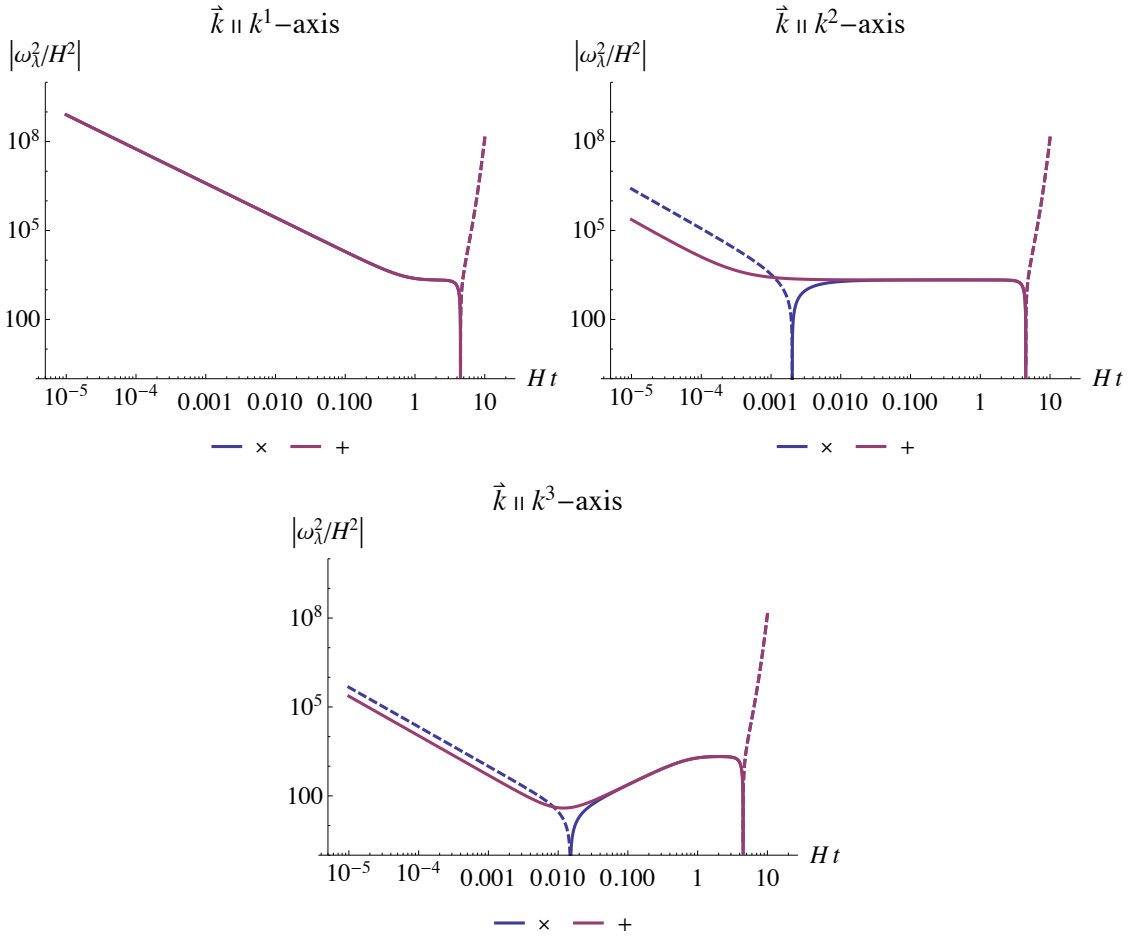

Figure 4.4: Time evolutions of $\omega_\times^2$ (blue) and ω_+^2 (red) for modes aligned with the k^1-axis (top-left), k^2-axis (top-right), and k^3-axis (bottom), for all of which the final wavenumber is $k_i = 100\, a_{\rm iso}\, H_\Lambda$ $(i = 1, 2, 3)$. The lines are dashed where $\omega_\times^2$ is negative. The background anisotropy parameter is $\Theta = \frac{8\pi}{6}$ corresponding to $(q_1, q_2, q_3) = (\frac{1}{\sqrt{3}}, 0, -\frac{1}{\sqrt{3}})$ and $(\Delta_1, \Delta_2, \Delta_3) = (\frac{1}{\sqrt{3}}, \frac{2}{\sqrt{3}}, \frac{1}{\sqrt{3}})$.

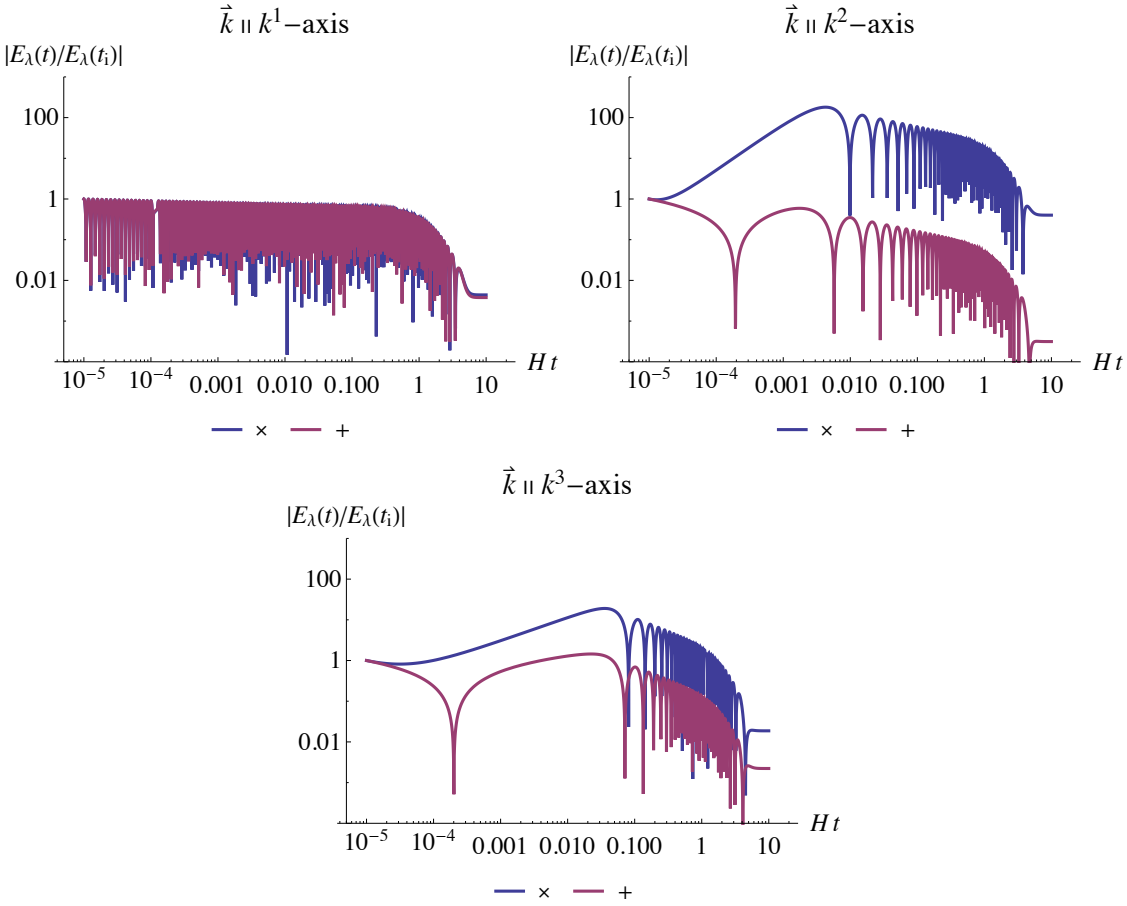

Figure 4.5: Waveforms of $E_\times$ (blue) and E_+ (red) for the modes aligned with the k^1-axis (top-left), k^2-axis (top-right), and k^3-axis (bottom). The initial time is $t_{\rm ini} = 10^{-5}\, H_\Lambda^{-1}$ and the other parameters are the same as in Figure 4.4.

or equivalently

$$H_\Lambda t_{\rm stall} = \frac{2\sqrt{2}}{3}\left[\frac{|9\Delta_i^2-1|}{2^{2-q_i}}\left(\frac{a_{\rm iso}H_\Lambda}{k_i}\right)^2\right]^{1/[2\,(2/3-q_i)]} . \tag{4.14}$$

For $\eta \ll \eta_{\rm stall}$, the equation of motion for the $\times$-mode is approximated as

$$\mu_\times'' + \frac{1-9\Delta_i^2}{4\eta^2}\,\mu_\times \approx 0 \tag{4.15}$$

and its general solution is given by

$$\mu_\times \approx C_+\,(H_\Lambda\eta)^{(1+3\Delta_i)/2} + C_-\,(H_\Lambda\eta)^{(1-3\Delta_i)/2} . \tag{4.16}$$

Hence, up to the time $\eta_{\rm stall}$, the growing mode behaves as $|E_\times| \propto (H_\Lambda\eta)^{3\Delta_i/2} \propto (H_\Lambda t)^{\Delta_i}$.

Once the shear term becomes subdominant after $\eta_{\rm stall}$, the $\times$-mode starts to oscillate obeying

$$\mu_\times'' + \frac{k_i^2}{(2^{1/3}a_{\rm iso}H_\Lambda\eta)^{3q_i}}\,\mu_\times \approx 0 . \tag{4.17}$$

This cannot be integrated analytically for a general q_i , but, since the exponents q_i only mildly depend on Θ , here we make a crude approximation that $(q_1,q_2,q_3) \approx (\frac{2}{3},0,-\frac{2}{3})$, which can be justified by a WKB analysis. Then, we have a rough estimate

$$|\mu_\times| \propto \begin{cases} \eta^{1/2} & (i=1) \\ \eta^0 & (i=2) \\ \eta^{-1/2} & (i=3) \end{cases} \tag{4.18}$$

and, therefore, we may estimate the amplitude of $E_\times$ between $t_{\rm stall}$ and $t_{\rm iso} = H_\Lambda^{-1}$ as

$$|E_\times| \propto (H_\Lambda t)^{-p_i} \quad \text{with} \quad (p_1,p_2,p_3) \equiv \left(0,\frac{1}{3},\frac{2}{3}\right) . \tag{4.19}$$

As we will show numerically later, although quantitatively not quite precise, this approximation captures certain qualitative features of the evolution of gravitational waves during the Kasner epoch.

The evolution of the +-mode can be deduced by setting $\Delta_i = 0$, see Equation (4.10). Hence E_+ oscillates constantly until $t_{\rm stall}$, and then decreasingly after $t_{\rm stall}$ as

$$|E_+| \propto (H_\Lambda t)^{-p_i} \,. \tag{4.20}$$

The background is isotropized at $\sim t_{\rm iso}$ and enters the standard de Sitter inflation phase. During inflation, amplitudes of the both modes decay exponentially as $E_\lambda \propto a^{-1} \propto \mathrm{e}^{-H_\Lambda t}$ until the modes exit the Hubble radius when $a(t) = k_i H_\Lambda^{-1}$, and are then frozen. The amplitude at the end of inflation is therefore suppressed by a factor $a(t_{\rm iso})\, H_\Lambda / k_i$ relative to the value at $t = t_{\rm iso}$.

Summing up all these effects, the linear growth factors for each polarization mode aligned with the principal axes are defined and estimated as

$$\begin{aligned} D_\times &\equiv \lim_{t\to\infty} \left| \frac{E_\times(t)}{E_\times(t_{\rm ini})} \right| \sim \frac{a_{\rm iso} H_\Lambda}{k_i} \, (H_\Lambda t_{\rm stall})^{p_i} \left(\frac{H_\Lambda t_{\rm stall}}{H_\Lambda t_{\rm ini}} \right)^{\Delta_i} , \\ D_+ &\equiv \lim_{t\to\infty} \left| \frac{E_+(t)}{E_+(t_{\rm ini})} \right| \sim \frac{a_{\rm iso} H_\Lambda}{k_i} \, (H_\Lambda t_{\rm stall})^{p_i} \,. \end{aligned} \tag{4.21}$$

Equation (4.14) implies that smaller q_i leads to larger $t_{\rm stall}$ as long as $k_i \gg a_{\rm iso}\, H_\Lambda$. Thus, the mode aligned with the k^3-axis enjoys the longest period of growth, see Figure 4.6 for comparison of the values of $t_{\rm stall}$ for the axis-aligned modes with the anisotropy parameter Θ varied. Note that $H_\Lambda t_{\rm stall}$ given by (4.14) for $i = 1$ formally saturates to 1 near $\Theta = \frac{7\pi}{6}$ (then $q_1 \approx \frac{2}{3}$), but, since the usefulness of (4.14) is limited in such a situation, we have not shown the corresponding values for $i = 1$ in Figure 4.6.

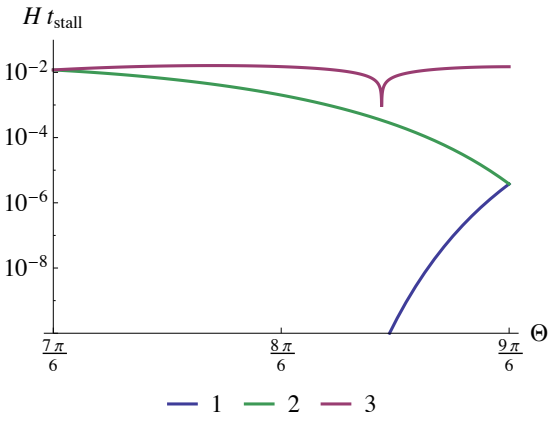

Figure 4.6: Θ-dependences of $t_{\rm stall}$ for the modes aligned with each principal axis with the final wavenumber $k_i = 100\, a_{\rm iso}\, H_\Lambda$ $(i = 1, 2, 3)$.

Substituting Equation (4.14) into (4.21), we can make the parameter dependence of the growth factors more explicit as

$$D_\times \propto \left(\frac{k_i}{a_{\rm iso}H_\Lambda}\right)^{P_{\times,i}} (H_\Lambda t_{\rm ini})^{-\Delta_i}\,, \quad D_+ \propto \left(\frac{k_i}{a_{\rm iso}H_\Lambda}\right)^{P_{+,i}} \tag{4.22}$$

with

$$P_{\times,i} = -1 - \frac{p_i + \Delta_i}{2/3 - q_i}\,, \quad P_{+,i} = -1 - \frac{p_i}{2/3 - q_i}\,. \tag{4.23}$$

The validity of this expression for $i = 1$ is also degraded when $\Theta \approx \frac{7\pi}{6}$ ($q_i \approx \frac{2}{3}$) for the same reason as above. In order to clarify the k_i dependences, we plot the indices $P_{\times,i}$ and $P_{+,i}$ in Figure 4.7. As for the $\times$-mode, since $P_{\times,3}$ is the largest of the three, the k^3-axis-aligned modes dominate at sufficiently large wavenumbers.

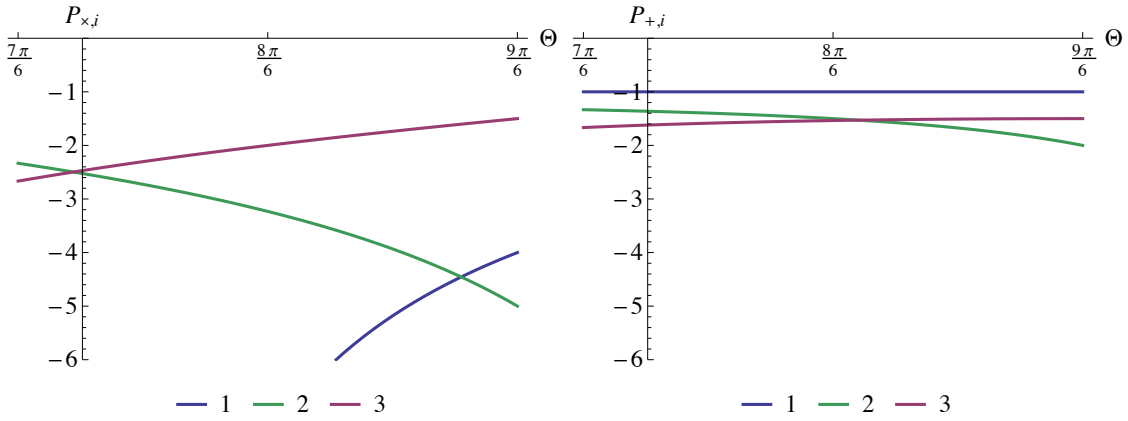

Figure 4.7: Θ-dependences of the indices $P_{\times,i}$ (left) and $P_{+,i}$ (right).

In the above analysis, we have implicitly assumed that the time scales are ordered as $t_{\rm ini} < t_{\rm stall} < t_{\rm iso}$, but this does not necessarily hold, as in the case of the k^1-axis-aligned mode exemplified in this section. If $t_{\rm stall} < t_{\rm ini}$, both polarization modes oscillate from the beginning with decaying amplitudes estimated by (4.19) and (4.20), and the growth factor is estimated as

$$D_\times \sim D_+ \sim \frac{a_{\rm iso}H_\Lambda}{k_i}\,(H_\Lambda t_{\rm ini})^{p_i}\,. \tag{4.24}$$

On the other hand, although this is not likely to occur, if $t_{\rm iso} < t_{\rm stall}$, the growth of gravitational waves does not stall until the time of isotropization and the growth factor

may be estimated as

$$D_\times \sim D_+ \sim \frac{a_{\rm iso} H_\Lambda}{k_i} \left(H_\Lambda t_{\rm ini}\right)^{-\Delta_i} . \tag{4.25}$$

Figure 4.8 shows the Θ-dependences of the growth factors for the axis-aligned modes with final wavenumber $k_i = 100\, a_{\rm iso}\, H_\Lambda$ $(i = 1, 2, 3)$ for the initial time $t_{\rm ini} = 10^{-5}\, H_\Lambda^{-1}$. The solid and dashed lines are the numerical and analytic estimate (4.21), respectively, which are in fairly good agreement with each other in the almost entire range of Θ. The k^1-axis-aligned mode is almost independent of Θ since it does not grow but constantly oscillates as implied by Equations (4.19) and (4.20). The k^2-axis-aligned and k^3-axis-aligned modes are comparable for the chosen set of parameters, although, as could be deduced from (4.22), at sufficiently large wavenumbers the k^3-axis-aligned $\times$-mode should dominate over the others.

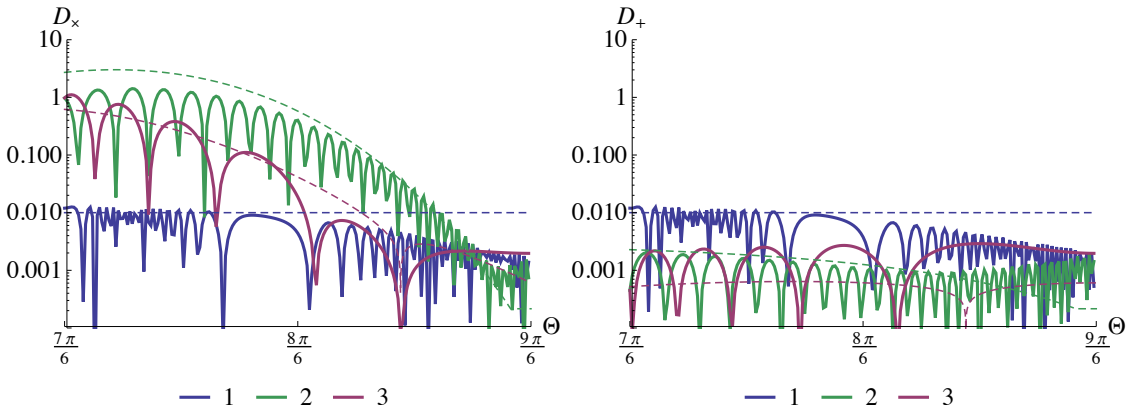

Figure 4.8: Θ-dependences of the linear growth factors $D_\times$ (left) and D_+ (right). The final wavenumber is $k_i = 100\, a_{\rm iso}\, H_\Lambda$ $(i = 1, 2, 3)$ and the initial time is $t_{\rm ini} = 10^{-5}\, H_\Lambda^{-1}$. The dashed lines indicate the analytic estimate given by (4.21), in fairly good agreement with the numerical calculations (solid).

4.3 Evolution of modes aligned between two principal axes

Then, we extend our analysis to modes whose wavevector $\vec{k}$ is not aligned with either of the principal axes but between two of them. For such modes, as discussed in Section 4.1, the direction of a wavevector $\vec{k}$ changes with time from the axis of faster expansion to the slower along one of the quarter circumferences C_i defined as in Figure 4.2. As in

Section 4.1, we introduce notations "(fast)" and "(slow)" for quantities associated with the faster and the slower axes, respectively. Wavevectors to be considered should have one vanishing component, $k_i = 0$ $(i = 1, 2, 3)$, while the other two, to be denoted as $k_i^{(\mathrm{fast})}$ and $k_i^{(\mathrm{slow})}$, are non-zero. To parameterize such a wavevector, we introduce an angle parameter ψ_i and a modulus k as given by Equation (4.4).

It is notable that the $\times$-component of the shear tensor $\sigma_\times^{(\mathrm{T})}$ still vanishes in this case, so, since $\xi = 0$, the two polarization modes of gravitational waves are decoupled. Therefore the evolution of each mode can still be analyzed separately.

As we will discuss shortly, the distribution of the intensity of gravitational waves on the circumferences C_i will serve as a key clue to establish the connection between the directional variation of gravitational-wave intensity and the pre-inflationary parameters. The situation on a circumference may be classified into the following three cases according to the final direction of the wavevector, i.e., the value of $\tan\psi_i$.

First, if the final direction of a mode satisfies $\tan\psi_i > 1$, the wavevector $\vec{k}$ remains close to the faster axis throughout the anisotropic Kasner regime. In terms of t_{mid} given by (4.6), the condition for this to realize may be written as

$$t_{\mathrm{mid}}(\psi_i) > t_{\mathrm{iso}} \quad \Leftrightarrow \quad \tan\psi_i > 1\,. \tag{4.26}$$

We will approximately evaluate the evolution of the modes of this kind by regarding their wavevectors as exactly aligned with the faster axis throughout the anisotropic phase.

Next, for modes with $\tan\psi_i < 1$, a turnover of the direction could happen at the time $t = t_{\mathrm{mid}}$ given by Equation (4.6). However, if

$$t_{\mathrm{mid}}(\psi_i) < t_{\mathrm{ini}} \quad \Leftrightarrow \quad \tan\psi_i < \left(\frac{3H_\Lambda t_{\mathrm{ini}}}{2}\right)^{2(q_i^{(\mathrm{fast})} - q_i^{(\mathrm{slow})})}\,, \tag{4.27}$$

the wavevector $\vec{k}$ is already close to the slower axis at the initial time $t = t_{\mathrm{ini}}$, hence no turnover occurs during the Kasner epoch. In this case the wavevector is regarded as aligned exactly with the slower axis throughout.

Finally, a turnover actually happens during the anisotropic phase if

$$t_{\mathrm{ini}} < t_{\mathrm{mid}}(\psi_i) < t_{\mathrm{iso}} \quad \Leftrightarrow \quad \left(\frac{3H_\Lambda t_{\mathrm{ini}}}{2}\right)^{2(q_i^{(\mathrm{fast})} - q_i^{(\mathrm{slow})})} < \tan\psi_i < 1\,. \tag{4.28}$$

We regard such modes as aligned with the faster axis before $t_{\rm mid}$ and with the slower axis after $t_{\rm mid}$. The analyses in the first and second cases above still apply to the time ranges $t < t_{\rm mid}$ and $t > t_{\rm mid}$, respectively.

4.3.1 Case 1: $t_{\rm mid}(\psi_i) > t_{\rm iso}$

For such a mode, we approximate the growth rate by the one for a mode exactly aligned with the faster axis and having a wavenumber $k_i = k_i^{(\rm fast)} = k \sin\psi_i$. Applying (4.21) or (4.24) with $q_i = q_i^{(\rm fast)}$, $\Delta_i = \Delta_i^{(\rm fast)}$, and $p_i = p_i^{(\rm fast)}$, we may estimate the growth factor for the $\times$-mode as

$$D_\times(\psi_i) \sim \frac{a_{\rm iso} H_\Lambda}{k} \times \begin{cases} \left(H_\Lambda t_{\rm stall}^{(\rm fast)}\right)^{p_i^{(\rm fast)}} \left(\frac{H_\Lambda t_{\rm stall}^{(\rm fast)}}{H_\Lambda t_{\rm ini}}\right)^{\Delta_i^{(\rm fast)}} & (t_{\rm ini} < t_{\rm stall}^{(\rm fast)}) \\ \left(H_\Lambda t_{\rm ini}\right)^{p_i^{(\rm fast)}} & (t_{\rm stall}^{(\rm fast)} < t_{\rm ini})\,, \end{cases} \tag{4.29}$$

where

$$H_\Lambda t_{\rm stall}^{(\rm fast)}(\psi_i) = \frac{2\sqrt{2}}{3} \left[\frac{\left|9(\Delta_i^{(\rm fast)})^2 - 1\right|}{2^{2-q_i^{(\rm fast)}}} \left(\frac{a_{\rm iso} H_\Lambda}{k \sin\psi_i}\right)^2 \right]^{1/[2\,(2/3 - q_i^{(\rm fast)})]} . \tag{4.30}$$

It is noted that, for both the circumferences C_2 and C_3, the k^1-axis serves as the axis of faster expansion, so $q_i^{(\rm fast)} = q_1 \geq \frac{1}{3}$ for $i = 2, 3$. Then, since $k > a_{\rm iso}\, H_\Lambda$ by assumption, a rough but strict upper limit on the time scale of the growth stall is given as

$$H_\Lambda t_{\rm stall}^{(\rm fast)}(\psi_i) \lesssim \left(\frac{k}{a_{\rm iso} H_\Lambda}\right)^{-3} \quad (i = 2, 3)\,. \tag{4.31}$$

This implies that growth of gravitational waves does not take place near the k^1-axis if the wavelength is sufficiently short such that $k \gg a_{\rm iso}\, H_\Lambda$.

4.3.2 Case 2: $t_{\rm mid}(\psi_i) < t_{\rm ini}$

Again, no turnover takes place. Similarly to Case 1 but with the use of $k_i = k_i^{(\rm slow)} = k\,\cos\psi_i$ instead of $k\,\sin\psi_i$, the growth factor is estimated as

$$D_\times(\psi_i) \sim \frac{a_{\rm iso}H_\Lambda}{k} \times \begin{cases} \left(H_\Lambda t_{\rm stall}^{(\rm slow)}\right)^{p_i^{(\rm slow)}} \left(\frac{H_\Lambda t_{\rm stall}^{(\rm slow)}}{H_\Lambda t_{\rm ini}}\right)^{\Delta_i^{(\rm slow)}} & (t_{\rm ini} < t_{\rm stall}^{(\rm slow)}) \\ (H_\Lambda t_{\rm ini})^{p_i^{(\rm slow)}} & (t_{\rm stall}^{(\rm slow)} < t_{\rm ini}) \end{cases} \tag{4.32}$$

with

$$H_\Lambda t_{\rm stall}^{(\rm slow)}(\psi_i) \approx \frac{2\sqrt{2}}{3} \left[\frac{\left|9(\Delta_i^{(\rm slow)})^2 - 1\right|}{2^{2-q_i^{(\rm slow)}}} \left(\frac{a_{\rm iso}H_\Lambda}{k\,\cos\psi_i}\right)^2\right]^{1/[2\,(2/3-q_i^{(\rm slow)})]} . \tag{4.33}$$

In contrast to the previous case, the exponent for this expression does not become large except on C_3 for a nearly axisymmetric background with $\Theta \approx \frac{9\pi}{6}$.

4.3.3 Case 3: $t_{\rm ini} < t_{\rm mid}(\psi_i) < t_{\rm iso}$

Finally, we consider the intermediate case in which a turnover occurs during the Kasner regime. We regard the wavevector $\vec{k}$ as aligned with the faster axis before $t_{\rm mid}$ and with the slower axis after $t_{\rm mid}$.

It is useful here to compare the three time scales $t_{\rm stall}^{(\rm fast)}$, $t_{\rm stall}^{(\rm slow)}$, and $t_{\rm mid}$. Shown in Figure 4.9 are their values evaluated on the circumferences C_1 (top-left), C_2 (top-right), and C_3 (bottom) for the parameters $k = 100\,a_{\rm iso}\,H$ and $\Theta = \frac{8\pi}{6}$. As we will discuss shortly, the $\times$-mode can grow during the time range indicated as gray-shaded regions.

Before the time of turnover $t_{\rm mid}$ is reached, i.e., below the green lines in Figure 4.9, the wavevector $\vec{k}$ is considered to be aligned with the faster axis and the analysis in Section 4.3.1 may be applied. The growth stalls at $t_{\rm stall}^{(\rm fast)}$ if it comes before $t_{\rm mid}$, but otherwise continues up to $t_{\rm mid}$. Indeed, in Figure 4.9, there are small intervals of $\tan\psi_i$ in which $t_{\rm mid} < t_{\rm stall}^{(\rm fast)}$.

After $t_{\rm mid}$, i.e., above the green lines in Figure 4.9, the wavevector $\vec{k}$ is considered to be aligned with the slower axis and the analysis in Section 4.3.2 may be applied. If $t_{\rm mid} < t_{\rm stall}^{(\rm slow)}$, then the mode continues (or resumes) to grow beyond $t_{\rm mid}$ up to $t_{\rm stall}^{(\rm slow)}$.

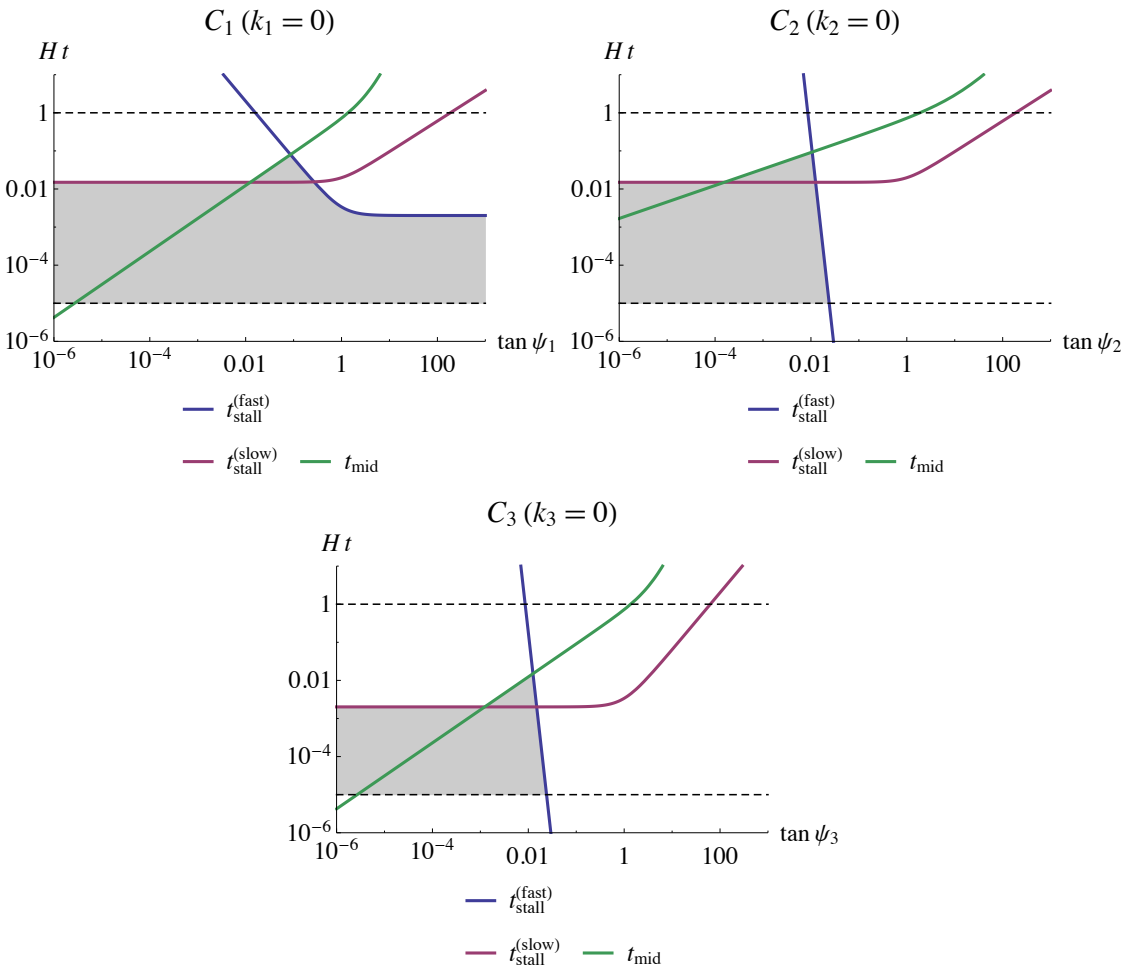

Figure 4.9: Time scales on the circumferences C_1 (top-left), C_2 (top-right), and C_3 (bottom) for $k = 100\,a_{\rm iso}\,H_\Lambda$ and $\Theta = \frac{8\pi}{6}$. The horizontal dashed lines correspond to $H_\Lambda t_{\rm iso} = 1$ and $H_\Lambda t_{\rm ini} = 10^{-5}$. For each value of $\tan\psi_i$, the mode can grow within the time range indicated in gray, see text.

Near the k^1-axis on the circumferences C_2 and C_3, it may happen that the time $t_{\rm stall}^{\rm (fast)}$ comes to earlier than $t_{\rm ini}$ and then growth is substantially suppressed. Indeed, for our choice of parameters, the values of $t_{\rm stall}^{\rm (fast)}$ evaluated on C_2 and C_3 are much earlier than $t_{\rm ini} = 10^{-5}\, H_\Lambda^{-1}$ as in the top-right and the bottom panels of Figure 4.9. If this is the case, a growth can only happen near the slower axes on these circumferences. Therefore, a criterion for growth in terms of the angle from the slower axis may be given by

$$t_{\rm stall}^{\rm (fast)} \gtrsim t_{\rm ini} \quad \Leftrightarrow \quad \psi_i \lesssim \left(\frac{k}{a_{\rm iso} H_\Lambda}\right)^{-1} (H_\Lambda t_{\rm ini})^{-(2/3 - q_i^{\rm (fast)})} \quad (i = 2, 3)\,. \tag{4.34}$$

In contrast, for the current choice of parameters, such suppression is not working on C_1 as understood from the top-left panel of Figure 4.9, where $t_{\rm stall}^{\rm (fast)}(\tan\psi_1 \gtrsim 1)$ is comparable to $t_{\rm stall}^{\rm (slow)}(\tan\psi_1 \lesssim 1)$ and never comes below $t_{\rm ini}$. However, for some parameters and wavelengths it may happen that $t_{\rm stall}^{\rm (fast)}$ on C_1 becomes earlier than $t_{\rm ini}$, leading to suppression of growth near the k^2-axis (the faster axis on C_1). In the next subsections, we will pay particular attention to this possibility.

4.3.4 Growth factors

In Figure 4.10, we show the linear growth factors for the $\times$-mode on the circumferences C_1 (top-left), C_2(top-right), and C_3 (bottom) for the parameters $\Theta = \frac{8\pi}{6}$, $t_{\rm ini} = 10^{-5}\, H_\Lambda^{-1}$, and $k = 100\, a_{\rm iso}\, H_\Lambda$. In each figure, ψ_i measures the angle from the axis of slower expansion. The analytic estimates based on the arguments in the previous sections are also plotted as dashed lines.

As understood from the figure, there is only weak contrast in growths on C_1, whereas rather sharp declines at some angle of $\mathcal{O}(0.01)$ from the slower axes on C_2 and C_3 are indicated. This implies that the region of high-intensity gravitational waves on the celestial sphere would form a belt-like pattern around a great circle containing C_1, which we will numerically confirm in the next subsection.

In Figure 4.11, we show waveforms of $E_\times$ (blue) and E_+ (red) for several modes on C_3, i.e., with $k_3 = 0$. The modes have a common final wavenumber $k = \sqrt{k_1^2 + k_2^2} = 100\, a_{\rm iso}\, H_\Lambda$ but different final directions parameterized by $\tan\psi_3 = k_1/k_2$: $\psi_3 = 10^{-1}$ (top-left), 10^{-2} (top-right) and 10^{-3} (bottom). The other parameters are the same as in Figure 4.10. It is observed that growths occur more efficiently as ψ_3 decreases, i.e., as the final direction of the wavevector gets closer to the k^2-axis. Indeed, there appears

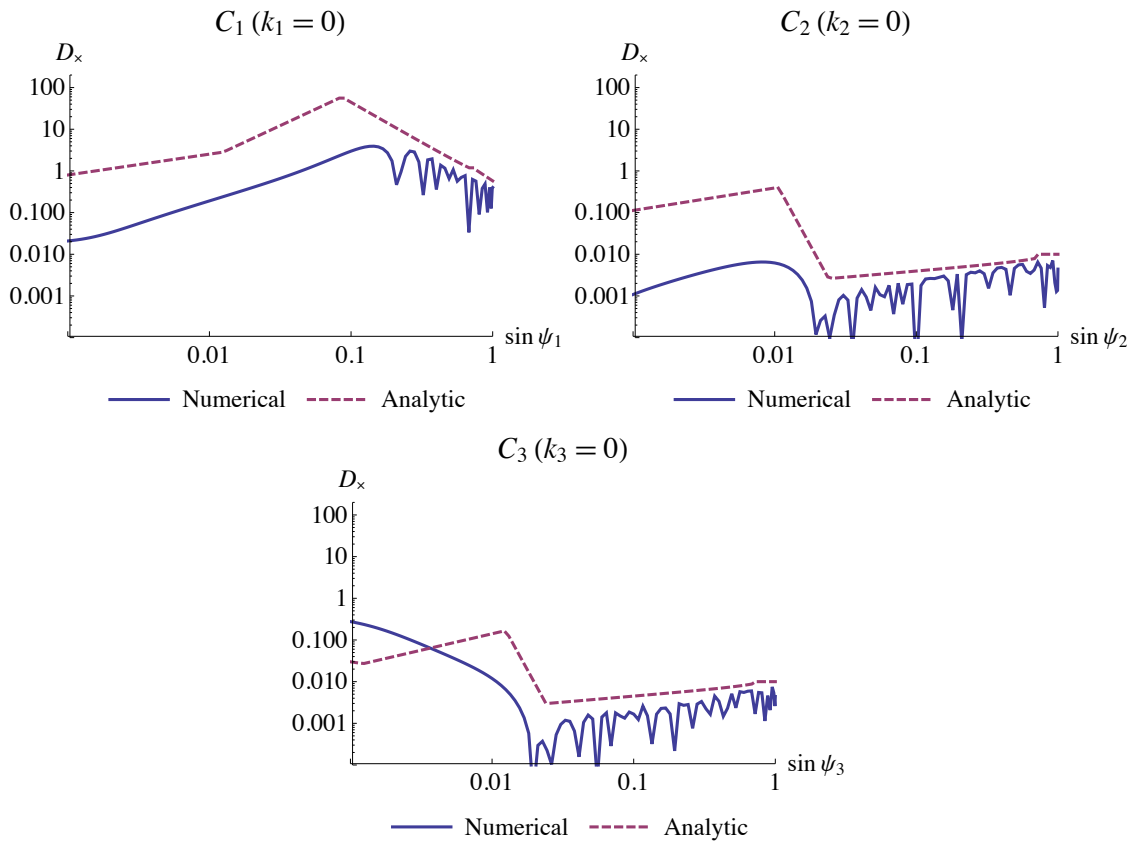

Figure 4.10: Linear growth factors for the $\times$-modes on the circumferences C_1 (top-left), C_2 (top-right), and C_3 (bottom). The background anisotropy parameter is $\Theta = \frac{8\pi}{6}$. The initial time and the final wavenumber are $t_{\rm ini} = 10^{-5}\,H_\Lambda^{-1}$ and $k = 100\,a_{\rm iso}\,H_\Lambda$, respectively.

a threshold value $\psi_3 \sim 10^{-2}$ for growth as implied by Equation (4.34). Note also that these figures are to interpolate the top panels of Figure 4.5.

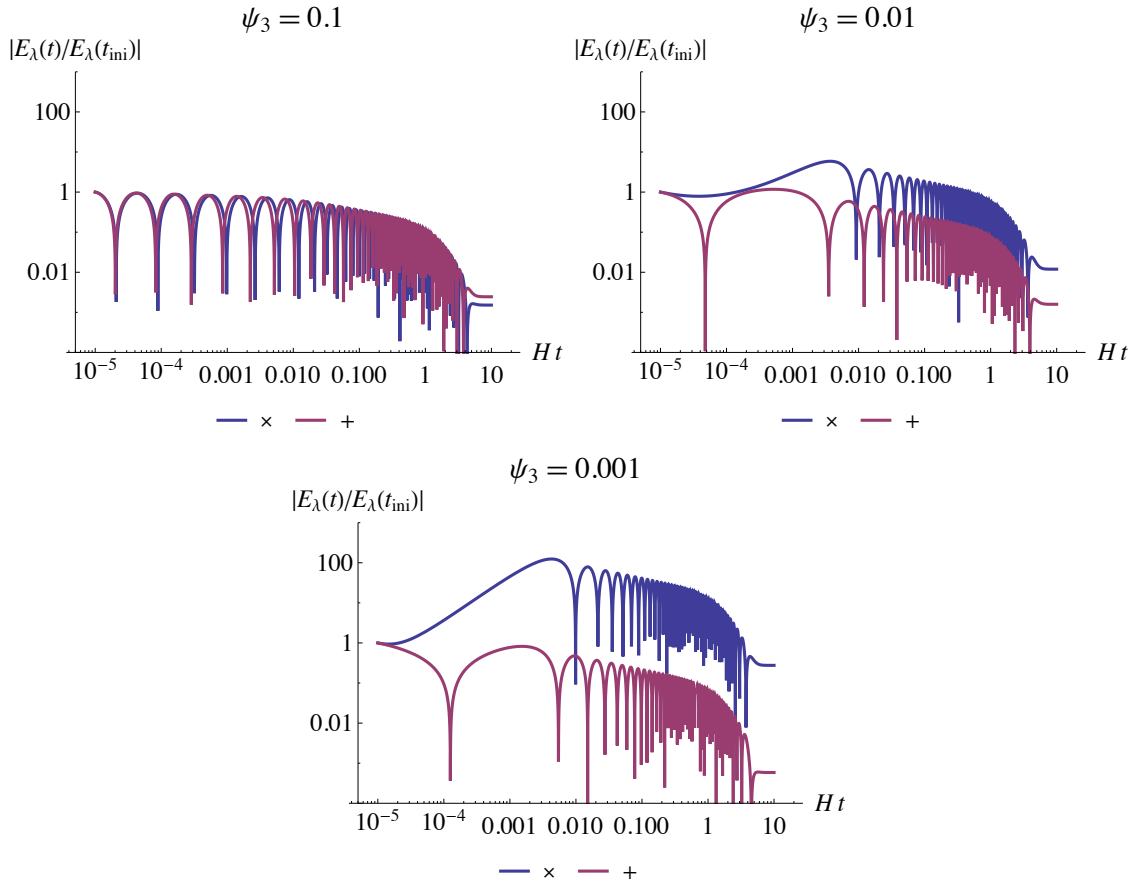

Figure 4.11: Waveforms of several modes on the circumference C_3 ($k_3 = 0$) with a common final wavenumber $k = 100\,a_{\rm iso}\,H_\Lambda$ but with different final directions $k_1/k_2 = \tan\psi_3$ for $\psi_3 = 10^{-1}$ (top-left), 10^{-2} (top-right), and 10^{-3} (bottom). The background anisotropy parameter and the initial time are $\Theta = \frac{8\pi}{6}$ and $t_{\rm ini} = 10^{-5}\,H_\Lambda^{-1}$, respectively.

It should be noted here that the situation on C_1 can change dramatically according to the wavenumber and the background parameters. As implied by (4.30), the time scale $t_{\rm stall}^{\rm (fast)}$ near the k^2-axis on C_1 ($\tan\psi_1 \gtrsim 1$) is a decreasing function of both k and Θ, the reason for the latter dependence being that the exponent $q_1^{\rm (fast)} = q_2$ is an increasing function of Θ. If $t_{\rm stall}^{\rm (fast)}$ declines to a value as small as $t_{\rm ini}$, then amplification of gravitational waves is prohibited near the k^2-axis. Therefore, a simple criterion for the growth on C_1 to occur uniformly may be given by

$$t_{\rm ini} \leq t_{\rm stall}^{\rm (fast)}(\psi_1 = \pi/2) = t_{\rm stall}^{(i=2)}\,. \tag{4.35}$$

In Figure 4.12, we show the boundaries in the $(\Theta, H_\Lambda t_{\rm ini})$-plane saturating the above inequality for several wavenumbers, which can be used to discriminate whether the growth factor on C_1 is uniform or not at a corresponding wavenumber.

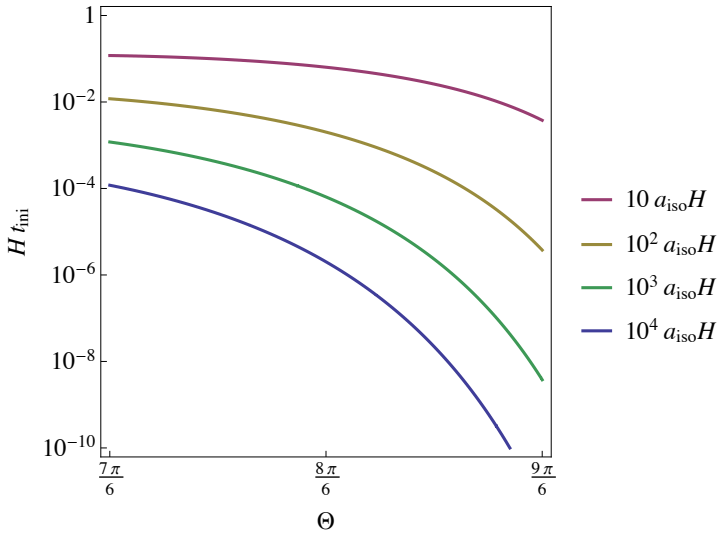

Figure 4.12: Boundaries in the $(\Theta, H_\Lambda t_{\rm ini})$-plane satisfying $t_{\rm ini} = t_{\rm stall}$ evaluated for the k^2-axis-aligned modes with several wavenumbers k_2. If a combination of the parameters $(\Theta, H_\Lambda t_{\rm ini})$ lies below a boundary for a given wavenumber k_2, then the corresponding k^2-axis-aligned mode is supposed to grow and the growth factor on C_1 would look rather uniform.

4.4 Evolution of modes pointing in general directions

Finally we discuss time evolutions of modes with a wavevector pointing in a general direction. As indicated in Figure 4.1, a wavevector $\vec{k}$ rotates from the k^1- to the k^3-axis (except on the circumference C_3). Since neither of the tensor components of the shear vanishes, the two polarization modes no longer evolve independently but affect each other. Hence we shall numerically solve the coupled equations of motion (2.109).

In Figure 4.13, we show all-sky maps of the growth factor for intensity $I \equiv \sqrt{E_+^2 + E_\times^2}$, which is invariant under rotations of polarization basis, for the anisotropy parameters $\Theta = \frac{8\pi}{6}$ (top) and $0.99 \times \frac{9\pi}{6}$ (bottom). The former represents a highly triaxial configuration while the latter is nearly axisymmetric around the k^3-axis, resembling the situation investigated in [GKP08].

An obvious feature seen in the top panels is significantly higher growth factor along the $k_1 = 0$ great circle. This is a manifestation of the result of the analysis in the previous

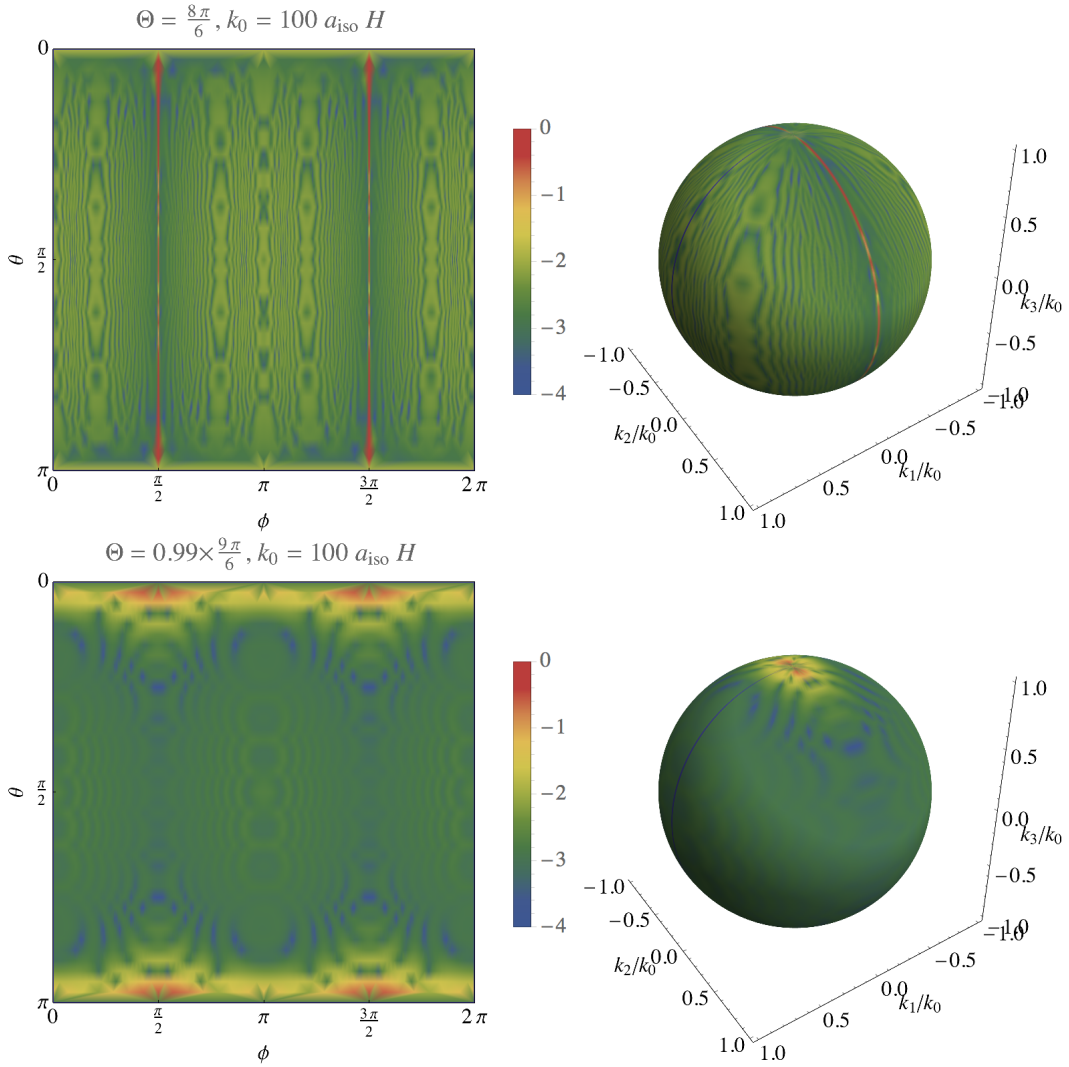

Figure 4.13: Qualitative difference in the intensity ratio $\log_{10}[I(\infty)/I(t_{\rm ini})]$ between the cases of $\Theta = \frac{8\pi}{6}$ (top) and $0.99 \times \frac{9\pi}{6}$ (bottom).

sections that the growth of gravitational waves only occurs in a narrow range near the slower axis on the circumferences C_2 and C_3. Indeed, the width of the belt-shaped region of higher growth factor is well estimated by $\psi_{i=2,3}$ given by Equation (4.34). On the other hand, in the bottom panels ($\Theta = 0.99 \times \frac{9\pi}{6}$) the growth is localized to near the k^3-axis.

As we shall explain now, this topological property is crucial in determining not only the directions of the principal axes of the early anisotropic expansion but also the degree of anisotropy Θ and the initial time of the anisotropic pre-inflationary stage $t_{\rm ini}$ with the aid of Figure 4.12.

Let us imagine all-sky observations of gravitational waves at multiple wavelengths become put into practice in the future, and we assume their initial conditions are given isotropically. If the gravitational waves from the anisotropic regime are detected at some (long) wavelength and the intensity map is determined to have a topology like the top panels of Figure 4.13, then the principal axis of the fastest expansion (in our notation, the x^1-axis) is determined as the normal direction to the plane containing the great circle of higher intensities. As for the pre-inflationary parameters, the combination of $(\Theta, H_\Lambda t_{\rm ini})$ in Figure 4.12 is restricted to lie below the boundary corresponding to the observation wavelength.

Our analyses further predict that, as one goes from longer wavelengths to shorter, the intensity maps will exhibit a transition from a circle-like one (as depicted in the top panels of Figure 4.13) to a localized one (bottom panels) at some critical wavelength. From the map after the transition, the axis of the slowest expansion (the x^3-axis) is determined to be the direction pointing the highest intensity region on the celestial sphere, after which the remaining axis (the x^2-axis) is also determined to be the orthogonal direction to the other two axes.

If such a transition is observed, the values of the parameters $(\Theta, H_\Lambda t_{\rm ini})$ in Figure 4.12 should lie on a curve corresponding to the critical wavelength. Then, once either of the two parameters is given observationally or theoretically, the rest can be determined.

Here, we assumed that the initial conditions of PGWs are isotropic for perspicuity. However, even if the initial conditions were not isotropic, the qualitative topological nature of the sky-map of the growth factor should have impacts on the final distribution of the intensity of PGWs. Particularly, the "uncomputable" region, previously mentioned in Chapter 3, can correspond to the higher growth region.

The success of observation of such topological nature would be not only useful for searching the initial anisotropy but also be a proof of the presence of a "pre-inflation" stage of the universe.

4.5 Discussions

Here, we discuss a very crude constraint on the gravitational-wave background from the anisotropic pre-inflationary phase using the CMB observations. Let us focus on the axis-aligned modes for simplicity. By doing so, we can take advantage of the fact that the two polarizations are decoupled, and hence, the power spectrum after inflation can be represented as a sum of those of the +-mode $\mathcal{P}^{\rm pre}_{\rm T+}$ and the ×-mode $\mathcal{P}^{\rm pre}_{\rm T\times}$ [GKP08; PPU08]. They are not identical in general because the two polarizations evolve differently on an anisotropic background and even their initial values are not necessarily the same. We here consider gravitational waves already existing at the initial time $t_{\rm ini}$. Denoting the values at $t_{\rm ini}$ as $\mathcal{P}^{\rm pre,ini}_{\rm T\lambda}$, the power spectra after inflation can be written in terms of the growth factor D_λ as

$$\mathcal{P}^{\rm pre}_{\rm T\lambda}(k_i) = D_\lambda^2\, \mathcal{P}^{\rm pre,ini}_{\rm T\lambda}(k_i)\,, \tag{4.36}$$

where k_i is the only non-zero component. If $\mathcal{P}^{\rm pre,ini}_{\rm T+}(k_i)$ and $\mathcal{P}^{\rm pre,ini}_{\rm T\times}(k_i)$ are of the same order, since $D_\times \gtrsim D_+$ in general, we may ignore the +-mode in comparison with the ×-mode at later times. Then, we can regard the total primordial power spectrum of the pre-inflationary gravitational waves as

$$\mathcal{P}^{\rm pre}_{\rm T}(k_i) \approx \mathcal{P}^{\rm pre}_{\rm T\times}(k_i) = D_\times^2\, \mathcal{P}^{\rm pre,ini}_{\rm T\times}(k_i)\,, \tag{4.37}$$

whose explicit k_i dependence, apart from the unknown initial part, is

$$\mathcal{P}^{\rm pre}_{\rm T}(k_i) \propto \left(\frac{k_i}{a_{\rm iso}H_\Lambda}\right)^{-2-\frac{2+6\Delta_i}{3(2/3-q_i)}} (H_\Lambda t_{\rm ini})^{-2\Delta_i}\ \mathcal{P}^{\rm pre,ini}_{\rm T\times}(k_i)\,. \tag{4.38}$$

The upper limit on the primordial tensor power spectrum is given in terms of the tensor-to-scalar ratio $\mathcal{P}_{\rm T}/\mathcal{P}_{\rm S} \equiv r \lesssim 0.27$ at around $k = 0.05\,{\rm Mpc}^{-1}$, where the scalar power spectrum is $\mathcal{P}_{\rm S}(k_{\rm pivot}) \sim 10^{-9}$ [Ade+16a]. Since it is expected that the k^3-axis-aligned mode grows the most at shorter wavelengths, we require the primordial tensor power spectrum of the mode traveling along the x^3-axis to be lower than $r\,\mathcal{P}_{\rm S}$ as a

conservative limit. An additional assumption to be made here is that the modes exiting the horizon at $t = t_{\rm iso}$ re-enter the cosmological horizon at sufficiently late times, namely $a_{\rm iso}\, H_\Lambda \sim a(t_0)\, H(t_0)$.

In the left panel of Figure 4.14, we show upper limits on the $\times$-mode initial power spectrum of the pre-inflationary gravitational waves $\mathcal{P}_{\mathrm{T},\times}^{\mathrm{pre,ini}}$ plotted against the anisotropy parameter Θ. The initial time is fixed to be $t_{\rm ini} = 10^{-5}\, H_\Lambda^{-1}$. The constraint becomes gradually stronger as Θ approaches to $\frac{7\pi}{6}$, reflecting the tendency observed in the left panel of Figure 4.8. In the right panel, we show lower limits on the initial time $t_{\rm ini}$. In this figure, we set $\mathcal{P}_{\mathrm{T}\times}^{\mathrm{pre,ini}} = 10^{-8}$.

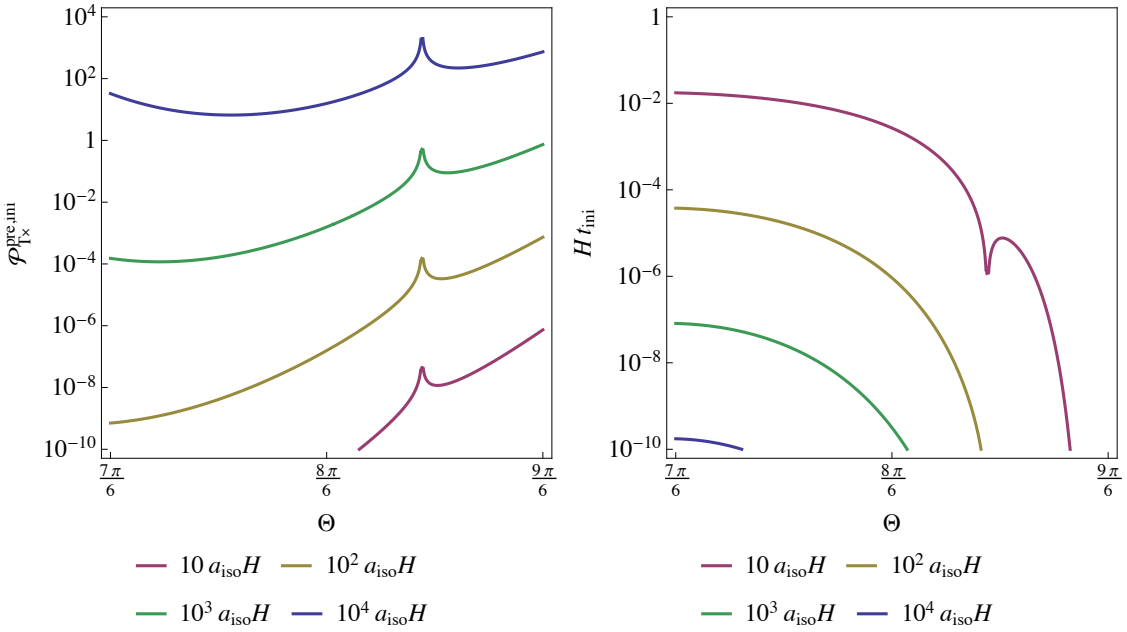

Figure 4.14: Left: Upper limits on the initial spectrum of the $\times$-mode $\mathcal{P}_{\mathrm{T},\times}^{\mathrm{pre,ini}}$ for wavenumbers $k_3 = 10\, a_{\rm iso}\, H_\Lambda$ (red), $10^2\, a_{\rm iso}\, H_\Lambda$ (yellow), $10^3\, a_{\rm iso}\, H_\Lambda$ (green), and $10^4\, a_{\rm iso}\, H_\Lambda$ (blue). The initial time is fixed as $t_{\rm i} = 10^{-5}\, H_\Lambda^{-1}$. Right: Lower limits on the initial time $H_\Lambda\, t_{\rm i}$ for the same set of wavenumbers. The initial amplitude of the $\times$-mode spectrum is fixed as $\mathcal{P}_{\mathrm{T},\times}^{\mathrm{pre,ini}} = 10^{-8}$.

Chapter 5

Conclusions

5.1 Summary of the thesis

As explained in Chapter 1, this thesis was devoted to a comprehensive study of PGWs generated from anisotropic pre-inflation.

In Chapter 2, we reviewed basic equations for cosmological perturbations in Bianchi type-I anisotropic spacetimes. A few important qualitative differences of calculations from those in the isotropic cases are summarized as follows:

1. The norm and direction of wavevectors are time-dependent.
2. The gauge-invariant variables are no longer composed independently of scalar, vector and tensor-type variables, due to the presence of shear in background.

Then, we showed polarization decomposition of the components of the first-order Einstein tensor.

After presenting the general formalism, we focused on the tensor perturbations in the Kasner–de Sitter background, where only the two polarization components are dynamical. As a typical example of triaxially anisotropic KdS, we took the anisotropic indices $(q_1, q_2, q_3) = (1/\sqrt{3}, 0, -1/\sqrt{3})$ $(\Theta = 8\pi/6)$ in most discussions in this thesis.

In Chapter 3, we considered quantization of PGW in the anisotropic pre-inflation model. In Section 3.1, we considered the problem of quantization of primordial perturbations in the presence of a pre-inflationary anisotropy of Bianchi type-I. Quantization in such background has been considered to have a trouble due to the diverging anisotropy as approaching to the initial singularity at $t = 0$ except for the "oblate" axisymmetric

case. We began with an argument that there should be a finite initial time $t_{\rm ini}$ circumventing the initial singularity. Then we suggested that the quantum initial condition for each mode should be set at some moment $t = t_*$ around or after $t_{\rm ini}$. With this initial condition, quantization and evaluation of expectation values was performed in a rather standard way.

In Section 3.2, we practically examined viability of three possible variables, ${}^{(i)}\chi_\lambda$ $(i = 1, 2, 3)$, as defined in (3.11), for the uses as mode functions for quantization of PGWs. As seen in Figure 3.2, due to the hierarchy ${}^{(1)}f \gg {}^{(2)}f \gg {}^{(3)}f$, the variable ${}^{(1)}\chi_\lambda$ was the best to use to approximate a harmonic oscillator with a constant frequency squared ${}^{(1)}\Omega_\lambda^2 \approx k_1^2$ for a wide range of wavenumber (k_1, k_2, k_3). The result also confirmed that interaction between the polarizations modes did not take significant effects at short wavelengths (see [PPU07] for a relevant analysis).

In Section 3.3, we discussed conditions for sensible quantization. We assumed that quantization in the triaxially anisotropic Kasner-de Sitter universe around some moment t_* can be carried out to good approximation if the following conditions are fulfilled:

- At least one of the transformed variables $\{{}^{(1)}\chi_\lambda, {}^{(2)}\chi_\lambda, {}^{(3)}\chi_\lambda\}$ has positive, nearly constant frequency squared.
- Interaction between the polarization modes are weak. Decoupling of the modes in the short wavelength regime has been partly confirmed in [PPU07], and we expect that the interaction is weak as long as the WKB approximation is valid.

These conditions provided us the means to determine the energy spectrum of the fields at $t = t_*$. However, the adequate quantum state is not determined at this stage. In the remainder of Chapter 3, we chose a typical situation in which the state with the lowest energy is realized at $t = t_*$. Moreover, we assumed that we could decide which of ${}^{(i)}\chi_\lambda$ was the most suitable choice of a variable to quantize for a given wavevector (k_1, k_2, k_3). Once a variable suitable for quantization was given, a standard procedure of second quantization could be carried out same as the standard way.

In Section 3.4, we applied our prescription to an evaluation of PGWs. For sufficiently short wavelengths, the predicted PGWs with our quantum initial conditions gave the almost isotropic, scale-invariant power spectrum with the same amplitude as de Sitter inflation, as understood from Equation (3.29) and Figure 3.4. This is consistent with the previous results of the analyses in the short wavelength regime [PPU07; PPU08]. We also presented the sky map in a nearly "prolate" axisymmetric background in Figure 3.5.

For very small $|k_1|$ or in the long wavelength regime with $k \lesssim \mathcal{O}(10)\, a_{\rm iso}\, H_\Lambda$, our variables ${}^{(i)}\chi_\lambda$ do not give a good approximation to harmonic oscillator.[1] The enhancement of PGWs near the k_3 axis as seen in Figure 3.4 is most probably merely a manifestation of the limitation of our approximations with the use of the variables ${}^{(i)}\chi_\lambda$. We did not even try to make any predictions if all ${}^{(i)}\Omega^2_\lambda$ are negative, which takes place in the vicinity of the great circle of $k_1 = 0$.

Nevertheless, we expect that the prediction can differ from that of de Sitter inflation if the WKB condition was violated or the frequency squared Ω^2_λ became negative during some period in the anisotropic regime. This could indeed happen in the regions where our current approximation method breaks down.

In Chapter 4, we performed a detailed analysis on the directional variations of a gravitational wave background in a (pre-)inflation model described by the general triaxial Kasner–de Sitter metric, in which the degree of anisotropy is parameterized by an angle parameter Θ . The purpose of the study was to give some more insights into the connection between such gravitational waves and the primordial anisotropies.

We divided the whole analysis into the following three steps. First, in Section 4.2, we investigated the evolution of gravitational waves whose wavevector is aligned with either of the principal axes of anisotropic expansion. We clarified that, with our choice of the polarization basis, the $\times$-polarization mode grows substantially while the shear term is giving a dominant contribution to the squared frequency $\omega^2_\times$. The amount of growth reflects two factors: (i) the slower the expansion along the axis is, the longer $\omega^2_\times$ remains negative; (ii) the larger the projected shear component $\sigma^{(\mathrm{T})}_+$ is, the faster the mode grows. There was a competition between the k^3- and k^2-axis-aligned modes since the former grows for longest while the latter "sees" the largest value of $\sigma^{(\mathrm{T})}_+$. In an analytical manner, we have obtained the explicit parameter dependencies of the growth factors as in Equation (4.22), clarifying that the k^3-axis-aligned $\times$-mode should dominate over the other modes at sufficiently large wavenumbers except for an axisymmetric background with $\Theta \approx \frac{7\pi}{6}$.

Second, in Section 4.3, we extended the analysis to the modes whose wavevector is aligned between two of the principal axes. The situations are different on each circumference C_i introduced as in Figure 4.2. We revealed that the distribution of gravitational-wave intensities on C_1 can change dramatically according to the background parameters

[1] Note that modes with $k < \mathcal{O}(1)\, a_{\rm iso}\, H_\Lambda$ are already on super-horizon scales at the beginning of de Sitter inflation. Classicality of such modes might be questioned.

Θ and $t_{\rm ini}$ as explained by Figure 4.12 : when Θ is sufficiently close to $\frac{9\pi}{6}$, a value corresponding to one of the axisymmetric limits, and $H_\Lambda\, t_{\rm ini}$ is sufficiently large, the growth of gravitational waves is localized to near the k^3-axis. In the opposite case, the growth takes place rather uniformly on C_1 . On the other circumferences C_2 and C_3 , we showed that the growth is localized to near the k^3- and k^2-axis, respectively, for wide ranges of parameters.

Third, in Section 4.4, we discussed time evolutions of modes with a wavevector pointing in a general direction. Specifically, we demonstrated all-sky maps of the growth factor of the pre-inflationary gravitational waves for the two anisotropy parameters $\Theta = \frac{8\pi}{6}$ (triaxial) and $0.99 \times \frac{9\pi}{6}$ (nearly axisymmetric) as in Figure 4.13. For $\Theta = \frac{8\pi}{6}$, the growth of gravitational waves occurs in a narrow range near the $k_1 = 0$ great circle on the sphere whose width can be well estimated by Equation (4.34), while for $\Theta = 0.99 \times \frac{9\pi}{6}$, the growth is localized to the k^3-axis. Using these results, we argued that the topological properties of the pre-inflationary gravitational waves in future all-sky, multi-wavelength observations might provide us a crucial probe for determination of the configuration of the primordial anisotropy, its degree Θ , and the initial time $t_{\rm ini}$.

Moreover, in Section 4.5, we gave some tentative constraints on the initial amplitude of the pre-inflationary gravitational waves, the anisotropy parameter Θ , and the initial time $t_{\rm ini}$ from the B-mode polarization of CMB observed by the Planck satellite.

A thorough inspection into the modes with small k_1 (corresponding to the "planar modes" studied in the "oblate" axisymmetric case [BPM15; DP12; DKP12; DKP14]) and long-wave length modes with $k \sim \mathcal{O}(10)\, a_{\rm iso}\, H_\Lambda$ is beyond the scope of this thesis, and we leave studies of possible signatures of primordial anisotropy in the sky map of such PGWs in future studies.

5.2 Concluding remark

The qualitative topological nature of the sky-map of the growth factor should have impacts on the final intensity of PGWs. Particularly, the "uncomputable" region where our quantization prescription is ineffective can correspond to the higher growth region. This might serve as a potential probe for the pre-inflationary initial anisotropy with future all-sky observations of gravitational waves. The success of observation of such

topological nature would be not only useful for searching the initial anisotropy but also be a proof of the presence of a "pre-inflation" stage of the universe.

Bibliography

[Abb+16a] B. P. Abbott *et al.*, "GW151226: Observation of Gravitational Waves from a 22-Solar-Mass Binary Black Hole Coalescence", Phys. Rev. Lett. **116** (2016), 241103, DOI: 10.1103/PhysRevLett.116.241103, arXiv: 1606.04855 [gr-qc].

[Abb+16b] B. P. Abbott *et al.*, "Observation of Gravitational Waves from a Binary Black Hole Merger", Phys. Rev. Lett. **116** (2016), 061102, DOI: 10.1103/PhysRevLett.116.061102, arXiv: 1602.03837 [gr-qc].

[Abb+17a] B. P. Abbott *et al.*, "GW170104: Observation of a 50-Solar-Mass Binary Black Hole Coalescence at Redshift 0.2", Phys. Rev. Lett. **118** (2017), 221101, DOI: 10.1103/PhysRevLett.118.221101, arXiv: 1706.01812 [gr-qc], [Erratum: Phys. Rev. Lett. **121** (2018), 129901].

[Abb+17b] B. P. Abbott *et al.*, "GW170608: Observation of a 19 solar-mass Binary Black Hole Coalescence", Astrophys. J. Lett. **851** (2017), L35, DOI: 10.3847/2041-8213/aa9f0c, arXiv: 1711.05578 [astro-ph.HE].

[Abb+17c] B. P. Abbott *et al.*, "GW170814: A Three-Detector Observation of Gravitational Waves from a Binary Black Hole Coalescence", Phys. Rev. Lett. **119** (2017), 141101, DOI: 10.1103/PhysRevLett.119.141101, arXiv: 1709.09660 [gr-qc].

[Abb+17d] B. P. Abbott *et al.*, "GW170817: Observation of Gravitational Waves from a Binary Neutron Star Inspiral", Phys. Rev. Lett. **119** (2017), 161101, DOI: 10.1103/PhysRevLett.119.161101, arXiv: 1710.05832 [gr-qc].

[Ade+14a] P. A. R. Ade *et al.*, "A Measurement of the Cosmic Microwave Background B-Mode Polarization Power Spectrum at Sub-degree Scales with POLARBEAR", Astrophys. J. **794** (2014), 171, DOI: 10.1088/0004-637X/794/2/171, arXiv: 1403.2369 [astro-ph.CO].

[Ade+14b] P. A. R. Ade *et al.*, "Detection of B-Mode Polarization at Degree Angular Scales by BICEP2", Phys. Rev. Lett. **112** (2014), 241101, DOI: 10.1103/PhysRevLett.112.241101, arXiv: 1403.3985 [astro-ph.CO].

[Ade+15] P. A. R. Ade *et al.*, "Joint Analysis of BICEP2/*Keck Array* and *Planck* Data", Phys. Rev. Lett. **114** (2015), 101301, DOI: 10.1103/PhysRevLett.114.101301, arXiv: 1502.00612 [astro-ph.CO].

[Ade+16a] P. A. R. Ade *et al.*, "*Planck* 2015 results. XIII. Cosmological parameters", Astron. Astrophys. **594** (2016), A13, DOI: 10.1051/0004-6361/201525830, arXiv: 1502.01589 [astro-ph.CO].

[Ade+16b] P. A. R. Ade *et al.*, "*Planck* 2015 results. XX. Constraints on inflation", Astron. Astrophys. **594** (2016), A20, DOI: 10.1051/0004-6361/201525898, arXiv: 1502.02114 [astro-ph.CO].

[Agh+18] N. Aghanim *et al.*, "*Planck* 2018 results. VI. Cosmological parameters" (2018), arXiv: 1807.06209 [astro-ph.CO].

[Ala+17] Shadab Alam *et al.*, "The clustering of galaxies in the completed SDSS-III Baryon Oscillation Spectroscopic Survey: cosmological analysis of the DR12 galaxy sample", Mon. Not. Roy. Astron. Soc. **470** (2017), 2617–2652, DOI: 10.1093/mnras/stx721, arXiv: 1607.03155 [astro-ph.CO].

[AS+12] Pau Amaro-Seoane *et al.*, "Low-frequency gravitational-wave science with eLISA/NGO", Class. Quant. Grav. **29** (2012), 124016, DOI: 10.1088/0264-9381/29/12/124016, arXiv: 1202.0839 [gr-qc].

[Bar80] James M. Bardeen, "Gauge-invariant cosmological perturbations", Phys. Rev. D **22** (1980), 1882–1905, DOI: 10.1103/PhysRevD.22.1882.

[BST83] James M. Bardeen, Paul J. Steinhardt, and Michael S. Turner, "Spontaneous creation of almost scale-free density perturbations in an inflationary universe", Phys. Rev. D **28** (1983), 679, DOI: 10.1103/PhysRevD.28.679.

[Ben+13] C. L. Bennett *et al.*, "Nine-year *Wilkinson Microwave Anisotropy Probe* (*WMAP*) Observations: Final Maps and Results", Astrophys. J. Suppl. **208**, 20 (2013), 20, DOI: 10.1088/0067-0049/208/2/20, arXiv: 1212.5225 [astro-ph.CO].

[BPM15] Jose J. Blanco-Pillado and Masato Minamitsuji, "The Initial State of a Primordial Anisotropic Stage of Inflation", J. Cosmol. Astropart. Phys. **1506** (2015), 024, DOI: 10.1088/1475-7516/2015/06/024, arXiv: 1501.07427 [hep-th].

[CC05] Jeff Crowder and Neil J. Cornish, "Beyond LISA: Exploring future gravitational wave missions", Phys. Rev. D **72** (2005), 083005, DOI: 10.1103/PhysRevD.72.083005, arXiv: gr-qc/0506015 [gr-qc].

[de 17] W. de Sitter, "On the relativity of inertia. Remarks concerning Einstein's latest hypothesis", Koninklijke Nederlandse Akademie van Wetenschappen Proceedings Series B Physical Sciences **19** (1917), 1217–1225, URL: https://www.dwc.knaw.nl/DL/publications/PU00012455.pdf.

[de 18] W. de Sitter, "On the curvature of space", Koninklijke Nederlandse Akademie van Wetenschappen Proceedings Series B Physical Sciences **20** (1918), 229–243, URL: https://www.dwc.knaw.nl/DL/publications/PU00012216.pdf.

[DKP12] Anindya Dey, Ely Kovetz, and Sonia Paban, "Non-Gaussianities in the cosmological perturbation spectrum due to primordial anisotropy II", J. Cosmol. Astropart. Phys. **1210** (2012), 055, DOI: 10.1088/1475-7516/2012/10/055, arXiv: 1205.2758 [astro-ph.CO].

[DKP14] Anindya Dey, Ely D. Kovetz, and Sonia Paban, "Power spectrum and non-Gaussianities in anisotropic inflation", J. Cosmol. Astropart. Phys. **1406** (2014), 025, DOI: 10.1088/1475-7516/2014/06/025, arXiv: 1311.5606 [hep-th].

[DP12] Anindya Dey and Sonia Paban, "Non-gaussianities in the cosmological perturbation spectrum due to primordial anisotropy", J. Cosmol. Astropart. Phys. **1204** (2012), 039, DOI: 10.1088/1475-7516/2012/04/039, arXiv: 1106.5840 [hep-th].

[EM69] G. F. R. Ellis and M. A. H. MacCallum, "A class of homogeneous cosmological models", Commun. Math. Phys. **12** (1969), 108–141, DOI: 10.1007/BF01645908.

[Fix+96] D. J. Fixsen *et al.*, "The Cosmic Microwave Background Spectrum from the Full *COBE* FIRAS Data Set", Astrophys. J. **473** (1996), 576, DOI: 10.1086/178173, arXiv: astro-ph/9605054 [astro-ph].

[Fri22] A. Friedmann, "Über die Krümmung des Raumes", Zeitschrift für Physik **10** (1922), 377–386, DOI: 10.1007/BF01332580.

[FNS17] Yu Furuya, Yuki Niiyama, and Yuuiti Sendouda, "Probing pre-inflationary anisotropy with directional variations in the gravitational wave background", J. Cosmol. Astropart. Phys. **1701** (2017), 009, DOI: 10.1088/1475-7516/2017/01/009, arXiv: 1609.02785 [astro-ph.CO].

[FNS19] Yu Furuya, Yuki Niiyama, and Yuuiti Sendouda, "A quantisation procedure in the presence of an initial Kasner singularity: primordial gravitational waves from triaxially anisotropic pre-inflation", Class. Quant. Grav. **36** (2019), 085007, DOI: 10.1088/1361-6382/ab0ca9, arXiv: 1904.02803 [gr-qc].

[Gam46] G. Gamow, "Expanding Universe and the Origin of Elements", Phys. Rev. **70** (1946), 572–573, DOI: 10.1103/PhysRev.70.572.2.

[GKP08] A. E. Gümrükçüoğlu, L. Kofman, and M. Peloso, "Gravity waves signatures from anisotropic preinflation", Phys. Rev. D **78** (2008), 103525, DOI: 10.1103/PhysRevD.78.103525, arXiv: 0807.1335 [astro-ph].

[GCP07] A. Emir Gümrükçüoğlu, Carlo R. Contaldi, and Marco Peloso, "Inflationary perturbations in anisotropic backgrounds and their imprint on the cosmic microwave background", J. Cosmol. Astropart. Phys. **0711** (2007), 005, DOI: 10.1088/1475-7516/2007/11/005, arXiv: 0707.4179 [astro-ph].

[Gut81] Alan H. Guth, "Inflationary universe: A possible solution to the horizon and flatness problems", Phys. Rev. D **23** (1981), 347–356, DOI: 10.1103/PhysRevD.23.347.

[GP82] Alan H. Guth and So-Young Pi, "Fluctuations in the New Inflationary Universe", Phys. Rev. Lett. **49** (1982), 1110–1113, DOI: 10.1103/PhysRevLett.49.1110.

[Haw82] S. W. Hawking, "The development of irregularities in a single bubble inflationary universe", Phys. Lett. B **115** (1982), 295, DOI: 10.1016/0370-2693(82)90373-2.

[Hub29] Edwin Hubble, "A relation between distance and radial velocity among extra-galactic nebulae", Proc. Nat. Acad. Sci. **15** (1929), 168–173, DOI: 10.1073/pnas.15.3.168.

[KKS97a] Marc Kamionkowski, Arthur Kosowsky, and Albert Stebbins, "A Probe of Primordial Gravity Waves and Vorticity", Phys. Rev. Lett. **78** (1997), 2058–2061, DOI: 10.1103/PhysRevLett.78.2058, arXiv: astro-ph/9609132 [astro-ph].

[KKS97b] Marc Kamionkowski, Arthur Kosowsky, and Albert Stebbins, "Statistics of cosmic microwave background polarization", Phys. Rev. D **55** (1997), 7368–7388, DOI: 10.1103/PhysRevD.55.7368, arXiv: astro-ph/9611125 [astro-ph].

[Kas21] Edward Kasner, "Geometrical Theorems on Einstein's Cosmological Equations", Am. J. Math. **43** (1921), 217–221, DOI: 10.2307/2370192.

[Kei+15] R. Keisler *et al.*, "Measurements of Sub-degree B-mode Polarization in the Cosmic Microwave Background from 100 Square Degrees of SPTpol Data", Astrophys. J. **807** (2015), 151, DOI: 10.1088/0004-637X/807/2/151, arXiv: 1503.02315 [astro-ph.CO].

[KM10] Hyeong-Chan Kim and Masato Minamitsuji, "Scalar field in the anisotropic universe", Phys. Rev. D **81** (2010), 083517, DOI: 10.1103/PhysRevD.81.083517, arXiv: 1002.1361 [gr-qc], [Erratum: Phys. Rev. D **82** (2010), 109904].

[KUP11] Lev Kofman, Jean-Philippe Uzan, and Cyril Pitrou, "Perturbations of generic Kasner spacetimes and their stability", J. Cosmol. Astropart. Phys. **1105** (2011), 011, DOI: 10.1088/1475-7516/2011/05/011, arXiv: 1102.3071 [gr-qc].

[Lem27] G. Lemaître, "Un Univers homogène de masse constante et de rayon croissant rendant compte de la vitesse radiale des nébuleuses extra-galactiques", Annales de la Société Scientifique de Bruxelles **47** (1927), 49–59.

[Mat+14] T. Matsumura *et al.*, "Mission Design of LiteBIRD", J. Low Temp. Phys. **176** (2014), 733–740, DOI: 10.1007/s10909-013-0996-1, arXiv: 1311.2847 [astro-ph.IM].

[MC81] V. F. Mukhanov and G. V. Chibisov, "Quantum fluctuation and a nonsingular universe", JETP Lett. **33** (1981), 532–535, URL: http://jetpletters.ac.ru/ps/1510/article_23079.pdf, [Pis'ma Zh. Eksp. Teor. Fiz. **33** (1981), 549–553].

[Nae+14] Sigurd Naess *et al.*, "The Atacama Cosmology Telescope: CMB polarization at $200 < \ell < 9000$", J. Cosmol. Astropart. Phys. **1410** (2014), 007, DOI: 10.1088/1475-7516/2014/10/007, arXiv: 1405.5524 [astro-ph.CO].

[Nak+16] Takashi Nakamura *et al.*, "Pre-DECIGO can get the smoking gun to decide the astrophysical or cosmological origin of GW150914-like binary black holes", Prog. Theor. Exp. Phys. **2016** (2016), 093E01, DOI: 10.1093/ptep/ptw127, arXiv: 1607.00897 [astro-ph.HE].

[PW65] A. A. Penzias and R. W. Wilson, "A Measurement of Excess Antenna Temperature at 4080 Mc/s.", Astrophys. J. Lett. **142** (1965), L419–L421, DOI: 10.1086/148307.

[PPU07] Thiago S. Pereira, Cyril Pitrou, and Jean-Philippe Uzan, "Theory of cosmological perturbations in an anisotropic universe", J. Cosmol. Astropart. Phys. **0709** (2007), 006, DOI: 10.1088/1475-7516/2007/09/006, arXiv: 0707.0736 [astro-ph].

[PPU08] Cyril Pitrou, Thiago S. Pereira, and Jean-Philippe Uzan, "Predictions from an anisotropic inflationary era", J. Cosmol. Astropart. Phys. **0804** (2008), 004, DOI: 10.1088/1475-7516/2008/04/004, arXiv: 0801.3596 [astro-ph].

[Pit+18] Cyril Pitrou *et al.*, "Precision big bang nucleosynthesis with improved Helium-4 predictions", Phys. Rept. **754** (2018), 1–66, DOI: 10.1016/j.physrep.2018.04.005, arXiv: 1801.08023 [astro-ph.CO].

[Rob35] H. P. Robertson, "Kinematics and World-Structure", Astrophys. J. **82** (1935), 284–301, DOI: 10.1086/143681.

[Rob36a] H. P. Robertson, "Kinematics and World-Structure II.", Astrophys. J. **83** (1936), 187–201, DOI: 10.1086/143716.

[Rob36b] H. P. Robertson, "Kinematics and World-Structure III.", Astrophys. J. **83** (1936), 257–271, DOI: 10.1086/143726.

[Sat81] Katsuhiko Sato, "First-order phase transition of a vacuum and the expansion of the Universe", Mon. Not. Roy. Astron. Soc. **195** (1981), 467–479, DOI: 10.1093/mnras/195.3.467.

[SZ97] Uroš Seljak and Matias Zaldarriaga, "Signature of Gravity Waves in the Polarization of the Microwave Background", Phys. Rev. Lett. **78** (1997), 2054–2057, DOI: 10.1103/PhysRevLett.78.2054, arXiv: astro-ph/9609169 [astro-ph].

[SKN01] Naoki Seto, Seiji Kawamura, and Takashi Nakamura, "Possibility of Direct Measurement of the Acceleration of the Universe Using 0.1 Hz Band Laser Interferometer Gravitational Wave Antenna in Space", Phys. Rev. Lett. **87** (2001), 221103, DOI: 10.1103/PhysRevLett.87.221103, arXiv: astro-ph/0108011 [astro-ph].

[Smo+92] George F. Smoot *et al.*, "Structure in the *COBE* Differential Microwave Radiometer First-year Maps", Astrophys. J. Lett. **396** (1992), L1–L5, DOI: 10.1086/186504.

[Sta82] A. A. Starobinsky, "Dynamics of phase transition in the new inflationary universe scenario and generation of perturbations", Phys. Lett. B **117** (1982), 175–178, DOI: 10.1016/0370-2693(82)90541-X.

[Suz+16] A. Suzuki *et al.*, "The POLARBEAR-2 and the Simons Array Experiments", J. Low Temp. Phys. **184** (2016), 1–6, DOI: 10.1007/s10909-015-1425-4, arXiv: 1512.07299 [astro-ph.IM].

[Wal83] Robert M. Wald, "Asymptotic behavior of homogeneous cosmological models in the presence of a positive cosmological constant", Phys. Rev. D **28** (1983), 2118(R)–2120(R), DOI: 10.1103/PhysRevD.28.2118.

[Wal37] A. G. Walker, "On Milne's Theory of World-Structure", Proceedings of the London Mathematical Society **42** (1937), 90–127, DOI: 10.1112/plms/s2-42.1.90.